The Role of High- and Low-Temperature Ocean Crust Alteration for the Marine Calcium Budget

Dissertation

zur Erlangung des Doktorgrades

der Mathematisch-Naturwissenschaftlichen Fakultät

der Christian-Albrechts-Universität

zu Kiel

vorgelegt von

Marghaleray Amini

Kiel

2007

Referent:.....

Koreferent:.....

Tag der mündlichen Prüfung:.....

Zum Druck genehmigt: Kiel,.....

Der Dekan

Abstract

Calcium (Ca) is a key element for the understanding of the chemical evolution of the ocean and for the global climate on long geological time scales. This is because Ca is interacting with the carbon cycle and is a major constituent of continental weathering. Beside continental runoff, mid-ocean ridges are of quantitative importance for the marine Ca elemental and isotope budget. Variations of hydrothermal circulation of seawater through oceanic crust have been recognized to play a significant role for the oceanic Ca mass and isotope balance. Hydrothermal activity leads to a chemical alteration of the circulating seawater at low- and high-temperatures during water-rock interaction, the formation of Ca-bearing minerals, and during phase separation. Within the framework of the subproject 'CARLA' in the 'Special Priority Program SPP 1144' Ca isotope ratios ($\delta^{44/40}$Ca) in hydrothermal fluids sampled from the Logatchev hydrothermal field (15°N/45°W) and the Ascension area (4-11°S) have been investigated in detail. It could be demonstrated that the Ca isotope compositions of the fluid endmembers undergo fractionation effects during the precipitation of anhydrite at high temperatures of > 300°C and most likely also due to phase separation processes. The Logatchev hydrothermal field and the Red Lion field at the Mid-Atlantic Ridge 15°N and 5°S, respectively provide hydrothermal circulation without evidence for phase separation of the circulating seawater. The transformation of seawater to a hydrothermal solution within the Logatchev and the Red Lion hydrothermal fields results in an increase of the Ca concentration of pristine seawater ($[Ca]_{SW}$) from about 10 mM to ~32 mM and ~16 mM in the hydrothermal fluid endmembers ($[Ca]_{HydEnd}$), thereby adopting a $\delta^{44/40}Ca_{HydEnd}$ of -0.95±0.07 ‰ and -0.90±0.44 ‰, respectively. $\delta^{44/40}Ca_{HydEnd}$ is higher than expected from the initial values ($\delta^{44/40}Ca_{initial}$). The enrichment of ^{44}Ca in the hydrothermal endmembers can be referred to precipitation of anhydrite. The much heavier $\delta^{44/40}Ca_{HydEnd}$ in hydrothermal fluids from the Turtle Pits field with a value of about -0.65 ‰ can be explained by high water-rock ratios, extensive anhydrite precipitation and potentially also due to phase separation. Ca isotopes may be discriminated during phase separation due to Cl^--complexation. The precipitation process of anhydrite can be described by the Rayleigh fractionation law implying a formation of the hydrothermal minerals in a nearly closed system. Ca isotope fractionation in these anhydrites is positively correlated to estimated precipitation temperatures in the range between ~100°C and ~350°C. The data show a temperature-dependency of Ca isotope fractionation in anhydrites less sensitive than deduced for calcium carbonate polymorphs.

Ca isotopes in hydrothermal calcites from serpentine-talc-tremolite schists indicate precipitation at temperatures above 100°C where $\Delta_{HydEnd-Cal}$ approaches zero. These calcites are formed due to high temperatures increasing the saturation state of the fluids for calcite. Ca isotope ratios in aragonites from leached serpentinites and from carbonate veins from ODP drill cores indicate aragonite precipitation at low temperatures between 10°C and 40°C corresponding to a Ca isotope fractionation of -1.32 ‰ to -1.82 ‰. While aragonites and calcites do not contribute at all to changes in the Ca isotope budget of the hydrothermal system, the high fractionation factors for the aragonites in combination with their frequent occurrence in weathered mafic and ultramafic rocks infer a reconsideration of the marine Ca isotope budget, in particular with regard to ocean crust alteration as these carbonates represent a significant sink in the marine Ca mass balance.

In order to provide an appropriate base for the isotopic composition of the oceanic crust and with regard to the paucity of data for the Ca isotope data of silicate rocks, this study reports the Ca isotopic compositions of eight MPI-DING glasses and the respective original powders, six USGS reference rock materials, the U-series isotope reference TML, the IAEA-CO1 (Carrara marble) and various non-certified rock samples. The samples were

selected in order to cover a wide range of different geologic settings and lithologies and by their importance in laboratory use. The Ca isotope ratios were obtained by thermal ionisation mass spectrometry using a $^{43/48}$double-spike method. Various chemical preparation techniques were applied in order to preclude chemical artifacts and to test for statistical variability. Analytical uncertainties for the reported $\delta^{44/40}$Ca data are less than 0.2 ‰ at 95 % confidence level. The different preparation methods resulted in identical values precluding chemical artifacts during sample processing. From the comparison between the original powder and the respective glasses variations in the Ca isotope ratios during the fusion process can be excluded. Individual analyses of different glass fragments indicate that the glasses are well-homogenized at the mm-scale with respect to their Ca isotope compositions. Within the analytical precision obtained no heterogeneities can be detected. This comprehensive data set provides first $\delta^{44/40}$Ca information values of reference rock materials for geochemical and in-situ microanalytical work. Variations in the Ca isotope compositions of different rock types, in particular between mafic and ultramafic rocks show strong evidence for a Ca isotope variability at p-T conditions of the mantle. Compared to mafic rocks the ultramafic rock samples consistently show up to 0.6 ‰ higher $\delta^{44/40}$Ca values. With respect to the predominance of ultramafic mantle rocks, the findings require a reconsideration of the currently assumed Bulk Earth value of about -0.9 ‰ adopted on volcanic rocks. Generally, this work evokes a reconsideration of the oceanic Ca budget with regard to variabilities in the Ca isotope compositions of hydrothermal solutions and the oceanic crust.

Kurzfassung

Calcium (Ca) spielt eine Schlüsselrolle im Verständnis der chemischen Entwicklung der Ozeane und des globalen Klimas auf langen geologischen Zeitskalen, da Ca ein wesentlicher Bestandteil der kontinentalen Verwitterung ist und mit dem Kohlenstoffkreislauf interagiert. Von ebenso quantitativer Bedeutung sind die Veränderungen des Ca-Flußes aus den mittelozeanischen Rücken im Hinblick auf deren Beitrag zur Ca-Konzentrations- und Isotopenbilanz des Meerwassers. Die hydrothermale Aktivität an den mittelozeanischen Rücken führt zu einer chemischen Modifikation während der Wechselwirkung zwischen Meerwasser und dem Gestein der Ozeankruste, der Bildung von Ca-reichen Mineralen und der Phasenseparation. Im Rahmen des Schwerpunktprogramms SPP 1144 wurde im Teilprojekt ‘CARLA’ Ca Isotopenverhältnisse ($\delta^{44/40}$Ca) in Fluidproben des Logatchev Hydrothermalfeldes (15°N/45°W) und der Hydrothermalfelder der Ascension-Region untersucht. Es konnte gezeigt werden, dass Ca Isotope im hydrothermalen Endglied bei der Bildung von Anhydrit bei Temperaturen von bis zu 300°C fraktioniert sind. Am Logatchev Hydrothermalfeld und Red Lion Hydrothermalfeld am mittelatlantischen Rücken bei 15°N bzw. 5°S findet hydrothermale Aktivität ohne Anzeichen von Phasenseparation im Untergrund statt. Die chemische Umwandlung von Meerwasser zum Hydrothermalfluid führt hier zu einer Anreicherung von Ca ($[Ca]_{SW}$) von etwa 10 mM auf 32 mM bzw. 16 mM mit einer einhergehenden Anpassung der Isotopensignatur auf $\delta^{44/40}Ca_{HydEnd}$ von -0.95±0.07 ‰ bzw. -0.90±0.44 ‰. Die Ca Isotopenwerte für die hydrothermalen Endglieder sind höher, als von den Gesteinswerten erwartet werden kann. Die Anreicherung an ^{44}Ca beruht auf der Bildung von Anhydrit mit gleichzeitiger Ca-Isotopenfraktionierung. Der um einiges höhere $\delta^{44/}40Ca_{HydEnd}$-Wert von -0.65 ‰ für Fluide vom Turtle Pits Hydrothermalfeld beruht auf ein höheres Wasser-Gesteinsverhältnis während der Zirkulation, der intensiven Ausfällung von Anhydrit aus dem Fluid und sehr wahrscheinlich einer zusätzlichen Ca-Isotopenfraktionierung

während der Phasenseparation. Eine Fraktionierung von Ca Isotopen mag auf die Chlor-Komplexierung von Ca zurückgeführt werden. Die Präzipitation von Anhydrit ähnelt einer Ausfällung in einem geschlossenen System und kann durch eine Rayleighfraktionierung beschrieben werden. Ca-Isotopenfraktionierungen in diesen hydrothermal ausgefällten Anhydriten zeigen eine positive Korrelation zur Bildungstemperatur wie sie über eine adiabatische Mischung von Meerwasser und Hydrothermalfluid auf etwa 100-350 °C abgeschätzt wurde. Die Temperaturabhängigkeit der Ca-Isotopenfraktionierung in Anhydriten scheint weniger empfindlich als in Kalziumkarbonaten zu sein.

Hoch-Temperatur-Kalzite aus Sepentin-Talk-Tremolit Adern bildeten sich bei Temperaturen >100°C und weisen daher kaum eine Ca-Isotopenfraktionierung ($\Delta_{HydEnd-Cal}$) auf. Die Ausfällung dieser Kalzite beruht auf den hohen Temperaturen und des damit einhergehenden Anstiegs des Sättigungsgrades der Fluide für Kalzit. Ca Isotope in Aragoniten aus dem ODP Bohrkern, die bei niedrigen Temperaturen zwischen 10 °C und 40 °C ausgefallen sind, zeigen eine Ca Isotopie von -1.32 ‰ bishin zu -1.82 ‰. Obgleich diese Aragonite direkt aus Meerwasser ausgefallen sind und daher wie die Hoch-Temperatur-Kalzite die nicht fraktioniert sind, nicht zu Änderungen des Ca-Isotopenbudgets des Logatchev-Hydrothermalsystems beitragen, erfordert ihre leichte Isotopensignatur und ihr häufiges Auftreten in verwitterter mafischen und ultramafischer Ozeankruste eine Nachprüfung der Ca-Bilanz des Ozeans, da diese Karbonate eine bedeutende Senke im marinen Ca-Haushalt darstellen.

Um eine möglichst genaue isotopische Zusammensetzung der Ozeankruste zu erhalten und im Hinblick auf den Mangel an Ca-Isotopendaten für Silikatgesteine, wurden in dieser Studie die Ca-Isotopenzusammensetzung von acht MPI-DING Gläsern und den zugrundeliegenden Gesteinspulvern, als auch von sechs USGS Gesteinsreferenzmaterialien, die U-Serien Isotopenreferenz TML, dem Carrara Marmor (IAEA-CO1) und zusätzlich verschiedene, nicht-zertifizierte Gesteinsproben untersucht. Die Proben wurden nach ihrer geologischen Herkunft und ihrer Bedeutung für den Laborgebrauch ausgewählt. Die Ca-Isotopenverhältnisse wurden mittels Thermionen-Massenspektrometrie (TIMS) nach der $^{43/48}$Ca-Doppel-Spike-Methode mit einer Präzision von etwa 0.2 ‰ (2-fache Standardabweichung) gemessen. Verschiedene chemische Aufbereitungstechniken wurden angewendet, um chemische Artefakte zu erkennen und die statistische Variabilität zu testen. Die verschiedenen Präparationsmethoden ergeben identische Werte innerhalb des analytischen Fehlers und schließen eine Beeinträchtigung der Ergebnisse durch die chemische Aufbereitung aus. Der Vergleich zwischen den geschmolzenen MPI-DING Gläsern mit den ursprünglichen Gesteinspulvern schließt weiterhin eine Kontamination während des Schmelzvorgangs aus. Die individuelle Analyse von verschiedenen Glassfragmenten zeigt, dass die Referenzgläser in Bezug auf Ca-Isotope im mm-Bereich homogen sind. Innerhalb der möglichen analytischen Auflösung kann keine Heterogenität festgestellt werden. Der umfassende Datensatz präsentiert erste Ergebnisse für die Ca-Isotopenzusammensetzung von verschiedenen Referenzmaterialien und stellt eine Grundlage für geochemische und mikroanalytische Arbeiten bereit. Variationen in der Ca-Isotopenzusammensetzung von unterschiedlichen Gesteinstypen, insbesondere zwischen mafischen und ultramafischen Gesteinen, weist auf eine Ca-Isotopenfraktionierung bei Druck- und Temperaturbedingungen des Mantels hin. Im Vergleich zu mafischen Gesteinen sind Ultramafite um bis zu 0.6 ‰ schwerer in ihrer Ca-Isotopie. Im Hinblick auf die überwiegende Bedeutung des ultramafischen Mantels, ist eine Nachprüfung des Bulk Earth-Wertes für Ca Isotope angebracht. Im Allgemeinen, fordert diese Arbeit eine nähere Untersuchung des ozeanischen Ca Budgets mit Hinblick auf die nachgewiesene Variabilität des hydrothermalen Eintrages und der Ozeankrustenzusammensetzung.

Table of Contents

3. Results

4. Discussion

References

Acknowledgements

Appendix

A1 – Description and localization of hydrothermal fluids

A2 – Description and localization of rock samples and mineral precipitates

A3 – Comparison of different digestion procedures

A4 – Comparison of different glass splits

1. INTRODUCTION

The present study was carried out within the framework of the German Special Priority Program SPP 1144 'From Mantle to Ocean: Energy-, Material-, and Life Cycles at Spreading Axes' started in 2003. The aim of this program is to investigate the mid-ocean spreading system at the Atlantic at different scales and as a whole in a multi-disciplinary study. The SPP 1144 comprises various projects consisting of different working groups.
The project 'CARLA: The Role of High- and Low-Temperature Ocean Crust Alteration for the Marine Calcium Budget' was accomplished by the present dissertation and focuses on the marine Ca cycle and the related fluxes between seawater and oceanic crust. Therein, the question of Ca isotope variations associated with hydrothermal processes and its impact on the global marine Ca budget will be addressed.

1.1 Global Calcium cycling

The global cycling of Calcium at the surface of the Earth and its evolution during Earth's history has been subject of a number of studies during the last two decades (e.g. Milliman, 1993; Hardie, 1996; Berner & Berner, 1996; Holland et al., 1996; Wallmann, 2001; Horita et al., 2002; Lowenstein et al., 2003; Berner, 2004; Demicco et al., 2003; Holland, 2005). Calcium is of particular interest because of its interference and close linkage with the global carbon cycle (De La Rocha & DePaolo, 2000; Heuser et al., 2005). Over geological time scales the Calcium balance in the ocean is believed to be directly related to pCO_2 variations in the atmosphere, and it thus may control climate changes (e.g. Demicco et al., 2003; Fantle & DePaolo, 2005). The understanding of the global Calcium cycle has recently received new input from studies of Ca isotopes that raises in turn new challenges.

1.1.1 Ca isotope systematics

Calcium (Ca) is the fifth most abundant element in the Earth's crust and becomes increasingly important for the understanding of biogeochemical processes (DePaolo, 2004). As a major cation in rocks and minerals and an essential constituent in organisms, it is involved in many inorganic and biological processes.
Ca is a white metallic alkaline earth element that occurs in nature never uncombined but mostly as salt, in particular as carbonates and sulfates or is sequestered in silicates. It has the Atomic number of 20 and an atomic weight of 40.08 amu and comprises six stable isotopes over a wide mass range with the following abundances proposed by Russell et al. (1978): 96.98 % ^{40}Ca, 0.642 % ^{42}Ca, 0.133 % ^{43}Ca, 2.056 % ^{44}Ca, 0.003 % ^{46}Ca, and 0.182 % ^{48}Ca.
The Ca isotope compositions may vary due to different effects. Naturally occurring variations of Ca isotopes during geological and biological processes are based either on the generation of ^{40}Ca as radioactive decay product of ^{40}K or on thermodynamically driven mass-dependent fractionation due to the high mass difference of up to 20 % between the Ca isotopes (DePaolo, 2004).

Radiogenic Calcium

^{40}Ca is the primary radiogenic daughter product from β^--decay of ^{40}K with a half-life of 1.25 billion years (Ga). The K-Ca system can therefore be used for geochronology (e.g. Marshall & DePaolo, 1982). The radiogenic enrichment of ^{40}Ca is determined by correcting measured $^{40}Ca/^{44}Ca$ or $^{40}Ca/^{42}Ca$ ratios for machine-induced fractionation using a fixed isotope ratio that is unaffected by radioactive decay (e.g. $^{42}Ca/^{44}Ca = 0.31221$; Russell et al., 1978). The ^{40}Ca excess is reported in the ε notation normalized to a standard material:

$$\varepsilon^{40/44}Ca_{(standard)} = (^{40}Ca/^{44}Ca_{(sample)} / {}^{40}Ca/^{44}Ca_{(standard)} - 1) \times 10^4.$$

Enrichment of radiogenic Ca can only be detected in K-rich samples of an according age that have accumulated enough ^{40}Ca to exceed the analytical resolution of about $\pm 1\varepsilon$ (DePaolo, 2004). For most samples the radiogenic enrichment of ^{40}Ca is negligibly small and can be barely resolved by the analytical methods to date.

Ca isotope analyses – double spike method

Hirt and Epstein (1964) first applied the double spike technique for Ca in order to correct for instrumental mass discrimination from the mass spectrometer. The method was further improved by Russell et al. (1978) providing resolution of isotopic differences at the permill level.

The double spike technique is based on the principals of isotope dilution (e.g. Heumann, 1988) where a well-defined synthetic Ca salt enriched in two naturally less abundant isotopes is added to the sample. Commonly, a combination of ^{43}Ca-^{48}Ca, ^{42}Ca-^{48}Ca but recently also ^{42}Ca-^{43}Ca (Gopalan et al., 2006) is used. The well-homogenized sample-spike mixture is then measured on the mass spectrometer, and the resulting ratios are corrected iteratively for instrumental bias by the known double-spike composition and according to an empirical law, mostly exponentially (e.g. Russell et al., 1978; Heuser et al., 2002). Analyses are carried out either by thermal ionization mass spectrometry (TIMS) (e.g. Heuser et al., 2002) or multicollector ICP-MS (e.g. Halicz et al., 1999). Both methods yield a typical precision of around 0.2 ‰ at the 2σ level.

Matrix-bearing samples require a chemical purification prior to the measurements in order to isolate Ca from interfering elements. Chemical separation of Ca is commonly carried out by cation exchange chromatography. As Ca isotope fractionation was observed during column chromatography (e.g. Heumann & Lieser, 1972; Russell & Papanastassiou, 1978), the samples should be mixed with the spike in prior, if a Ca yield of 100 % can not be assured. Hence, the double-spike correction may not only account for instrumental bias but also for fractionation effects during chemical preparation.

Ca isotope notation and standardization

Stable Ca isotope ratios are commonly expressed as permill deviation from a standard material that is ideally analyzed within the same analytical run:

$$\delta^{44/40}Ca_{(standard)} = (^{44}Ca/^{40}Ca_{(sample)} / {}^{44}Ca/^{40}Ca_{(standard)} - 1) \times 10^3.$$

Attempts have been made to find an agreement for a common internationally accepted and certified reference material or standard for Ca isotopes in order to facilitate inter-laboratory comparisons. Hence, Hippler et al. (2003) and the International Union of Pure and Applied Chemistry (IUPAC) proposed to refer on the Ca carbonate standard NIST SRM 915a provided by the National Institute of Standards and Technology, USA. However, the availability of NIST SRM 915a was recently exhausted, and it is now replaced by SRM 915b that has to be manifested yet for the use in Ca isotope analytics. Many authors refer rather to seawater (Zhu & Macdougall, 1997; Schmitt et al., 2003a/b; Hensley, 2006). As the residence time of Ca of around 1 million years (Ma) exceeds the oceans mixing time (~10^3 a) (Broecker & Peng, 1982), the isotopic compositon of modern seawater is well-homogenized. The $\delta^{44/40}$Ca of the SRM 915a relative to modern seawater has been confined to a $\delta^{44/40}$Ca of -1.88 ± 0.04 ‰ (Hippler et al., 2003). With respect to potential variations in the Ca isotope composition of seawater during Earth history and its small content of radiogenic Ca, Skulan et al. (1997) suggested the value for Bulk Earth to be the more appropriate reference. The Bulk Earth value have been taken over from Russell et al. (1978), who defined for the Ca isotope composition of Bulk Earth the Ca isotope value of a natural CaF_2 being close to the average Ca isotope composition of various igneous rocks. Hence, a $\delta^{44/40}$Ca of about -1 ‰ relative to seawater ($\delta^{44/40}Ca_{(SW)}$) was assumed for the Ca isotope composition of Bulk Earth. Several authors (Skulan et al., 1997; DePaolo, 2004; Fantle & DePaolo, 2005) followed this suggestion and adjusted an ultrapure $CaCO_3$ salt to this value. Recently, this standard material is only used as an intralaboratory delta-zero reference and quality-control material. However, the use of delta-zero materials with natural compositions in contrast to synthetically composed reference standards is advantageous due to matrix effects that lacks in standards not mimicking natural concentration pattern.

Mass-dependent Ca isotope fractionation

Mass-dependent Ca isotope fractionation was remained undetected for a long time due to analytical limitations. Recent advances in the analytical techniques of Ca isotope investigations have greatly improved the precision and instrumental efficiency (e.g. Russell et al. 1978; Halicz et al., 1999; Heuser et al., 2002; Fietzke et al., 2004) and allow now to examine isotopic variations of Ca in more detail. Ca isotope fractionation occurs during diffusion, evaporation, dissociation reactions and biological-mediated processes.

The first Ca isotope fractionation effects were observed on extraterrestrial materials. Large Ca isotope variations were found in Ca-Al-rich inclusions (CAI) and Ca-rich aggregates (CA) in meteorites and were attributed to a loss of lighter Ca isotopes into the near-vacuum during evaporation (e.g. Lee et al., 1978; Niederer & Papanastassiou, 1984). Terrestrial materials are commonly less strongly fractionated in their Ca isotope compositions. Currently, a natural fractionation of up to 6 ‰ is known (Skulan & DePaolo, 1999). Present studies consistently show a preferential incorporation of ^{40}Ca in the mineral phase for Ca mineral precipitation from aqueous solutions (Gussone et al., 2003; Schmitt et al., 2003a/b; Hensley & Macdougall, 2003; Marriott et al., 2004; Lemarchand et al., 2004). In addition, Ca isotopes are subject to biological fractionation most likely causing a successive lightening of Ca isotope compositions along the trophical levels through the food chain. Ca isotope variations in minerals, in particular in $CaCO_3$ that is the major constituent of calcerous organisms and sedimentary deposits result from biogeochemical processes and may record physico-chemical conditions at the time of their formation.

For instance, the recently observed temperature-dependency of Ca isotope fractionation in foraminifera (e.g. Nägler, 2000; Gussone et al., 2003, 2005) may be used for paleothermometry. An additional application of Ca isotope variations deals with the investigation of global Ca fluxes. This is of particular importance as the Ca balance in the ocean is believed to be directly related to pCO_2 variations in the atmosphere, thus potentially controlling climate changes (e.g. Demicco et al., 2003; Fantle & DePaolo, 2005).

In order to utilize Ca isotope variations as a biogeochemical tool for understanding and reconstructing recent and ancient processes, the underlying physico-chemical mechanisms have to be constrained. A number of studies were carried out in order to deduce the theoretical principles of Ca isotope fractionation (e.g. Richter et al., 2003; Gussone et al., 2003; Lemarchand et al., 2004). Ca isotope fractionation may be the result of the two mechanisms, equilibrium and/or kinetic fractionation. Equilibrium isotope fractionation is based in principle on differences in the zero-point energy of chemical compounds of different isotopic compositions (Urey, 1947). Because the energy levels are mass-dependent, isotopes are discriminated in a chemical compound according to the bond strength, in that chemical species with stronger bonds preferentially incorporate the heavier isotopes. As a consequence, the isotope signature is a result of the abundances of chemical substances, and isotopic variations occur due to net changes in the chemical composition. As the distribution of isotopes in coexisting phases reflect differences in chemical activity, equilibrium isotope fractionation decreases with increasing temperatures (Richter et al., 2003).

While there is no net chemical reaction in equilibrium fractionation, kinetic effects are related to chemical and diffusional exchange reactions (O'Neill et al., 1969). Thereby, chemical and physical kinetic fractionations are distinguished (Richter et al., 2003). Chemical kinetic fractionation occurs during unidirectional processes, when reaction rates differ between different isotopes (Richter et al., 2003). Chemical isotope fractionation dictates an enrichment of the lighter isotopes in the reaction product as isotopically lighter educts react more readily due the higher ground-state vibration frequency of the lighter isotope (Zhu, 1999). This mechanism is often associated with biologically induced fractionation effects. Physical kinetic fractionation, on the other hand, accounts for mass transport processes within one phase (diffusion) or between two phases (evaporation). Isotopes are separated due to their relative mobilities expressed as self-diffusion coefficient that is mass-dependent, but notably not temperature-dependent. Therefore, physical kinetic isotope fractionation may serve as an underlying mechanism for fractionation processes at high temperatures, where equilibrium fractionation becomes negligibly small (Richter et al., 2003).

Ca isotope variations during high-temperature processes

In recent studies, significant isotope variations are focused rather during biogeochemical cycles, whereas fractionation effects at high temperatures exceeding 100 °C or even during petrogenetic magma evolution and melt segregation are barely considered. This is because equilibrium fractionation as assumed for mineral precipitation becomes negligible at high temperatures and in addition, the few data currently existing for different rock types suggest no or only small variations (Skulan et al., 1997; DePaolo, 2004).

However, Hensley (2006) reported very low values for the Ca isotope compositions of hydrothermal anhydrites with the Ca isotopes being most likely fractionated from the parental solution, seawater and/or hydrothermal fluid.

Hydrothermal anhydrites are commonly formed at temperatures above 150 °C. Furthermore, a significant Ca isotope fractionation between two different silicate melts was unequivocally demonstrated by experimental studies (Richter et al., 2003). Richter et al. (2003) detected an isotopic difference of up to 7 ‰ at a temperature of 1450 °C along a concentration gradient in a diffusion couple consisting of a rhyolitic (0.5 % CaO) and a basaltic melt (10.38 % CaO). Thereby, the lighter isotopes of Ca diffuse faster than the heavier, and the rhyolite beomes subsequently lighter, while the heavier isotopes are enriched in the basaltic melt. A closer consideration of the deduced diffusivities indicates that the diffusing species are much larger than the intrinsic masses of the individual Ca isotopes, potentially comprising the mass of the anorthite formula ($CaAl_2Si_2O_8$) (DePaolo, 2004). With respect to the experiments of Richter et al. (2003) and the findings for other stable isotope systems, especially for Mg that can be considered to be a chemical analog for Ca, there is potential for Ca isotope fractionation at magmatic temperatures. However, a direct proof in natural systems by a systematic investigation of various rock types is still lacking.

1.1.2 The oceanic Ca budget

The oceanic Ca budget has been subject to a number of studies (e.g. Hart, 1973; Thompson, 1983; Berner & Berner, 1987; Zhu & Macdougall, 1998; Berner & Berner, 2004) due to the high Ca content in the ocean and its importance in the global CO_2 cycle. Ca is the fifth most abundant constituent of ocean water (~10 mM or ~400 ppm) and moreover a major cation in seawater. Spatial and temporal variations in the Ca inventory of the ocean reflect variability in the relative contributions of Ca to the ocean, mainly from continental weathering and ocean floor hydrothermal fluxes (e.g. Zhu & Macdougall, 1998; DePaolo, 2004).

Oceanic Ca fluxes

Continental run-off, oceanic weathering, mid-ocean ridge hydrothermal activity, and carbonate sedimentation have been recognized to be the major factors controlling the marine Ca cycle (Fig. 1.1). Continental weathering and riverine influx, submarine magmatism and associated hydrothermal activity and seafloor weathering, and in addition a diagenetic flux due to cation exchange processes are considered to be the major sources for the marine Ca budget (Berner & Berner, 1996). The supplied Ca freight is in turn removed from the ocean by the deposition of carbonates and evaporites as primary modern sink for marine Ca (Fig. 1.1). 70 % of the ocean's inventory of Ca of $1450*10^{16}$ mol stems from the rivers, wherein Ca is the major cation essentially derived from rock weathering, in particular sedimentary carbonates and silicates. This is complemented by the input from hydrothermal processes and seafloor weathering of up to 20 % (Berner & Berner, 1996) during which Ca is released from the oceanic crust by water-rock reactions ranging from high-temperature hydrothermal processes to low-temperature ocean crust alteration (Berner & Berner, 1996).

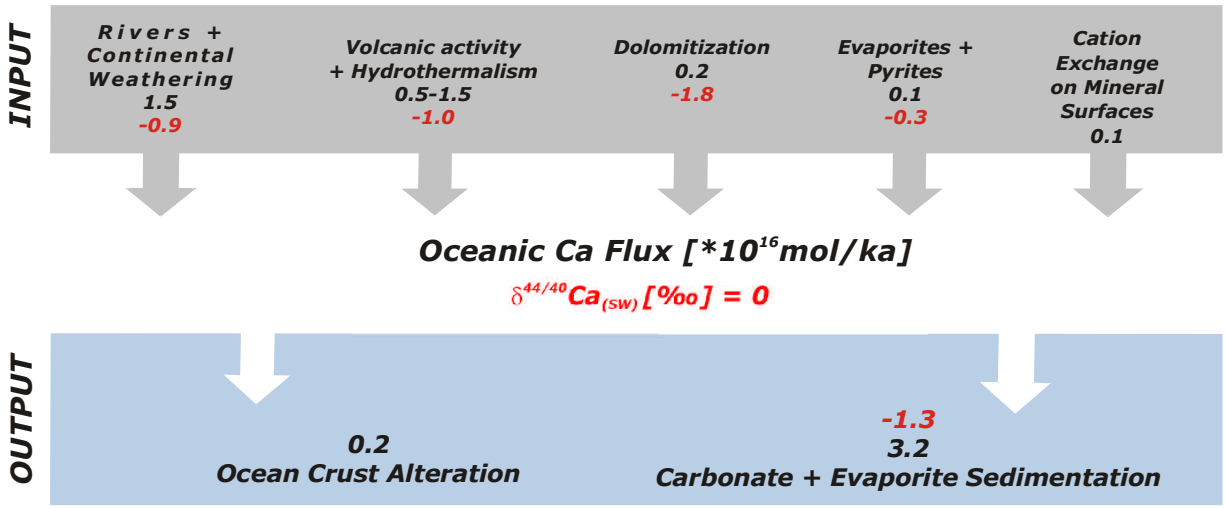

Fig. 1.1, Model currently assumed for the modern oceanic Ca budget with flux rates (dark numbers) and the known isotopic compositions relative to seawater (red numbers). The total oceanic Ca inventory comprises $1450*10^{16}$ mol/ka. Data compiled from Milliman, 1993; Berner & Berner, 1996; Alt & Teagle, 1999; Wallmann, 2001; Schmitt et al., 2003a; Gussone et al., 2003; Berner, 2004; DePaolo, 2004; Böhm et al., 2006).

Geochemical budgets of Ca have been investigated by means of the isotopic compositions of oceanic Ca and its major input and output fluxes (Fig. 1.1) (e.g. Zhu & Macdougall, 1998; De La Rocha & DePaolo, 2000; Schmitt et al., 2003a; Chang et al., 2004; Schmitt & Stille, 2005; Böhm et al., 2006). The riverine input has been determined by the weighted average of eight world rivers to a Ca isotope composition of -1.1 ‰ relative to modern seawater ($\delta^{44/40}Ca_{(SW)}$) (Schmidt et al. 2003a). This is close to a $\delta^{44/40}Ca_{(SW)}$ for the hydrothermal input of around -0.95 ‰ (Schmitt et al., 2003a). Both match the currently assumed value for oceanic crust (Skulan et al., 1997; Zhu & Macdougall, 1998; DePaolo, 2004) and Bulk Earth (Russell et al., 1978; Skulan et al., 1997). Disregarding the considerably wide range displayed by the riverine Ca isotope flux (-1.7 to -0.6 ‰) as well as by the hydrothermal input (-0.8 to -1.1 ‰), the overall Ca isotope input approximates the output by carbonate sedimentation of presumably -1.3 ‰ relative to seawater (De La Rocha & DePaolo, 2000) and implies that for Ca the modern ocean is isotopically close to steady state, that is the input is compensated by the output flux.

The steady state question

Several authors suggested that the total Ca input into the ocean is not balanced by the deposition of carbonates, but exceeded by the latter due to high sedimentation rates (e.g. Milliman, 1993; Berner & Berner, 1996; Milliman & Droxler, 1996). These and further studies showed that most likely the ocean is currently not at steady state with respect to Ca and that the Ca concentration of the oceans have varied significantly during the Phanerozoic (Hardie, 1996; Stanley & Hardie, 1998; Horita et al., 2002). Likewise, the Ca isotopic composition of the ocean is supposed to have changed up to 0.5 ‰ throughout geologic time scales (e.g. De La Rocha & DePaolo, 2000; Fantle & DePaolo, 2005; Heuser et al., 2005; Farkaš et al., 2007). In particular, Fantle & DePaolo (2005) demonstrated a significant imbalance in the current Ca isotope budget of the oceans. They reported an average Ca isotope composition of around -1.45 ‰ relative to modern seawater for marine bulk carbonate sediments formed over the last 20 Ma.

In case of steady state or close to steady state and with regard to the integration over such a long time period, this value represents the significant oceanic Ca sink and should resemble the average Ca isotopic influx to the ocean of around -1 ‰. The significant deviation points to a major gap in the current oceanic Ca budget.

Assuming that isotopic variabilities result rather from intrinsic changes in the Ca isotope compositions than being implied by net changes of the individual fluxes as has been proposed by Schmitt et al. (2003b), there are currently several explanations under debate to resolve this question. Ca isotope variations may be evoked either by imbalances between continental Ca input and carbonate sedimentation in the oceans due to variations of continental weathering fluxes (e.g. De La Rocha & DePaolo, 2000; Fantle & DePaolo, 2005), or by the existence of a large reservoir of isotopically fractionated Ca in continental deposits (Tipper et al., 2006), or as proposed by Heuser et al. (2005) and later adapted by Farkaš et al. (2007) the ocean's inventory of Ca varies due to the formation of dolomite from carbonate generating a Ca flux without an associated CO_3^{2-} flux (e.g. Berner, 2004; Holland & Zimmermann, 2000). In addition, output fluxes by the deposition of evaporites, recently determined to fractionate Ca isotopes (Böhm, pers. comm.) is less constrained. However, all three hypotheses are burdened with inconsistencies and uncertainties and even taken together do not result in a sufficiently high isotopic difference resolving the problem. An alternative explanation is recently suggested by Böhm et al. (2007), who assumes that the formation of carbonates during low-temperature alteration of the oceanic crust is presently not considered adequately in the Ca isotope budget and may provide 'the missing link'.

Low-temperature alteration carbonates

A number of studies indicated that Ca-bearing mineral phases such as aragonite, calcite, anhydrite and subordinately hydrous Ca-silicates (e.g. prehnite, zeolites), are formed during different stages of ocean crust alteration (e.g. Staudigel et al., 1981). At temperatures below 100 °C $CaCO_3$ is formed in vesicles and veins within the oceanic crust as a result of seafloor weathering. These low-temperature alteration carbonates are common to crustal depths of at least 500 m (Alt & Teagle, 1999, Alt et al., 2003) and have been recognized to play an important role in the global carbon cycle (Caldeira, 1995). During their formation as a late-stage product by circulation of cold, oxygenated seawater through the oceanic crust (e.g. Bonatti et al., 1980; Rosner et al., 2006), they represent about 10 % of the oceanic Ca sink (Alt & Teagle, 1999; Berner & Berner, 1996; Milliman, 1993), thereby consisting of about 70 % of seawater-Ca. The remaining 30 % Ca stems from the host-rocks.

Little is known about the isotopic compositions of these carbonates, although they may play a key role in the Ca isotope budget of the ocean. Small or even no Ca isotope fractionation in these carbonates would lead to an increase of the total Ca isotope output flux from the ocean and lower the imbalance between input and output flux as discussed above. Model calculations show that zero fractionation would shift the oceanic output of Ca about 0.2 ‰ towards higher values. In concert with the effect of dolomitization this offset is sufficiently high to fully explain the isotopic difference between output and input fluxes as reported by Fantle & DePaolo (2005). If, on the other hand, the low-temperature alteration carbonates are rather strongly fractionationated, the effect on the output-$\delta^{44/40}$Ca must be related to other effects, such as evaporite deposition. In summary, depending on the Ca isotopic composition of the low-temperature alteration carbonates, seafloor weathering may have a significant impact on the Ca isotope budget of the ocean and require further investigation (Böhm et al., 2007).

1.1.3 The Ca hydrothermal flux

Hydrothermal Ca fluxes from mid-ocean ridges are one of the key controls for the the marine Ca mass balance. Submarine volcanism has been recognized to be beside continental influx a major source for the ocean's inventory of Ca. The oceanic Ca flux occurs due to the release of Ca from the substratum to the circulating seawater during water-rock reactions (e.g. Hart, 1973; Thompson, 1983; Berner & Berner, 1987; Zhu & Macdougall, 1998; Berner & Berner, 1996). Additionally, Ca is removed from the ocean by the formation of Ca-bearing minerals, such as Ca carbonate polymorphs (calcite and aragonite), anhydrite, and Ca-silicates. Commonly, the Ca supply to the ocean by hydrothermal venting is assumed to be homogeneous and constant through time displaying a Ca isotope signature of an average ocean crust (Skulan et al., 1997; Zhu & Macdougall, 1998; Schmitt et al., 2003a; Fantle & DePaolo, 2005). However, the extent of the chemical and isotopic exchange of Ca between seawater and oceanic crust during hydrothermal circulation is still poorly constrained.

So far only Schmitt et al. (2003a) attempted a closer examination of Ca exchange processes in axial hydrothermal systems by analyzing hydrothermal vent fluids for their Ca isotopic compositions. They report values between -0.78 ‰ and -1.11 ‰ for the Ca isotope ratios in hydrothermal fluids from different vent fields at the Mid-Atlantic Ridge (MAR) and the East Pacific Rise (EPR). The investigated hydrothermal fields differ significantly in their physico-chemical conditions such as temperature, pressure, water-to-rock ratio, the nature of the substratum, magmatic activity, tectonic setting etc.. The EPR is a fast-spreading ridge with a hydrothermal system at shallow depths (Von Damm et al., 1997). Fluid samples derived from this vent are amongst the hottest and are supposed to have suffered under phase separation. Additionally, the basement of the hydrothermal system at EPR is basaltic. Whereas the vent site at the MAR, the Rainbow Field (Douville et al., 2002) is ultramafic-hosted. Although the analytical uncertainties given by Schmitt et al. (2003a) do still not allow defining significant differences between the different vent fields, the relatively wide range of up to 0.3 ‰ displayed by the Ca isotope ratios in the hydrothermal fluids may imply a variability of the Ca content and isotopic compositions due to the above-mentioned parameters.

In summary, the few existing data indicate that the hydrothermal pathway of Ca is much more complex than previously assumed and may not just simply represent a compositional equilibration between seawater and the oceanic crust. In contrast, spatial and temporal variations of hydrothermal Ca influx probably cause an imbalance in the oceanic Ca budget and challenge existing models on the global Ca budgets.

Hydrothermal anhydrite

There is strong evidence for a Ca isotope fractionation of up to 1 ‰ during the precipitation of anhydrites ($CaSO_4$) from hydrothermal fluids (Hensley, 2006) with the lighter isotope sequestered in the anhydrite. Anhydrite is an abundant component in hydrothermal systems and a strong Ca isotope fractionation in hydrothermal anhydrites may significantly influence the hydrothermal Ca flux by two means. Commonly, anhydrite is considered to be quickly and almost quantitatively removed by off-ridge dissolution and thus supplied back to the ocean (Berner & Berner, 1996).

On the other hand, it has been recently suggested (Alt et al., 2003) that anhydrite may be preserved in deeper parts of the oceanic crust at higher temperatures above 100 °C. A preservation of significant amounts of anhydrites within the ocean's crust would represent an important sink for light Ca isotopes, strongly influencing the Ca isotopic compositions of their parental solutions that are issued as hydrothermal fluids into the ocean. However, a systematic investigation of anhydrites in greater depths of the oceanic crust, especially of their Ca isotopic composition, is still lacking.

1.2 Hydrothermal activity

1.2.1 Hydrothermal processes

Hydrothermal activity was first discovered in 1977 at the Galapagos spreading centers and has now proven to be quite abundant with more than 40 locations on the world ridge-crest system (Fig. 1.2) (Von Damm, 1990). The occurrence of the hydrothermal vent fields differ widely. They are found at distinct settings, from ultrafast-spreading (East Pacific Rise, EPR) to slow-spreading (Mid-Atlantic Ridge, MAR) centers, supplying fluids of various chemical compositions and temperatures, from ambient seafloor temperatures of ~2 °C to hot fluids of > 400 °C.

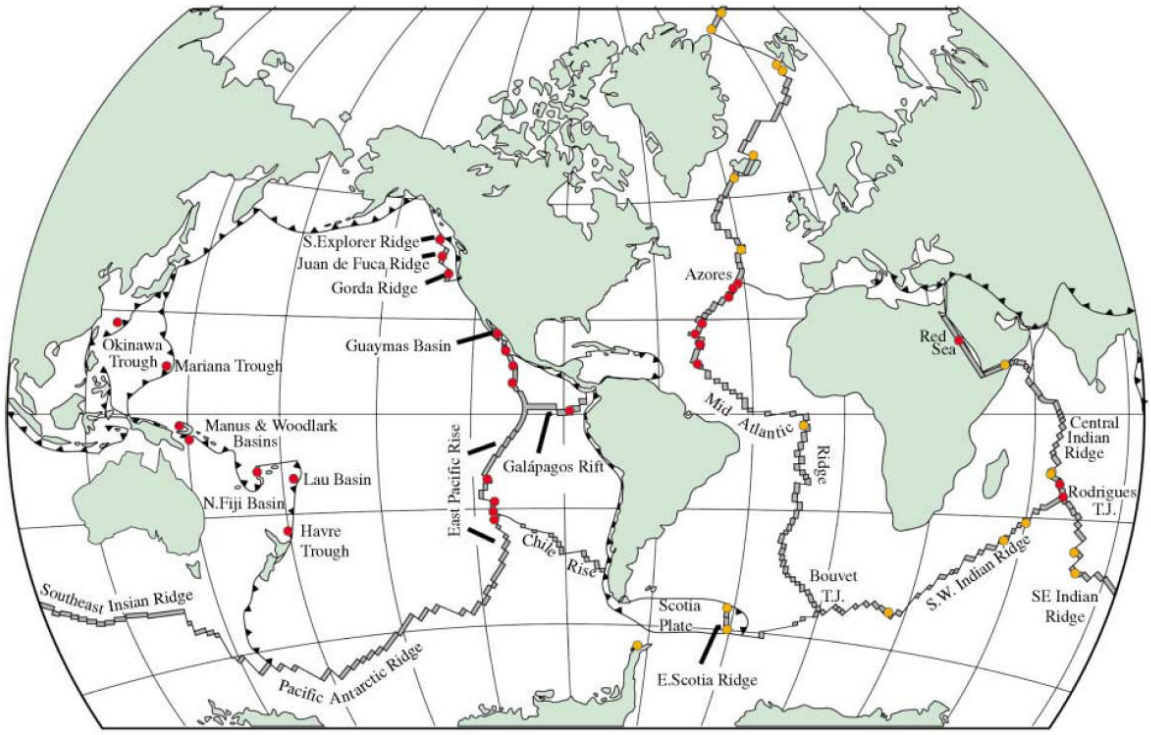

Fig. 1.2, Schematic world map with locations of directly observed (red circles) or anticipated by chemical anomalies in the superjacent water-column (orange circles) active hydrothermal vents along the global ridge crest. From ‚Treatise on Geochemistry' (2005).

The flux of water through oceanic crust during hydrothermal convection was estimated to equal the total seawater volume within 1 Ma (Hannigton et al., 2001). Hydrothermal circulation provides energy and material transfer between the oceanic crust and seawater and controls the chemical composition of past and present seawater (e.g. Elderfield and Schulz, 1996; Hardie, 1996). The chemical compositions of the hydrothermal effluents into the ocean result from the interaction of seawater and the oceanic crust. Water-rock interactions during convective circulation in hydrothermal systems lead to either an addition or removal of chemical species of the penetrating seawater as well of the entrained oceanic crust and thus affect oceanic mass balances over space and time (Berner & Berner, 1996).

During convective circulation pristine seawater is penetrating the oceanic crust and underlies at exceptional temperature and pressure conditions a succesive chemical modification towards a hydrothermal fluid composition, which is subsequently mixed up by ambient seawater before exciting on the seafloor (Fig. 1.3). The composition of this pure fluid that is inaccessible for direct sampling has to be deduced by retracting the mixing proportions of seawater. Experimental studies on seawater-basalt interaction at hydrothermal conditions (e.g. Bischoff & Dickson, 1975; Seyfried & Bischoff, 1979) show that Magnesium (Mg) is almost quantitatively removed from the solution forming Mg-OH silicates at temperatures above 150 ° C and is balanced mainly by protons (H^+) and the rock inventory of Ca (Ca^{2+}). Hence, the intrinsic chemical composition of the hydrothermal fluid endmember is calculated by the extrapolation to a fluid with zero Mg concentration. This method has proven to be the best approximation for correcting seawater entrainment during the sampling of high-temperature hydrothermal solutions (Elderfield & Schultz, 1996) and provides the opportunity to compare different vent fluids.

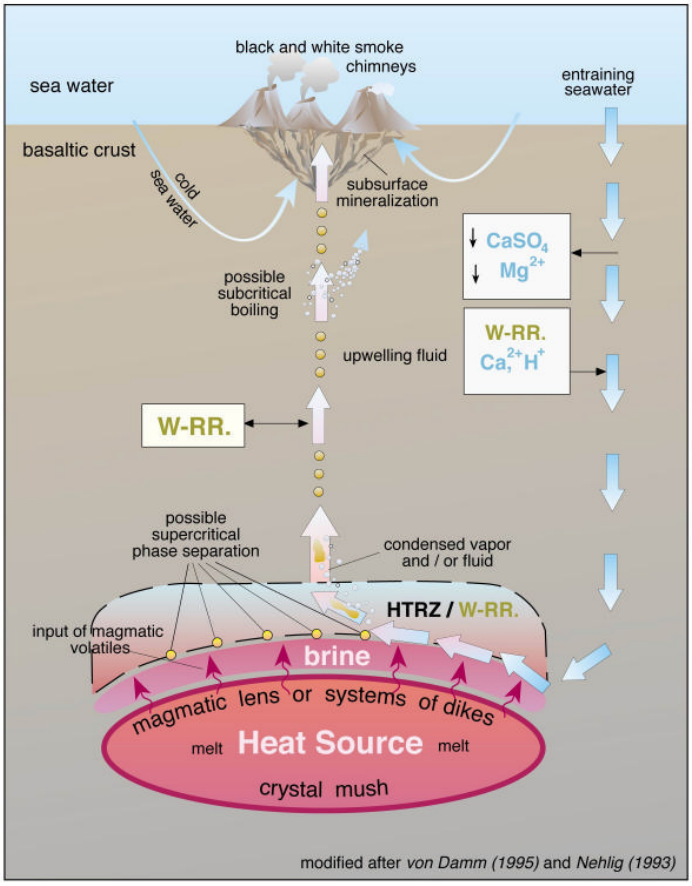

Fig. 1.3, Model of submarine hydrothermal circulation with recharge, reaction and discharge zone. The recharge zone is characterized by anhydrite precipitation. 'W-RR.' refers to water-rock reaction, mainly exchange processes of Mg^{2+} for Ca^{2+} and/or H^+. 'HTRZ' ro high-temperature reaction zone, where sub- or supercritical phase separation may occur leading to a separation of the hydrothermal fluid into a brine and a vapor phase. The heat source is provided either by a magmatic lens or by a recently intruded dike complex. In the subsurface hydrothermal fluid is admixed with ambient seawater resulting in hydrothermal mineralization. From Kuhn (pers. comm.).

Compositional varibilities during hydrothermal circulation is strongly influenced by physico-chemical conditions such as temperature, depth and bedrock composition of the hydrothermal system. Three stages are distinguished within a hydrothermal convection cell (Fig. 1.3). Downward entrainment of seawater occurs in the broad and diffuse *‚recharge zone'*, where seawater experiences first compositional changes at increasing temperatures and pressures. During progressive heating in this downflow zone most of the seawater-sulfate (SO_4^{2-}) is removed as anhydrite precipitates at temperatures > 140 °C. SO_4^{2-} is balanced by additional Ca^{2+} leached from the bedrock as a result of water-rock reaction. In addition, further major and trace metal cations, e.g. of Si, Fe and Mn are leached from the host-rock. Due to the generation of H^+ the pH is continuosly lowered, thereby titrating seawater-alkalinity. Water-rock interaction proceeds more quickly in the *'reaction zone'* that is the hottest and mostly deepest part of the hydrothermal cell. The downflowing fluid approaches the heat source, either a magma lens or a recently intruded dike. Depending on the temperature and pressure conditions phase separation and/or a direct input of magmatic gases, in particular He and CO_2 may occur. The buoyant fluids rise finally within the *'discharge zone'* to the seafloor and are admixed by ambient seawater in the subsurface. The contact between the hot and mostly reducing and acidic fluids with cold oxygenated seawater leads to the precipitation of hydrothermal minerals such as anhydrite, sulfides, Fe-Mn oxyhydroxide and also carbonates. Extensive reactions between hot fluid and seawater lead to the formation of fine-grained particles venting as black or white smoke and to massive deposits of hydrothermal precipitates especially of anhydrite and sulfides forming imposing chimney structures. Many chimneys are surrounded by diffuse venting hydrothermal fluids presumably cooled subsurface below 35 °C. Diffuse flows are sufficiently cooled down to be discharged of much of the metal sulfide load and hence do not smoke. Due to density gradients diffuse effluents are identified as 'shimmering water' and provide often habitats for diverse biological populations such as mussel fields.

Effects of phase separation on the hydrothermal fluid composition

Phase separation is accepted to be a major process forming hydrothermal fluids (Von Damm et al., 2003). Crossing the critical point at ~407 °C and ~298 bar, seawater is separated in two phases (Fig. 1.4), a vapor-like phase, enriched in volatile, gaseous species, and in a high-salinity liquid phase (brine). Thereby, large variations of > 10 % in the chloride (Cl^-) content of the circulating seawater are induced (Bischoff & Rosenbauer, 1985). Hydrothermal fluids commonly pass through this two-phase condition in their subseafloor reaction path, where they are separated into a low-chlorinity vapor phase and high-chlorinity liquid or brine phase (Von Damm et al., 1997). The separation into two phases occurs in terms of subcritical and supercritical phase separation (Fig. 1.4). Subcritical phase separation occuring as boiling is referred to the fluid that crosses the vapor/liquid phase boundary below the critical point of seawater, i.e. at lower pressure (p) and/or temperature (T). This leads to the generation of a low-chlorinity vapor of variable amounts within a large amount of a high-chlorinity brine that is enriched in salts and metals and depleted in volatile species such as the gaseous species CO_2, H_2S and H_2. The farther away from the critical point the more vapor fraction being continuously enriched in Cl^- is produced. Supercritical phase separation occurs when a fluid crosses the phase boundary above the seawater-critical point (higher p-T). In this case two fluid phases appear with their compositions depending on the p-T conditions.

Generally, one of the phases shows a higher density and salinity and condenses to small brine droplets within the second, low-salinity liquid representing rather a continuous 'vapor' phase. Both phases become increasingly similar when the critical point is approached (Von Damm et al., 1997).

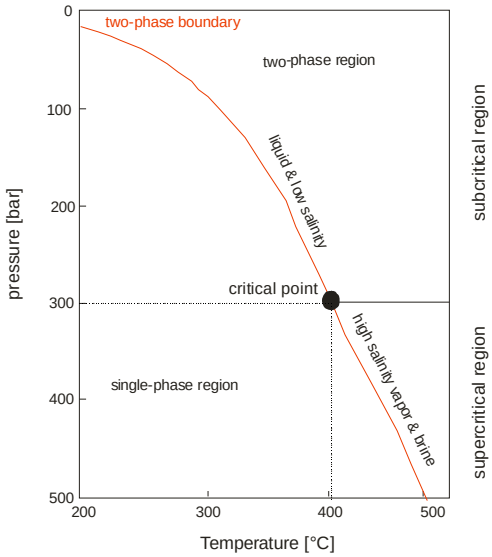

Fig. 1.4, Two-phase curve for 3.2 ‰ NaCl solution representing standard seawater as a function of temperature and pressure. After Bischoff & Rosenbauer (1984).

The two phases undergo phase segregation prior to exciting onto the seafloor (Von Damm et al., 1997). The vapor jets out rapidly, while the brine settles lower in the structure due to its higher density resulting in a longer residence time of the brine in the oceanic crust relative to the corresponding vapor (Von Damm et al., 1997). It is expected that element discrimination and isotope fractionation increases during phase separation as a function of the high-density contrast between the two phases away from the critical point (Bonifacie et al., 2005). Hence, a fractionation between LREE and HREE by a factor of 3 has been reported during phase separation (Shmulovich et al., 2002; Humphris & Bach, 2005). The LREE/HREE ratio is lower in the vapor compared to the brine solution.

Phase separation results in a significant deviation in the Cl^- content of the two phases. Cl^- enrichment or depletion influences the chemical behaviour of other elements and is generally the result of a combination of authigenic mineralization and phase separation related processes like complexation and vaporisation of volatiles. In some cases, an excessive enrichment of Cl^- may lead to the precipitation of chloride salts such as halite (Butterfield et al., 1997). Commonly, Cl^- determines the bulk transport properties of the fluid through charge balance and complexation. As the fluids are acidic and sulfate is removed, Cl^- is the major anion, and at elevated pressures and temperatures most of the cations, in particular the divalent ones will be transported as chloro-complexes (Edmonds & Edmond, 1995). As a result of chloro-complexation most cations are conservative with respect to Cl^- and show a linear positive relation to Cl^- in phase-separated hydrothermal fluids (Edmonds & Edmond, 1995), if phase separation is the only process.

Chloro-complexation shifts the equilibrium between a secondary mineral phase containing Ca and Sr (like epidote) and a fluid phase towards larger concentrations in the solution as metal stability in solution can be greatly enhanced by aqueous metal-ligand complex formation. Commonly, the type of complexation is determined by the concentration of ligands in the fluids, temperature, redox state, pH and ionic strength. Potential fractionation effects become increasingly important at higher temperature as the strength of the metal ligands complexes increase (Metz & Trefry, 2000). Temperature and salinity are the key factors controlling the solubility and distribution of trace metals in hydrothermal systems (Metz & Trefry, 2000). Generally, there is a strong functional dependence between the solubility and temperature and total chloride concentration as the stability of complexes increase with increasing temperature (Douville et al., 1999). An exception is boron being unique in its behaviour as it is not chloro-complexed and at least in basaltic-hosted systems its concentration seems not to be solubility-controlled (Von Damm et al., 2003).

1.2.2 The Logatchev hydrothermal field (LHF)

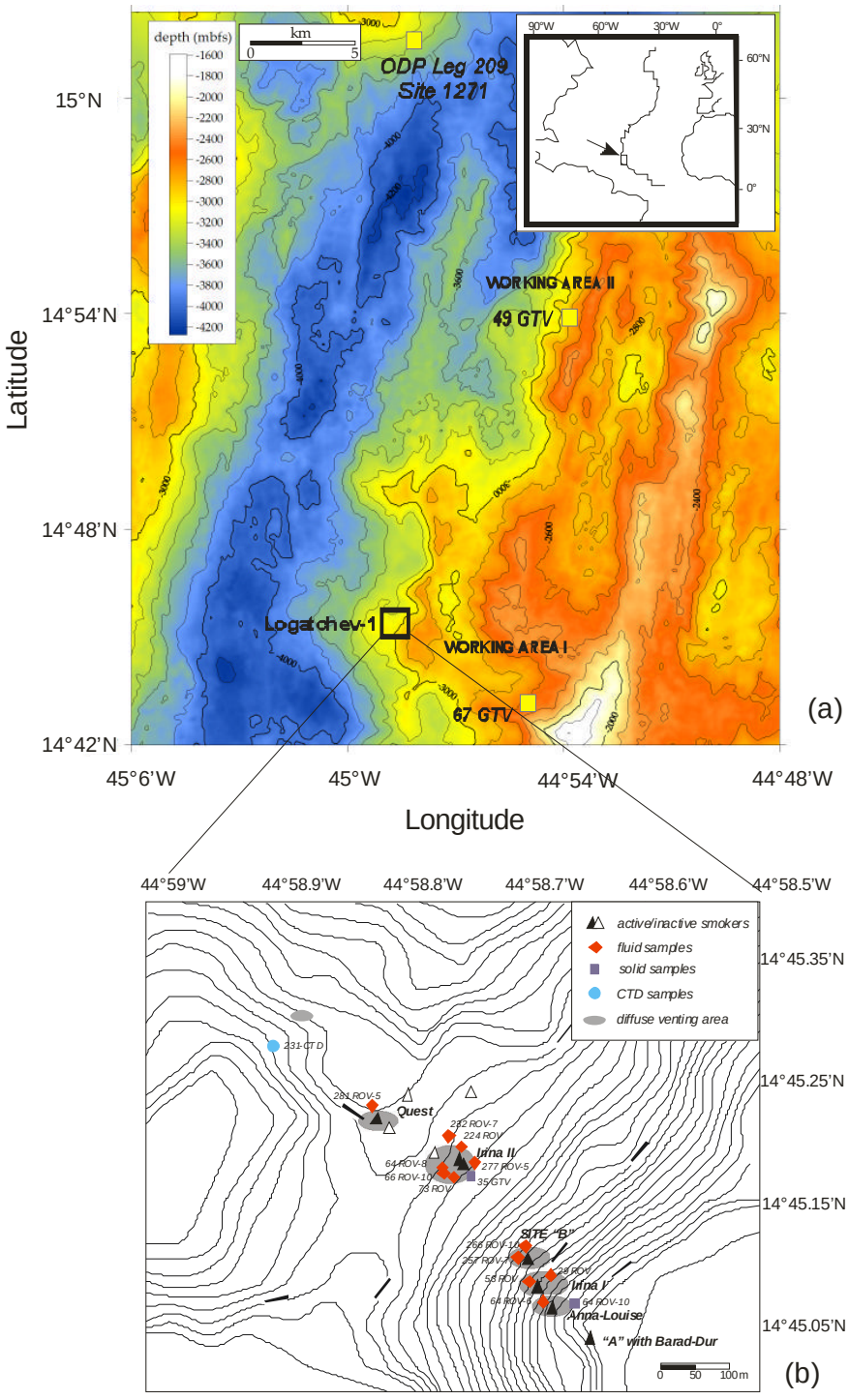

Fig. 1.5, (a) Location of the Logatchev hydrothermal field at the Mid-Atlantic Ridge (MAR) and the working areas sampled in this study; **(b)** Detailed map of the active LHF-1. From Augustin (pers. comm.).

The Logatchev hydrothermal field (LHF) is located at the slow-spreading Mid-Atlantic Ridge (MAR) at 14°45'N/44°59'W about 50 km south of the transform fault at 15°20'N (Fig. 1.5a). Hydrothermal activity occurs in a water depth of ~3000 m on a small plateau within the rift valley. This area is characterized by large tectonic extension with scarce volcanic activity (Escartin and Cannat, 1999; Fujiwara et al., 2003). The basement at the Logatchev field comprises serpentinized peridotites, coarse-grained magmatic cumulates and subordinate basaltic and gabbroic fragments (~20 %) (Kuhn et al., 2004; Lackschewitz et al., 2005). Talus of ultramafic and mafic rocks is covered by sediments of locally up to 1 m thickness (Kuhn et al., 2004). These sediments are often capped by a silicified hydrothermal crust. Low-temperature precipitates such as Fe-Mn oxides as well as massive sulfide structures are developed throughout the Logatchev field (Kuhn et al., 2004; Lackschewitz et al., 2005). The Logatchev field provides a tectonically controlled, ultramafic-hosted hydrothermal system with constant fluid supply and chemistry. Preliminary age dating suggests that hydrothermal activity has been occurring for at least 10^5 a indicating a long-lived, stable system.

Four fields, known as Logatchev-1 and –4 are described with Logatchev-1 being active while the remainders are only indicated by sulfide structures and dead mussel fields. The active Logatchev-1 field (LHF-1) has been subject to intensive investigations during SPP 1144 (Fig. 1.5a). Its central part consists of two main regions of high hydrothermal activity comprising two larger vent areas, a complex comprising the four vent sites ANNA-LOUISE, IRINA, SITE 'B', and the newly discovered site QUEST and the large mound of IRINA II with black smoker chimneys on top.

SITE 'A' consists of a single black smoker, 5 m high, on top of a sulfide talus mound. The other four sites Quest, SITE 'B', IRINA and ANNA-LOUISE are so-called 'smoking craters' consisting of a talus mound with a crater rim and a central depression. In these environments of vigorous fluid venting, mussel beds were absent. In contrast, the four chimneys of IRINA II are densely overgrown with mussels, where diffuse fluid venting occurs. A maximum temperature of 353° C has been reported for the Logatchev field (Douville et al., 2002). Both, low- and high-temperature fluids resemble in their chemical compositions indicating a single fluid source. The Logatchev hydrothermal field has shown a rather constant fluid composition for about the last 10 a (e.g. Douville et al., 1999; Schmidt et al., in press) suggesting rather a mature, non-boiling system.

1.2.3 Hydrothermal activity at the 'Ascension area' (4 – 11°S)

Hydrothermal activity along the southern Mid-Atlantic Ridge (MAR) was reported as recently as by the discovery of hydrothermal vent system in the 'Ascension Area' (Fig. 1.6) between 4 and 11°S (German et al., 2005; Haase et al., 2005). As yet, two hydrothermal vent fields at 5°S and around 9°S (Lilliput) have been directly observed, but strong plume signals indicate further vent sites around 8°S (Nibelungen) (Devey et al., 2005).

The hydrothermal system at 5°S situated in the neovolcanic zone of the Mid-Atlantic Ridge (MAR 5°S) consists of the three active vent fields Turtle Pits, Wideawake and Red Lion. The Turtle Pits field is centered at 4°48.58'S/12°22.42'W in a water depth of 2990 m within a small depression on a flank of a volcanic edifice.

This young post-eruptive, basaltic-hosted vent field consists of two mound areas composed of sulfide debris with several small active black smokers at the top of the mounds and is supposed to have been subject to recent volcanic activity (Haase et al., 2005). Extremely hot vent fluids, unexpectable for the slow-spreading MAR (Haase et al., subm.), are emanating from the smokers. A stable average temperature of 407 °C with a maximum at 408.5 °C, above the critical point of 407 °C was recorded by in situ measurements (Koschinsky et al., 2006). This is the highest temperature ever reported for hydrothermal vent fluids. The high temperatures, visible boiling, and extreme values for the chemical composition of the fluids clearly indicate phase separation near the critical point of seawater at Turtle Pits with the fluids representing the vapor phase (Koschinsky et al., 2006).

About 200 m to the East of Turtle Pits at 4°60'S, the diffuse-flow mussel field Wideawake is located at a water depth of 3000 m. The vent field is densely overgrown by *Bathymodiolus sp*. mussels, interestingly intercalated by vesicomyid clams (cf. *Calyptogena sp.*). Vent fluids are characterized by temperatures of about 18° C and by a chemical composition similar to the adjacent Turtle Pits field indicating the same fluid source but being diluted by entraining seawater in the subsurface.

In contrast, fluids from the Red Lion hydrothermal field around 2 km north to Turtle Pits (4°47.76'S) and in a water depth of 3050 m are chemically distinct to those from Turtle Pits and Wideawake. The fluids are emanating from four active chimneys that are characterized by flange growth. The chemical composition and also the fluid temperatures ranging between 196 °C and 349 °C exhibit no obvious indications for phase separation and resemble vent fluids from the Logatchev hydrothermal field. The fluid composition suggests that the influence of recent volcanic activity on the hydrothermal systems is confined to the Turtle Pits vent field implying venting of vapor-type fluids but is not affecting the Red Lion vent field with its seawater-salinity fluids and the much lower vent fluid exit temperatures (Haase et al., subm.). The Red Lion and Turtle Pits/Wideawake fields are obviously not supplied by the same fluid source.

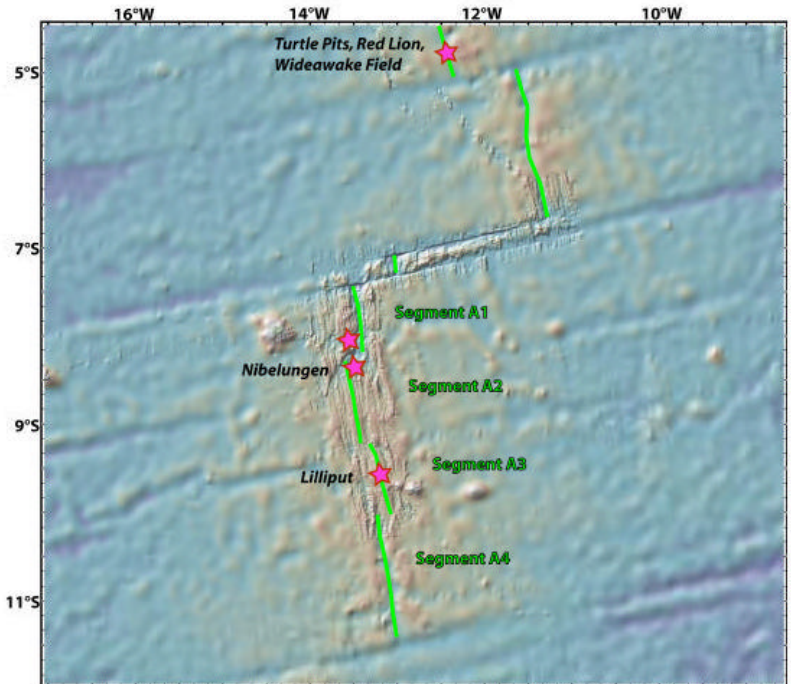

Fig. 1.6, Map of the ‚Ascension area' (4°S - 11°S) with active hydrothermal vent fields (red stars). The vent sites 'Nibelungen' and 'Lilliput' are indicated by strong plume signals. From Koschinsky et al. (2006).

The Lilliput area is located at 9°33'S in a shallow water depth of ~1500 m. Although strong plume signals are indicating active hot vents sites in the vicinity, up to now only diffuse venting on the seafloor could be unequivocally identified.

1.3 Aim of the study

The primary goal of this study is to constrain Ca isotope fractionation processes and the Ca isotope budget at low- and high-temperatures in axial hydrothermal convection systems and to provide a critical assessment of the Ca hydrothermal flux. The aim is to trace the hydrothermal pathway of Ca and to further constrain processes related to hydrothermal Ca cycling, in particular water-rock reactions, hydrothermal mineral precipitation, and phase separation. Up to now, little is known about the Ca isotope systematics in subsurface processes and actually no information exists about the Ca isotope behaviour in phase-separated, high-temperature aqueous solutions. Hydrothermal circulation at the Logatchev field offers the opportunity to study water-rock interactions under different conditions as diffuse as well as discrete venting occurs throughout a diversity of lithologies and displaying thus an average hydrothermal flux. The comparison of the hydrothermal fluids from the vent fields of the Ascension area, in particular at the MAR 5°S provides new insights into the process of phase separation and the overall controls on hydrothermal fluid compositions. Therefore, this work intends to characterize these different hydrothermal systems for their Ca elemental and isotopic budgets.

The lack of Ca isotope data in silicates and hence the difficulty to relate the hydrothermal fluid compositions properly to the basement lead to a systematic investigation of the Ca isotopic compositions of various silicate rocks including well-established geological reference materials. Thereby, efforts are made to complement the existing studies (Skulan et al., 1997; Zhu & Macdougall, 1998; Richter et al., 2003; DePaolo, 2004) and to provide a comprehensive data set over a wide range of geological reservoirs. This helps to clarify the question of naturally occurring fractionation processes at mantle temperatures, and its dependency on source, melting degree and magma evolution.

The present work contributes to a better understanding of Ca exchange between oceanic crust and hydrosphere and addresses by means of Ca directly the main objectives of SPP 1144, namely the mass transfer from the mantle into the ocean and the controlling factors for hydrothermal circulation in the subsurface.

2. MATERIALS and METHODS

2.1 Sample Materials

2.1.1 Sample collection

Sampling of water and hydrothermal vent fluids

Three sample types were retrieved; water column samples, diffuse outflows and in situ fluid samples from discrete vent sites. Water column samples were recovered by the CTD/rosette, equipped with 24 Niskin flasks à 10 l volume. Hydrothermal fluid samples were collected by three Niskin flasks (5 l volume) and the recently constructed Kiel Pumping System (KIPS; Garbe-Schönberg et al., 2005), both mounted on the remotely operating vehicle ROV QUEST from the MARUM/Univ. Bremen (Fig. 2.1).

Fig. 2.1, The KIPS system mounted on the tool sled of the ROV *QUEST* (MARUM/Univ. Bremen) during cruise MARSÜD (M64/1). From Haase et al. (2005).

The KIPS is equipped with 15 bottles à 675 ml that are filled by a pumped flow-through system. This system provides in situ sampling of hydrothermal fluids from inside the vent orifices. Thereby, a bended titanium nozzle with an online temperature probe is inserted directly into the outflow by the ROV's manipulator arm. The fluids are pumped through PFA tubing either directly or via a complex remotely controlled multiport valve system into 15 single PFA Teflon flasks. The whole system consists of inert materials (titanium, Teflon) in order to largely prevent chemical affection of the samples.

Up to 30 ml of the sampled fluids were filled into PE bottles for element and isotope analyses and partly acidified for radionuclide measurements. The samples are denoted by the number of the station and an appendix indicating the sample technique. Hence, samples taken by CTD/rosette are labelled by 'CTD', ROV samples taken by the Niskin bottles are denoted as 'ROV N', and the KIPS samples are appended by 'ROV B' and the respective bottle number.

Fluid sampling for alkalinity and dissolved inorganic carbon (DIC) analyses

Between 100 and 250 ml of fluid samples were withdrawn from the fluid samplers (CTD/rosette, Niskin bottles and/or KIPS) following standard operation procedure (SOP 1) as described in DOE (1994). The fluids were filled slowly through a silicon tube into borosilicate ground neck glass bottles with the tube opening placed at the bottom of the bottles and were allowed to overflow in order to avoid air bubbles. Due to the temperature gradient between bottom and surface seawater, a head space of around 1 % of the bottle volume was left for water expansion. For CTD/rosette samples and those taken by Niskin flasks the glass bottles were rinsed with the samples in prior, while for hot vent fluids the glass bottles were precleaned thouroughly by Millipore water (18.2 MΩ) due to limited sample amounts.

Up to 5 ml of the samples were analysed for alkalinity onboard immediately after sampling, before the samples were poisoned by about 0.1 ml of a saturated $HgCl_2$ solution for high-precision analyses of alkalinity and DIC in the home laboratory. The bottles were sealed by greased and clipped stoppers and stored dark at room temperatures. The seawater salinity reference material IAPSO and the certified reference material (CRM) provided by A. Dickson from the Scripps Institution of Oceanography, La Jolla/CA (batch 60, bottle 88) were treated and stored such as the samples.

Rock recovery

Rocks and mineral precipitates were collected by TV-Grab or by the manipulator arm of the ROV providing rather selective sampling in contrast to the sample recovery by TV-Grab. The samples were characterized in terms of lithology and petrography before cataloguing and labeling. The respective sampling method is expressed in the sample name (‘GTV’ or ‘ROV’).

2.1.2 Samples from the Logatchev hydrothermal field (LHF)

Seventeen hydrothermal vent fluid samples from the active Logatchev hydrothermal field-1 (LHF-1) at 14°45’N on the Mid-Atlantic Ridge (MAR) (Fig. 1.5b) were investigated. Also examined were the Ca and Sr isotope compositions of 14 solid samples from the Logatchev field and ODP drill cores from south of the 15°20’N fracture zone (Fig. 1.5a). The samples were taken during the R/V METEOR cruises HYDROMAR I (M60/3; Kuhn et al., 2004) and II (M64/2; Lackschewitz et al., 2005). A list of samples and their locations is given in Tab. A1 and A2 in the Appendix and indicated in Fig. 1.5. Hydrothermal solutions with variable admixture of entrained seawater were collected from active black smoker chimneys as well as over mussel bed areas with diffuse fluid venting (Fig. 1.5b). In addition, four CTD/roesette samples of background seawater were collected (Tab. A1).

Serpentinites, carbonates and anhydrites were collected in order to compare the compositions of hydrothermal fluids and mineral precipitates (Tab. A2). Representative rock samples recovered by ROV and TV-Grab during cruise HYDROMAR I were leached in order to measure their Ca and Sr isotopic compositions. The rock samples comprise one moderately altered and three strongly serpentinized peridotites. Sample 49GTV-1A3 was recovered at working station II around 15 km northeast of the Logatchev field (Fig. 1.5a).

This ultramafic rock sample is moderately altered and contains carbonate-filled fractures. The sample group of 67GTV-2 comprises strongly altered and fractured peridotites. Except for 67GTV-2A, which contains talc- and quartz-bearing veins, the fractures of the other specimen are filled with aragonite (Augustin, pers. comm.).
In addition, hydrothermal precipitates, specifically anhydrites from LHF-1 and calcium carbonates from nearby ODP holes (Leg 209), were included in this study. Sample 35GTV-7/4 consists of fairly isolated, mm-sized anhydrite crystals recovered from underneath a silicified crust in the vicinity of IRINA II. Sample 64ROV-10C from the smoking crater rim of ANNA-LOUISE is an assemblage of anhydrite and sphalerite (Fig. 1.5b). Two deformed calcite veins from serpentine-talc-tremolite schists at ODP Leg 209, Site 1271 (Fig. 1.5a) were also investigated. The rocks hosting the carbonate veins are serpentinized harzburgites and dunites. The calcite veins have likely formed synkinematically in a detachment fault environment, while the aragonite veins are late extensional vein fills related to uplift and faulting of the rift mountains. More detailed information on the tectonic setting, rock types and alteration history are provided in the ODP Leg 209 Initial Reports (Kelemen et al., 2004).

2.1.3 Samples from the 'Ascension area' (4 – 11°S)

Ten fluid samples, six anhydrites and two basaltic glasses were selected from the hydrothermal vent fields at the MAR 5°S and 9°S (Fig. 1.6) for this study and are included in Tab. A1 and A2. The samples were recovered during the R/V METEOR cruise MARSÜD (M64/1; Haase et al., 2005). The fluids are admixtures of pure hydrothermal fluid and seawater and comprise three samples from the Turtle Pits field with fluid amounts of up to 63 %, two vent fluids from the nearby Wideawake with around 10 % hydrothermal contribution, four samples from vent sites at Red Lion (3 – 65 % fluid) and one sample from the diffuse outflow at Lilliput (5 % fluid) (Fig. 1.6; Tab. A1). The fluid samples from Turtle Pits are likely phase-separated representing the vapor phase.
All of the anhydrite samples are derived from Turtle Pits field (Fig. 1.6; Tab. A2). Anhydrite sample 114ROV-5B was scratched out from surrounding chalcopyrite within a zoned black smoker chimney. The both anhydrites from station 123ROV are from the interior of an inactive recrystallized sulfide chimney. 130ROV-1C is a fragment of an anhydrite chimney, and the both anhydrites from 139ROV were separated from an association of different sulfides.
The two basaltic glasses 109GTV-1 and -2 were also recovered at Turtle Pits at a water depth of 2998 m (Fig. 1.6; Tab. A2). They consist of fresh glassy pieces from a sheet flow (cf. Haase et al., 2005).

2.1.4 Various rock materials

For the investigation of Ca isotope variations in different rock types, several well-investigated rock samples, mainly reference materials were selected (Tab. 2.1). These samples offer the advantage to be investigated in detail for their elemental and most isotopic composition and to cover a wide range of different geologic reservoirs.

Tab. 2.1, Compilation of various rock materials analyzed for their Ca isotope compositions.

sample	rock type
commonly used references	
NIST SRM 915a	calcium carbonate
IAPSO	seawater
MPI-DING glasses	
ATHO-G	rhyolite
StHs6/80-G	andesitic ash
T1-G	quartz diorite
KL2-G	tholeiite - Kilauea
ML3B-G	tholeiite - Mauna Loa
GOR128-G	komatiite (Cret.-Tert.)
GOR132-G	komatiite (Cret.-Tert.)
BM90/21-G	peridotite
original rock powders	
StHs6/80	andesitic ash
T1	quartz diorite
KL2	tholeiite - Kilauea
ML3B	tholeiite - Mauna Loa
BM90/21	peridotite
USGS reference materials	
BHVO-2	tholeiitic basalt
BIR-1	tholeiitic basalt
BCR-2	tholeiitic basalt
W-2	diabase
DTS-1	dunite
PCC-1	peridotite
other certified materials	
TML	table mountain latite
IAEA-CO1	Cararra marble
non-certified rock samples	
Onverwacht 5019	komatiite (~3.5 Ga)
Onverwacht 5031	komatiite (~3.5 Ga)
82LM 66A (Res) [+]	magnesiocarbonatite
82LM 66A (Cc) [†]	Carbonate phase
83HV 26 (Res) [+]	calciocarbonatite
83HV 26 (Cc) [†]	Carbonate phase

[+] silicate residue after leaching
[†] leached carbonate fraction

MPI-DING glasses and powders

The MPI-DING reference suite consists of the eight igneous rock samples ATHO-G, StHs6/80-G, T1-G, KL2-G, ML3B-G, GOR128-G, GOR132-G and BM90/21-G. These materials cover a wide range from highly silicious to ultramafic compositions (Tab. 2.1). The rock powders are molten to glass beads for in situ microanalysis. The melting process was carried out by direct fusion without using a flux agent (Dingwell et al., 1993). The preparation and overall investigation of the glass fragments are described in detail by Jochum et al. (2000, 2006). In addition, the Ca isotope compositions of the MPI-DING reference glasses StHs6/80-G, T1-G, KL2-G, ML3B-G, and BM90/21-G were compared to those of their original rock powders.

USGS reference materials

Six USGS igneous rock reference materials were analyzed for their Ca isotope compositions. The samples comprise the Icelandic basalt BIR-1, the Columbia River Basalt BCR-2, the Hawaiian tholeiitic basalt BHVO-2, the diabase W-2, the peridotite PCC-1 and the dunite DTS-1 (USGS, 2000).

Other reference materials

As an internationally accepted standard for U-Th activity analyses the Table Mountain Latite TML (e.g. Williams et al., 1992; Turner et al., 2004) was investigated. Since carbonatic samples are often dated by U-Th method, hence, in concert with the MPI-DING glass ATHO-G the possibility to use a common reference material for the determination of age and Ca isotope ratios will be given.

With regard to its importance in stable isotope standardization, the $\delta^{13}C$- and $\delta^{18}O$-reference material IAEA-CO1 (Carrara marble) of the International Atomic Energy Agency was analyzed for its Ca isotope composition.

Non-certified geological materials

In order to extend the spectrum of magmatic melts with regard to Ca isotope studies two carbonatites deriving from Fuerteventura/Canary Islands and Cap Verde (Hoernle et al., 2002) were measured. The calcio-carbonatite 83HV26 and the magnesio-carbonatite 82LM66A represent the two groups of high-Ca/low-Mg (calciltic) and low-Ca/high-Mg (dolomitic) oceanic carbonatites. The two fractions of these samples, the carbonate and silicate phase have been investigated separately (Tab. 2.1).

Since both komatiites GOR128-G and GOR132-G within the MPI-DING sample suite are very young (Cretaceous-Tertiary) and show an atypical composition for komatiites (e.g. Hauff et al., 2000; Echeverria, 1980), two typical Archaen komatiites from the Onverwacht Group in South Africa (Nesbitt et al., 1979; Jochum et al., 1991) were added to the rock compilation (Tab. 2.1).

2.2 Analytical Methods

2.2.1 Ca isotope analyses

Sample decomposition

Prior to Ca isotope analyses, the silicate samples had to be dissolved in order to release Ca from the silicate cage. Generally, all procedures were carried out under clean lab conditions. Deionized and further purified water (18.2 $M\Omega*cm^{-1}$), and ultrapure acids were used throughout. The purity of the used reagents was monitored by the determination of blanks. Within every dissolution series a blank and an aliquot of the BHVO-2 were prepared and measured. Approximately 0.02 to 0.2 g of the rock sample material and the leached residues of the carbonatites were weighed in precleaned screw-top Savillex PFA vials and subject to two differing digestion techniques.

First, a common HF-HNO_3 acid attack was applied in order to destroy the silicate frame. Depending on the sample size, about 2 ml HF and 1 ml conc. HNO_3 were added to the samples and heated to 120 °C in closed beakers for 48 hours. The dissolved samples were then dried down and treated three times by conc. HNO_3 and once by 6N HCl in order to get rid off the fluorides. After evaporation the solutions were taken up by 2.2N HCl and attention was paid that the solutions were clear. Aliquots from these stock solutions were then processed through the analytical experiments. In addition, the seawater salinity standard IAPSO was subjected to the same dissolution procedure ($IAPSO_{diss}$) and compared to untreated aliquots.

The Ca recovery from the ultramafic samples (DTS-1, PCC-1, BM 90/21, BM90/21-G, GOR128-G, GOR132-G) was achieved in addition by a method using HBr prior to the HF-HNO_3 dissolution (Nägler & Kamber, 1996). The samples were treated by 8.8M HBr and heated at ~160 °C for 72 hours in closed vessels. During the heating the samples were ultrasonicated several times for ~10 min. Thereby, the cations are released from the crystal cage. The yellow-brownish solutions were centrifuged and decanted. While the residues consisting of the silicate framework were treated then further by HF-HNO_3 such as described above, the supernatants were preserved and merged afterwards with the residual dissolutions.

With this technique the critical exposure of Ca to HF in these low-Ca samples is largely prevented and thus fractionation effects during potential CaF_2-formation precluded. Because of additional handling, the blank of this digestion process is more than three times higher than the direct dissolution by HF-HNO_3. Therefore, the Ca isotope composition of the blank was determined and the results accordingly corrected. In the following, '$Diss_{HF}$' will refer to the direct dissolution and '$Diss_{HBr}$' to the digestion with a pretreatment by HBr.

Chemical Purification

Matrix-bearing samples, i.e. fluids and silicates had to be processed through a chemical separation in order to isolate Ca from potentially interfering elements such as potassium, strontium, and magnesium. In this study, a commonly used chromatographic clean-up for seawater and basalts, which is based on cation exchange and HCl elution was applied. Depending on the sample type fluid or rock, the reference materials IAPSO and/or BHVO-2, and a blank were processed in every separation course.

The komatiites, the peridotites and the dunite were separated by 1.2 ml columns (BioRad) that were filled with the cation exchange resin MCI Gel, CK08P (75-150 µm). Around 4 µg Ca was eluted by 8 ml of 1.5N HCl. For all other samples a column size of 0.6 ml and 5 ml HCl was used to yield the same amount of Ca.

The quality of the separation was checked by individual elution schemes and a Ca yield of up to 80 % was collected. Potentially occurring fractionation of the Ca isotopes on the column (Heumann & Lieser, 1971; Russell & Papanastassiou, 1978) was taken into account by adding the $^{43}Ca/^{48}Ca$-double spike to the sample in prior of the column chemistry.

Carbonates, anhydrites and leachates from serpentinites and carbonatites were not subject to column chromatography, but directly analyzed after dissolving and spiking. Working splits of the carbonate veins and anhydrite crystals were picked or scratched out from the host-rocks in order to obtain fairly pure phases. Carbonates and anhydrites were dissolved in 2.2N and 6N HCl, respectively. The serpentinites and carbonatites were leached by 0.5N HCl.

Ca isotope analyses

Aliquots of the samples have been analyzed for their Ca isotopic compositions by thermal ionization mass spectrometry (TIMS) in the laboratories of the Leibniz-Institut für Meereswissenschaften IFM-GEOMAR in Kiel/Germany. The analyses were performed in dynamic mode using the $^{43}Ca/^{48}Ca$-double spike technique (e.g. Russell et al., 1978). A spike composition as used by Heuser et al. (2002) and Gussone et al. (2003) was used (Tab. 2.2). Mass fractionation was corrected by exponential law.

Tab. 2.2, The composition of the used $^{43}Ca/^{48}Ca$-double spike 'Kaiser-Karl'. After Gussone et al. (2003).

Isotope	40	42	43	44	48
Concentration [ng/ml]	77	4	420	26	561
Atomic [%]	8	0.4	40.6	2.4	48.6

The measurements were carried out on a ThermoFinnigan Triton Tl using a routine method close to that described by Heuser et al. (2002). Thereby, a total amount of about 300 ng Ca was loaded with a Ta activator onto outgassed Re filaments. Ca isotopes were measured by an integration time of 4s for 7 blocks à 22 scans when a signal of 4 V was achieved.

Stable Ca isotope values are indicated in the proposed δ notation ($\delta^{44/40}Ca_{standard} = {}^{44}Ca/{}^{40}Ca_{sample} / {}^{44}Ca/{}^{40}Ca_{standard} - 1) \times 10^3$) (Eisenhauer et al., 2004). The data are referred to IAPSO as a reference for seawater ($\delta^{44/40}Ca_{(SW)}$), measured within each analytical run and being crosschecked by the carbonate standard NIST SRM 915a. During the course of this study, the average long-term value for IAPSO comprising 135 single measurements was 1.82 ± 0.15 ‰ (2sd) ($^{44}Ca/^{40}Ca = 0.02121920$) relative to SRM 915a. This is in accordance with the proposed values for modern seawater (Hippler et al., 2003). The results are averages of replicated analyses from at least 3 discrete chromatographic column separations. Overall analytical uncertainties are less than 0.2 ‰ indicated as 2 standard deviation (2sd).

A total procedural blank including the preceeding sample decomposition and column separation of less than 2 % was determined for $Diss_{HF}$, being negligible for any blank corrections. The sample digestion procedure $Diss_{HBr}$ exhibited a Ca blank of 16 ng with an isotopic composition of -1.08 ‰. The results of this experiment were therefore blank-corrected.

We checked selected rock samples (Tab. 3.11) for an enrichment of radiogenic ^{40}Ca in order to ensure that no radiogenic ^{40}Ca from the decay of ^{40}K is superimposing the Ca isotope compositions (in particular in the Archaen komatiites and the high-K samples ATHO-G and StHs6/80). For that reason, $^{40}Ca/^{44}Ca$ ratios of unspiked aliquots were measured at a signal of 10 V for at least 14 blocs à 20 scans by an integration time of 4s. Measured $^{40}Ca/^{44}Ca$ ratios were normalized to a $^{42}Ca/^{44}Ca$ value of 0.31221 (Russell et al., 1978). The radiogenic $^{40}Ca/^{44}Ca$ ratios are denoted as ε values ($({}^{40}Ca/{}^{44}Ca_{sample} / {}^{40}Ca/{}^{44}Ca_{standard} - 1) \times 10^4$) relative to the seawater salinity standard IAPSO. Samples displaying an $\varepsilon^{44/40}Ca_{(SW)}$ close to 0 were analyzed once. Other samples were measured twice. The typical analytical uncertainty of repeats was ±2 ε units (2sd).

Analytical uncertainties

For an appropriate assessment of the overall analytical uncertainty, the main sources of uncertainties during the experimental processing must be estimated. Many systematic error sources are canceled out by relating the results to a standard material (here IAPSO) that was treated in the same analytical procedure. Following the suggestions of Goldstein et al. (2003), this calibration standard was crosschecked by a second standard (NIST SRM 915a) analyzed during the course of the analyses. In this regard, contributions of the blank, sample-spike ratios, and instrumental bias to the analytical uncertainty can be neglected. For this reason an extensive error propagation is disregarded and only some particular error sources are briefly summarized and discussed in the following.

A source of uncertainty is certainly the use of non-representative amounts of sample material. Between 20 and 100 mg of sample amounts was digested. This is considered as analytical test portion masses for high precision isotope analyses (Jochum et al., 2006). With regard to in situ-microanalytical work this study may not provide information on micro-heterogeneity in the µm-scale taken quench crystallized mineral phases into account.

The ultramafic samples provide challenges to the analysts because of their particular matrix with high Fe and Mg content and the presence of barely soluble minerals such as spinels that might not be decomposed by the digestion methods used here. However, thorough adjustments of the column chromatographic procedure checked by individual elution schemes were carried out weakening this possible source of error and ascertaining the values. Uncertainties due to shifts between the two delta-zero materials could not be observed during the course of this study and the Ca isotope ratios of IAPSO and the NIST SRM 915a standard matched to each other and with their long-term values within the given precision.

Generally, variations between the analytical runs were smaller than the precision given by the analytical method. External precision is less than 0.2 ‰ (2sd). In summary, large affections by sample handling and the analytical procedure can be precluded and the measured values can be ascribed mainly to intrinsic properties of the sample materials.

2.2.2 $^{87}Sr/^{86}Sr$

Radiogenic Sr isotope ratios in fluid samples and in rock leachates were measured on a MC-ICPMS (VG Elemental Axiom) and a TIMS (ThermoFinnigan TRITON) at IFM-GEOMAR in Kiel, Germany, following standard chemical separation (Sr-Spec, 50-100 mesh; 0.6 ml) and measurement procedures (e.g. White & Patchett, 1983). Blanks were less than 1 ‰ of the total sample amount and therefore neglected.

The Logatchev fluid samples from HYDROMAR I were analyzed by MC-ICPMS. On-Top zero baselines were determined in order to account for potential Sr and Rb blanks and the Kr background. A detailed description of the method is given in Fietzke and Eisenhauer (2006). The measured ^{85}Rb was used to correct for the ^{87}Rb contributions to the signal on mass 87 using $^{87}Rb/^{85}Rb$ of 0.38565. During the course of the project, 5 NBS 987 standards were measured yielding a $^{87}Sr/^{86}Sr$ ratio of 0.71025(2) (2sd). In addition 3 measurements of the IAPSO seawater standard yielded 0.70920(1) (2sd).

The $^{87}Sr/^{86}Sr$ ratios of the fluid samples taken during the cruises HYDROMAR II and MARSÜD as well as of the anhydrites and the rock leachates were measured by TIMS. Thereby, 8 analyses of the NBS 987 standard yielded a value of 0.710248(3) and 3 analyses of IAPSO result in 0.709153(2) (2sd).

The ODP vein carbonates were measured by Martin Rosner at Woods Hole Oceanographic Institution in Woods Hole/USA. For the seven samples, Sr was separated by conventional ion chromatographic element separation using AG 50W-X8 ion exchange resin (200-400 mesh; 3ml). Sr, Kr and Rb ion yields of the resulting solution were analyzed by MC-ICPMS (ThermoFinnigan NEPTUN). Measured raw ion yields were corrected for Kr and Rb interferences after a method reported in Jackson and Hart (2006). Repeated measurements (n = 6) of reference material NBS 987 yielded a mean $^{87}Sr/^{86}Sr$ ratio of 0.71025(1) (2sd). The values of all measurement procedures are in good agreement with each other and with published ratios (e.g. McArthur & Howarth, 2004).

2.2.3 Element concentrations (Sr, Mg, Ca)

The concentrations of Mg, Ca, and Sr in sampled mixtures of hydrothermal fluid and seawater were determined by ICP-OES using a simultaneous CCD instrument with radial plasma observation (Spectro Ciros SOP) at the Institute of Geosciences, Univ. Kiel/Germany. A micronebulizer (200 µl*min^{-1} sample uptake, SeaSpray, Glass Expansion) in combination with a cyclonic spray chamber was used to minimize sample consumption. Samples were 10-fold diluted prior to analysis, and a 1 mg*L^{-1} Yttrium solution was added as an internal standard. Analytical results are averages of three replicate measurements with 45 s acquisition time each using the following wavelengths: Mg 279.079 nm, Ca 315.887 nm, Sr 407.771 nm. The stability of the instrument was monitored by re-analyzing samples in regular intervals, and precision calculated from these sample replicates was 0.5, 1.6, and 2.1 % (rsd = relative standard deviation) for Mg, Ca, and Sr, respectively. The seawater reference standard IAPSO was analysed together with the samples.

2.2.4 Uranium isotope ratios ($^{234}U/^{238}U$)

Hydrothermal fluid samples were analyzed for their Uranium isotopic ($^{234}U/^{238}U$) compositions by MC-ICPMS (VG Elemental Axiom). Prior to analyses a $^{233}U/^{236}U$-double spike was added, and a separation and purification by ion exchange chromatography using AG-1 X8 (100-200 mesh) and a combination of HNO_3 and H_2O for elution was carried out. Total blanks were less than 20 pg and with regard to the U amount of at least 10 ng negligible.

Samples from HYDROMAR I were analyzed using 2 ng U after the method of Fietzke et al. (2005). For these samples an analytical uncertainty of about 2 % (rsd = relative standard deviation) could be achieved (Tab. 3.1). Whereas the precision was enhanced by an order of a magnitude for the fluid samples from the cruise HYDROMAR II, where larger sample amounts containing up to 10 ng U could be processed (Tab. 3.1).

2.2.5 Mg isotope ratios ($\delta^{26}Mg$)

Five hydrothermal fluid samples were selected for the determination of their Mg isotope composition (Tab. 3.1). A sample amount containing 5-10 µg Mg was separated from the matrix by a two-stage column chemistry (BioRad AG 50W X8; 200-400 mesh; 0.75 ml). The alkaline elements, Mg and Ca were eluted successively by HCl of decreasing acidity. Mg analyses were performed on MC-ICPMS (VG Elemental Axiom) using bracketing standard technique (Galy et al., 2001), whereby the seawater salinity standard IAPSO was crosscalibrated by a 2.5 ppm Mg solution of Dead Sea Metal Standard (DSM-3). Mg isotope ratios ($\delta^{26}Mg$) are indicated in the δ notation relative to the Dead Sea Metal standard (DSM-3). IAPSO yielded a $\delta^{26}Mg$ of -0.76 ± 0.10 ‰ (2sd) relative to DSM-3 (Tab. 3.1) and is in good agreement to the value of about -0.82 ‰ reported in previous studies (Young & Galy, 2004; De Villiers et al., 2005).

With a procedural blank of less than 2.6 ng corrections were negligibly. Instrumental fractionation was corrected exponentially. $^{25}Mg/^{24}Mg$ ratios were monitored as an internal control. Overall analytical uncertainties were less than 0.1 ‰. Further details of the analytical procedure in particular of the column chemistry can be found in Wombacher et al. (2006).

2.2.6 $\delta^{11}B$ analyses

Seven fluid samples of low (6 %) to high (88 %) fluid amounts were selected for the analysis of boron isotopes (Tab. 3.1). The measurements were carried out on a ThermoFinnigan Triton (TIMS) applying negative ion method without any chemical preparation in prior. Around 5 ng of boron was directly loaded onto degassed zone-refined Re filaments and analyzed at a filament temperature of around 950 °C. Due to large mass fractionation occurring during the negative ion method, only measured ratios at the beginning of the analyses but at least for 3 blocs à 20 cycles with an integration time of ~8 s were considered. The measurements were stopped when the ratios deviated more than 0.4 ‰ from the values at the beginning of the measurements.
The measured $^{11}B/^{10}B$ ratios were calibrated against the NIST standard SRM 951 and crosschecked by IAPSO as seawater reference. The isotopic compositions are expressed as permill deviation from SRM 951. Three analyses of IAPSO yielded an average value of 39.9±0.4 ‰ (2sd) relative to SRM 951. Typical analytical precision is about ±1 ‰ (2sd).

2.2.7 Alkalinity and dissolved inorganic carbon (DIC)

The determination of alkalinity and dissolved inorganic carbon (DIC) was carried out at the Leibniz-Institut für Meereswissenschaften IFM-GEOMAR, Kiel/Germany. Alkalinity was measured by two different methods. A simple back titration for onboard analyses and a high-precision, open-cell titration (Anderson & Wedborg, 1985) in the home laboratory were carried out. DIC was determined by a coulometric method (Johnson et al., 1985) after proper sampling and sample storage.

Alkalinity onboard analyses – back titration

Alkalinity was determined onboard for samples of very less amounts and for a cross-check with later analyses due to potential modifications by H_2S oxidation and/or $CaCO_3$ precipitation. The measurements are carried out by a titration device after Galina Pavlova. 1 ml of sample was diluted by 4 ml of Millipore water, and 0.02 ml of a mixture of methylorange and methylenblue as indicator was added. The mixture was titrated by 0.01M HCl until turning to a stable pink color. The released CO_2 and H_2S, respectively were driven out by N_2. The results are averages of at least three replicated measurements. Analytical uncertainties are less than 0.7 %.

Potentiometric determination of total alkalinity (TA) – open-cell titration

For high-precision results alkalinity was determined potentiometrically by an automated open-cell titration. The measurements were carried out on the VINDTA device (Versatile Instrument for the Determination of Titration Alkalinity) (Mintrop et al., 2000). This system consists of a water-jacketed open cell, a magnetic stirrer, water-jacketed pipette, an automated burette and a pH-meter and provides an automated, computer-controlled titration of alkalinity by hydrochloric acid. The whole system as well as the samples are temperated at ~25 °C by a circulating bath. Prior to analyses the cell is flushed by 0.7M NaCl solution and calibrated by the CRM provided by A. Dickson from the Scripps Institution of Oceanography, La Jolla/CA (SIO). IAPSO was run as a quality control.

Alkalinity is deduced by an electrochemical cell that records the change of pH due to incrementally addition of 0.1M HCl. The addition of HCl was adapted to the titration curve with higher resolution near the alkalinity equivalence point. An online curve-fitting procedure was used to calculate total alkalinity (TA) from the H^+. Precision is better than 2 ‰.

Coulometric determination of dissolved inorganic carbon (DIC)

Dissolved inorganic carbon was determined coulometrically by the SOMMA device (Single-Operator Multiparameter Metabolic Analyzer), a computer-controlled closed-cell system (Johnson et al., 1993). Thereby, the carbon dioxide formed by acidification is expelled from the sample by an inert gas into a reagent containing ethanolamine. The thus generated hydroxyethylcarbamid acid is then titrated coulometrically by hydroxide ions evolved at the cathode, while at the anode silver is oxidized. Changes in pH are monitored colorimetrically with tymolphtaleine as indicator. The intensity of the generated current is a measure for the CO_2 content and is converted online into concentration values.

Prior to analyses fresh reagants were prepared and the system was calibrated by the CRM Dickson. A minimum of 150 ml sample amount is required. Samples and reagents are kept at a constant temperature. Analytical uncertainties are about ±2µM.

3. RESULTS

3.1 The Logatchev hydrothermal field (LHF)

3.1.1 The Ca and Sr isotope systematics

The results for the fluid samples from the Logatchev field are summarized in Tab. 3.1 and those for the solid samples in Tab. 3.2. The $\delta^{44/40}Ca_{(SW)}$ ratios of the fluids are inversely correlated with their corresponding Ca contents (Fig. 3.1a). Similarly, the measured Mg and Ca concentrations are inversely correlated, indicating that Ca concentrations in the hydrothermal fluids are higher than in seawater. The contribution of hydrothermal fluids in the samples can be calculated from their Mg concentrations (e.g. Von Damm, 1985) based on the assumption that the Mg concentration of pure hydrothermal fluid is equal to zero. From binary mixing calculations a Ca concentration of 32±1 mM is computed for the hydrothermal endmember ($[Ca]_{HydEnd}$). The endmember Ca isotope composition ($\delta^{44/40}Ca_{HydEnd}$) of the hydrothermal vent fluid of -0.96±0.09 ‰ (95 % confidence interval) was calculated by extrapolating the $\delta^{44/40}Ca$ data to a [Mg]/[Ca] value of zero (Fig. 3.1a).

Similar to Ca, the Sr concentrations and $^{87}Sr/^{86}Sr$ ratios are inversely correlated (Fig. 3.1b). Mixing calculations between seawater and hydrothermal fluid result in a Sr endmember concentration ($[Sr]_{HydEnd}$) of 125±5 µM and a $^{87}Sr/^{86}Sr$ value of 0.7034(4) (at 95 % confidence level) for the hydrothermal fluid endmember ($^{87}Sr/^{86}Sr_{HydEnd}$) (Fig. 3.1b). Binary mixing calculations using Ca and Sr isotopes lead, independently of the Ca concentrations, to a value of -0.93±0.10 ‰ (95 % confidence interval) for $\delta^{44/40}Ca_{HydEnd}$ (Fig. 3.1c) being statistically indistinguishable from the value calculated above (Fig. 3.1a). For further discussions an error-weighted mean value of -0.95±0.07 ‰ was adopted for $\delta^{44/40}Ca_{HydEnd}$. The $\delta^{44/40}Ca_{(SW)}$ of the seawater samples from the CTD reference stations are consistent within error to the IAPSO seawater salinity standard (Tab. 3.1).

The carbonates from the alteration veins recovered by ODP Leg 209 exhibit $\delta^{44/40}Ca_{(SW)}$ values between -0.66 and -1.70 ‰ (Tab. 3.2) but form two distinct groups. Calcites are significantly enriched in ^{44}Ca ($\delta^{44/40}Ca_{(SW)}$ of -0.66 and -0.97 ‰) compared to the aragonites ($\delta^{44/40}Ca_{(SW)}$ ranges from -1.32 to -1.70 ‰). The calcite samples also differ in their Sr isotope ratios displaying fairly unradiogenic $^{87}Sr/^{86}Sr$ ratios of about 0.7039, while the $^{87}Sr/^{86}Sr$ ratios of the aragonites are around 0.70915(2) and close to the seawater value (Tab. 3.2).

The $\delta^{44/40}Ca_{(SW)}$ of the leached peridotites vary between -1.48 and -1.82 ‰ and are therefore similar to the aragonites from the ODP drill cores. This similarity in Ca isotope compositions might suggest that the Ca released during leaching resided mainly in aragonite. Both anhydrite samples (35GTV-7/4 and 64ROV-10C) show $\delta^{44/40}Ca$ values of around -1.1 ‰ relative to seawater. Based on the relative proportions of Sr in seawater ($[Sr]_{SW}$ = 87 µM) and the fluid endmember ($[Sr]_{HydEnd}$ = 125 µM), Sr isotope compositions suggest that the anhydrite sample 35GTV-7/4 precipitated from a mixture of at least 41 % seawater and 59 % hydrothermal fluid, while 64 ROV-10C was derived from a fluid containing 78 % seawater (Fig. 3.1c).

Tab. 3.1, Results for the Ca and Sr isotopic compositions in hydrothermal fluid and seawater samples from the Logatchev hydrothermal field (LHF). Fluid amounts are calculated after zero Mg concentration.

sample ID	fluid amount [%]	Mg conc. [mM]	B conc. [µM]	U conc. [nM]	Ca conc. [mM]	Sr conc. [µM]	$^{87}Sr/^{86}Sr$	$\delta^{44/40}Ca_{(SW)}$ [‰]	2sem	*n*	$^{234}U/^{238}U$ [dpm]	sd	$\delta^{26}Mg_{(DSM)}$ [‰]	$\delta^{11}B_{(SRM\ 951)}$ [‰]
IAPSO	0	54	420	12.6	10.55	87	0.70918	0	0.04	*135*	1.16	0.02	-0.76	39.9
HYDROMAR I														
fluid samples														
29 ROV-2 B2	4	52.3	416	12.5	10.9	87.5	0.70883	-0.07	0.13	*12*	1.14	0.02	-0.78	37.7
29 ROV-3 B7	4	52.3	414	12.4	11.5	89.2	0.70897	-0.03	0.1	*6*	1.13	0.02		
53 ROV-4 B2	21	44.0	407	11.1	15.9	104.1	0.70759	-0.55	0.09	*12*	1.14	0.03	-0.78	39.4
53 ROV-5 B3	6	51.4	409	12.8	12.5	91.2	0.70864	-0.13	0.09	*5*	1.16	0.03		
53 ROV-7 B4	6	51.4	415	12.9	11.5	87.8	0.70884	-0.17	0.14	*4*	1.15	0.02	-0.81	
64 ROV-6 B2	7	50.2	408	12.9	11.5	88.1	0.70891	-0.14	0.2	*6*	1.15	0.02		38.3
64 ROV-8 B3	7	50.2	409		10.9	87.8	0.70883	-0.02	0.11	*4*				
66 ROV-10 B3	11	49.4	406	12.6	12.5	90.5	0.70864	-0.14	0.09	*5*	1.13	0.03	-0.79	
73 ROV-3 B2	11	49.4	409	12.7	12.5	91.3	0.70859	-0.14	0.15	*6*	1.12	0.02		
73 ROV-6 B3	13	48.5	403		12.5	91.6	0.70858	-0.11	0.09	*5*				
73 ROV-8 B3	16	48.5	405	11.6	13.5	91.6	0.70811	-0.29	0.08	*5*	1.13	0.04	-0.80	39.0
CTD/rosette samples														
17 CTD-6	0				10.3			-0.05	0.1	*3*				
17 CTD-16	0				10.0			0.08	0.1	*3*				
HYDROMAR II														
fluid samples														
224 ROV B15	72	16.1	343	2.6	24.7	109.4	0.70477	-0.88	0.11	*7*	1.14	0.005		27.1
232 ROV-7 B9	0	57.1	427	12.7	11.4	89.2	0.70914	0.00	0.07	*6*	1.14	0.003		
257 ROV-8 B10	88	7.1	345	3.6	30.4	121.1	0.70394	-0.90	0.11	*8*	1.14	0.004		22.7
266 ROV-10 B10	74	14.7	354		26.8	114.7	0.70458	-0.75	0.14	*7*				27.8
277 ROV-5 B2	11	50.6	410		12.9	88.1	0.70791	-0.35	0.12	*7*				
281 ROV-5 B2	51	28.1	370	7.6	20.9	105.3	0.70591	-0.72	0.1	*5*	1.14	0.003		
CTD/rosette samples														
217 CTD	0					91.6		-0.06	0.01	*2*				
231 CTD-8	0					93.0		0.03		*2*				

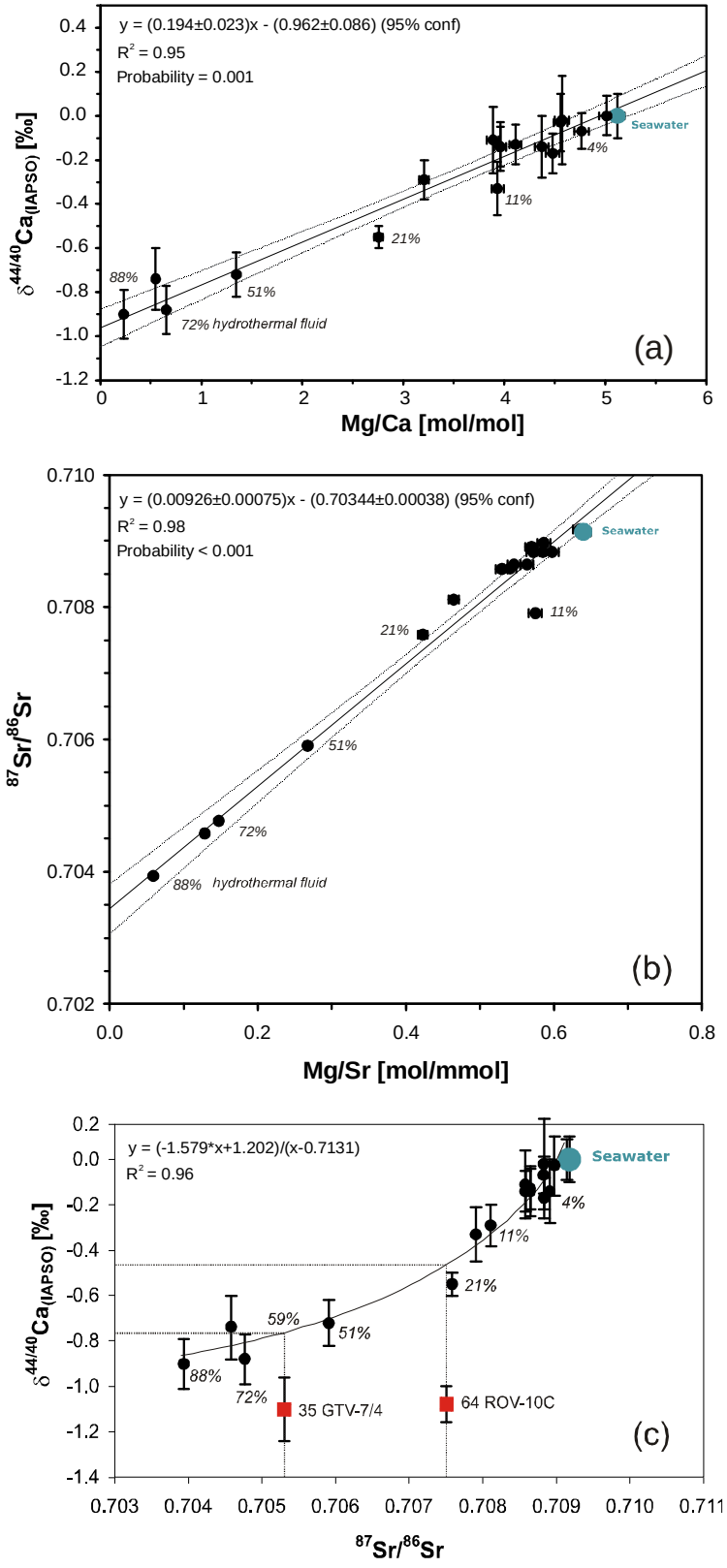

Fig. 3.1, (**a**) The Ca isotope values ($\delta^{44/40}$Ca) of the fluid samples are shown as a function of their corresponding Mg/Ca ratio. Labels next to the data points indicate the relative contribution of the hydrothermal fluid calculated from their Mg concentrations assuming that the Mg concentration of the hydrothermal fluid is zero. The approximating linear function is interpreted to represent a binary mixing curve of two endmembers being seawater one endmember and hydrothermal solution the other endmember. From the intercept of the binary mixing curve with the y axis a value for the $\delta^{44/40}Ca_{HydEnd}$-value of the hydrothermal fluid can be estimated to be -0.96±0.09 ‰ (95 % confidence) relative to IAPSO.
(b) The $^{87}Sr/^{86}Sr$-values of the sampled fluids are shown as a function of their corresponding Mg/Sr ratios. Similar to the Ca isotopes the approximating linear curve is interpreted to represent binary mixing between seawater and the hydrothermal fluid. From the intercept of the mixing curve with the y axis a $^{87}Sr/^{86}Sr_{HydEnd}$ value of 0.7034(4) for the hydrothermal endmember can be deduced.
(c) Plotting $\delta^{44/40}$Ca as a function of the $^{87}Sr/^{86}Sr$ ratios results in a non-linear hyperbolic binary mixing function. From the intercept of the function with the y axis a $\delta^{44/40}Ca_{HydEnd}$ of -0.93 ± 0.10 ‰ (95 % confidence) for the hydrothermal endmember can be computed.
The marked Sr isotope composition (dotted line) of anhydrite sample 35 GTV-7/4 reveals an emanation from a mixture of 41% seawater and 59 % hydrothermal fluid corresponding to a fluid $\delta^{44/40}$Ca value of -0.77±0.08 ‰, while anhydrite sample 64 ROV-10C is derived from a fluid with $\delta^{44/40}$Ca of -0.46±0.04 ‰.

Tab. 3.2, Results for the Ca and Sr isotopic compositions in rock samples and mineral precipitates from the Logatchev hydrothermal field (LHF), the ODP Leg 209 carbonate veins and the formation temperatures of the mineral precipitates as estimated by isenthalpic mixing.

sample ID	T [°C][1] ($\delta^{18}O_{(VSMOW)}$)	T [°C][2] ($\delta^{44/40}Ca_{(IAPSO)}$)	T* [°C][3] ($^{87}Sr/^{86}Sr$)	$^{87}Sr/^{86}Sr$	$\delta^{44/40}Ca_{(IAPSO)}$ [‰]	2sem	*n*
LHF							
anhydrites							
35 GTV-7/4			234	0.70533	-1.10	0.14	*4*
64 ROV-10C			113	0.70750	-1.08	0.08	*3*
Serpentinite leachates							
49 GTV-1A-3 (L)		25			-1.48	0.08	*4*
67 GTV-2A (L)		12		0.70916	-1.74	0.15	*4*
67 GTV-2B (L)		9		0.70916	-1.82	0.09	*4*
67 GTV-2C (L)		13		0.70928	-1.75	0.10	*4*
ODP Leg 209							
calcites							
1271A 1R2 28-31	130			0.70393	-0.97	0.19	*4*
1271A 5R1 30-33	160			0.70385	-0.66	0.08	*9*
aragonites							
1271B 1R1 8-15	4	16		0.70916	-1.70	0.09	*5*
1271B 14R1 58-62	10	41		0.70915	-1.32	0.09	*5*
1271B 15R1 53-57	13	28		0.70915	-1.52	0.15	*8*
1274A 12R2 9-13	6	27		0.70915	-1.53	0.15	*8*
1274A 13R1 61-66	3	20		0.70917	-1.64	0.07	*8*
1274A 15R1 61-65	6	27			-1.54	0.05	*9*

[1]calculated after Friedman & O'Neill (1977) and Böhm et al. (2000)
[2]calculated using inorganic aragonite fractionation line (Gussone et al., 2003)
[3]calculated by isenthalpic mixing using by Sr isotope ratios (Bach, pers. comm.)

3.1.2 $^{234}U/^{238}U$, $\delta^{26}Mg$ and $\delta^{11}B$ in hydrothermal fluids

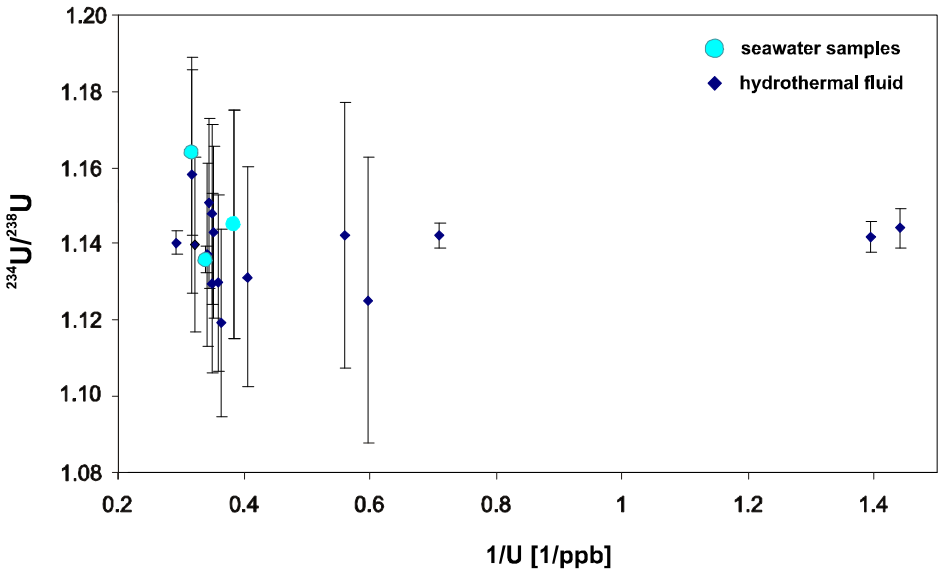

Fig. 3.2, U isotope ratios versus U concentrations. The isotopic composition of the fluids displays seawater signature independent from U concentrations and the hydrothermal fluid fraction. Samples with large error bars were measured by very less sample amounts. See text for further explanation.

While U concentrations in the fluid samples are inversely correlated with the fluid amounts as deduced by Mg, the analyses of Uranium isotope ratios $^{234}U/^{238}U$ do not show a correlation to the U contents and/or the hydrothermal fluid portions (Tab. 3.1; Fig. 3.2). All of the samples including those with high amounts of pure fluid (88 % and 72 %) display seawater activity ratios of around 1.14 matching the $^{234}U/^{238}U$ ratio of IAPSO of 1.16 ± 0.02 (sd) within the analytical uncertainties. U concentrations tend to decrease with increasing fluid amounts (Fig. 3.2), since the samples with the highest content of pure fluid 224ROVB15 (72 %) and 257ROV-8B10 (88 %) are substantially depleted in U compared to seawater displaying concentrations of 0.69 and 0.72 ng/g (ppb), respectively (Tab. 3.1; Fig. 3.2).

This is the case for the Mg isotope measurements. There is no trend obvious for the Mg isotope compositions in the fluids. The $\delta^{26}Mg_{(SW)}$ values range between 0.03 ‰ to 0.07 ‰ and are thus, with regard to the analytical uncertainty of 0.1 ‰ undistinguishable to that of the Mg isotope composition of IAPSO (Tab. 3.1; Fig. 3.3).

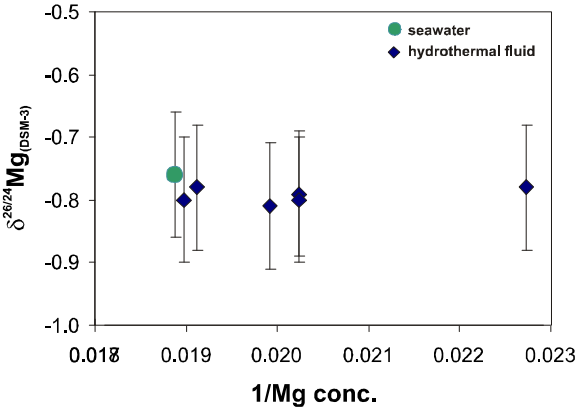

Fig. 3.3, Mg isotope ratios are seemingly not fractionated during hydrothermal circulation as the isotopic compositions of the fluid samples resembles seawater. Mg concentrations are used for the calculation of the amount of pure fluid with Mg content equal zero for the hydrothermal endmember.

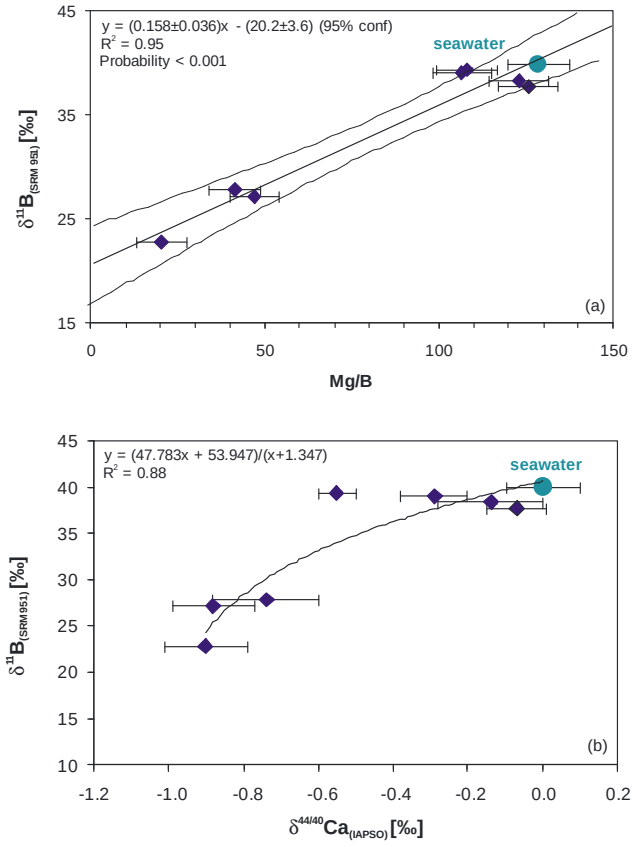

Fig. 3.4, **(a)** B isotope ratios are inversely correlated to the respective concentration values. **(b)** B versus Ca isotope ratios indicate a positive correlation.

In contrast to U and Mg, first boron isotope analyses ($\delta^{11}B$) listed in Tab. 3.1 seem to indicate a systematic between B concentrations and isotopes and in addition between $\delta^{11}B$ and $\delta^{44/40}Ca$ (Fig. 3.4). Boron isotope ratios are negatively correlated to the respective concentration values (Fig. 3.4a), while $\delta^{11}B$ and $\delta^{44/40}Ca$ are positively correlated showing binary mixing pattern between seawater and a hydrothermal fluid composition (Fig. 3.4b). Only sample 53ROV-B2 resembles a $\delta^{11}B$ value close to seawater despite of its relatively high fluid amount of 21 % and low Ca isotope composition. Endmember calculations using B concentrations yield for $\delta^{11}B$ a value of 20.5±3.6 ‰ relative to SRM 951. Using Ca isotope ratios, a $\delta^{11}B$ of 21.5±4.3 ‰ can be computed.

3.1.3 Total alkalinity (TA) and dissolved inorganic carbon (DIC)

The results for total alkalinity (TA) and dissolved inorganic carbon (DIC) are presented in Tab. 3.3. The alkalinity of the CTD samples as well as of the diffuse vent samples range between 2.0 and 2.3 mM, which is in accordance with the value of 2.33 yielded by IAPSO and assumed for surface ocean water. Hydrothermal fluid samples from smoking vent sites are decreased down to 0.5 mM for the samples with the highest fluid amount. Onboard determinations of alkalinity are consistent with the potentiometric analyses within 2 % (Tab. 3.3). For further discussion only the high-precision values are considered. Dissolved inorganic carbon (DIC) varies between 1 and 2.7 mM with ~2.2 mM for seawater (CTDs and IAPSO).

Carbonate ion concentrations [CO_3^{2-}] were calculated iteratively by the two parameters TA and DIC using the algorithm of Ware et al. (1991). Sensitivity and equilibrium constants for the CO_2-H_2O system were used from Millero (1995) and Millero et al. (2006) for the calculation of the equilibrium and dissociation constants K_0, K_W, K_1 and K_2. The dissociation constant K_B for the boron species was computed after Dickson (1990). From the carbonate ion concentrations the solubility product for calcite (K_{sp}^{cc}) was determined by the temperature-relation after Mucci (1983) (Tab. 3.3). Contributions of silicates and phosphates to the alkalinity are neglected.

Tab. 3.3, Measured alkalinity, DIC, respective salinity and pH values, and the hence deduced parameters carbonate ion concentration [CO_3^{2-}], solubility constant for calcite K_{sp}^{cc} and pH. Alkalinity was measured by two different methods for selected samples. The computed pH was compared to the pH measured immediately after the withdrawal of the samples.

Sample	fluid [%]	Ca [mM]	TA[1] (mM)	TA[2] [mM]	DIC [mM]	S [psu]	T [°C]	pH[3]	pH[4]	*[CO_3^{2-}] [mM]	†K_{sp}^{cc}
IAPSO	0	10.55		2.33		35	25	8.1			
217 CTD	0	10.55		2.216	2.218	34.2	2		8.04	0.1	0.42
231 CTD-8	0	10.55		2.288	2.201	33.7	2		8	0.073	0.76
224 ROV B15	72	24.7	0.527	0.562	2.459	31.6	225	4.9	4.97	0.0093	0.006
232 ROV-7 B9	0	11.4	2.011	2.283	2.196	33.6	225	7.8	5.85	0.17	0.007
249 ROV-7 B10	75	19	1.09	0.620	2.648	34.0	205	5.2	4.96	0.0094	0.015
261 ROV-6 B2	60	23.9		2.307	2.211	34.2	200		5.96	0.18	0.018
266 ROV-10 B8	67	30.4	0.585	0.659	0.989	32.9	300	5	5.08	0.003	0.003
277 ROV-4 B10	5	12.9		2.269	2.152	34.0	170	7.4	6.16	0.17	0.045
277 ROV-4 B8	4	11	2.289	2.253	2.233	33.8	170	7.5	6.11	0.16	0.044
281 ROV-2 B10	8	10.72	1.072	1.163	1.095	32.1	280	6.5	5.57	0.023	0.001
281 ROV-5 B2	51	20.88		1.424	1.817	57.2	280	6.5	4.59	0.085	0.011

[1]measured onboard by back titration
[2]measured by potentiometric titration
[3]measured onboard
[4]deduced by TA and DIC
*after Ware et al. (1991)
†after Mucci (1983)

3.2 The hydrothermal system in the 'Ascension area'

3.2.1 Ca and Sr isotope compositions of the fluids

The results for the hydrothermal fluids from the 'Ascension area' are reported in (Tab. 3.4). The diffuse outflow sample of Lilliput (200ROV-B11/13) displays expectedly in both, Sr and Ca isotopes as well as contents a seawater composition, because of its low fluid amount of 5 % deduced by Mg concentrations (Koschinsky et al., 2006).

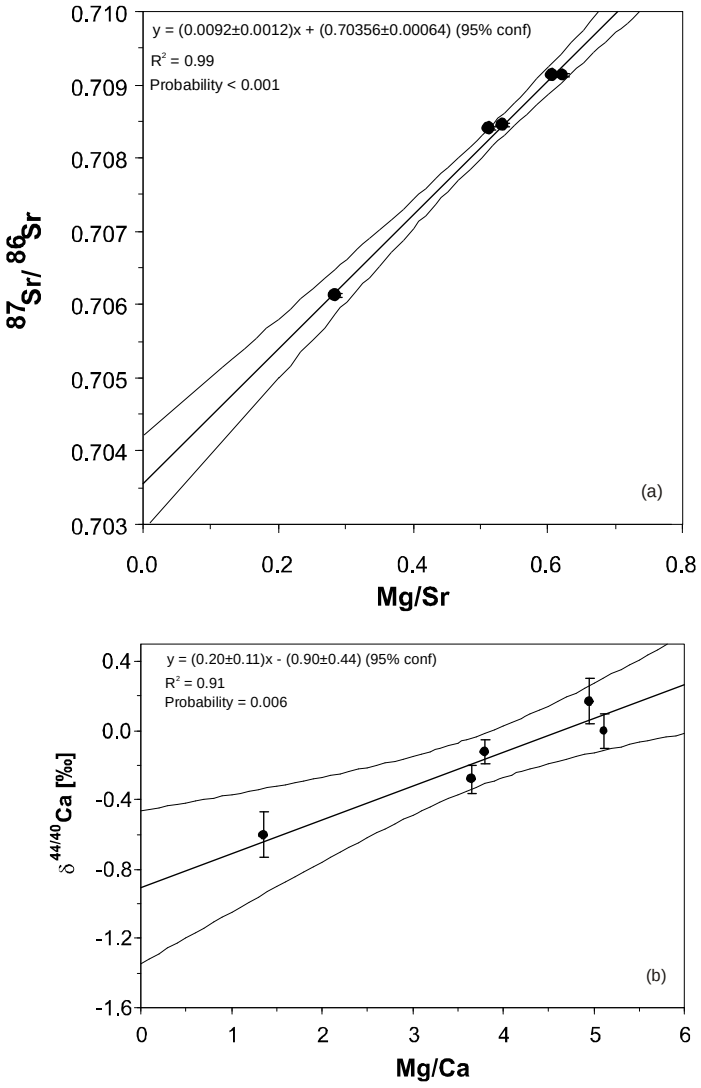

Fig. 3.5, **(a)** Sr isotope compositions in fluid samples from the hydrothermal field Red Lion at the MAR 5°S. **(b)** The fluid samples exhibit a Ca endmember composition close to that of the Logatchev field (Ch. 3.1). The small sample number results in relatively large statistical uncertainties.

The fluids taken at Red Lion cover a wide range of mixing proportions between seawater and hydrothermal fluid from almost pure seawater to up to 65 % pure hydrothermal fluid. Sr contents and radiogenic Sr isotope ratios at Red Lion are inversely correlated and lead to a composition for the hydrothermal endmember of 56±9 µM and a $^{87}Sr/^{86}Sr$ of 0.7035(1) (at 95 % confidence level) when extrapolating Mg/Sr to zero (Fig. 3.5a). This is also the case for Ca. Binary mixing calculations point to a Ca content of 16±1 mM with an isotopic composition of $\delta^{44/40}Ca_{(SW)}$ = -0.90±0.44 % (Fig. 3.5b).

Similar to Red Lion, the three samples from Turtle Pits provide 63 % fluid amount. But in contrast, endmember calculations yield for the hydrothermal endmember a Sr concentration of 31±2 µM and a $^{87}Sr/^{86}Sr$ of 0.7069(1) (at 95 % confidence level), and a Ca content of 9.5±1.5 mM with a $\delta^{44/40}Ca_{(SW)}$ of -0.65±0.58 ‰ (Fig. 3.6a).

The two samples from Wideawake represent diffuse effluents and are consistent in their Ca and Sr composition with the seawater salinity reference IAPSO (Tab. 3.4).

Tab. 3.4., Ca and Sr compositions of the hydrothermal fluid samples from the 'Ascension area'.

sample ID	site	fluid amount* [%]	Mg conc. [mM]	Ca conc. [mM]	Sr conc. [µM]	$^{87}Sr/^{86}Sr$	$\delta^{44/40}Ca_{(SW)}$ [‰]	2sem	*n*
IAPSO		0	54	10.55	87	0.70913	0	0.04	*135*
Ascension area									
MARSÜD									
114 ROV N2	TURTLE PITS	0	54.3	10.5	87.5	0.70914	0.16	0.07	*5*
123 ROV-B11	TURTLE PITS	15	46.1	40.1	79.5	0.70898	0.02	0.06	*5*
141 ROV-11	TURTLE PITS	63	20.1	10	52	0.70827	-0.35	0.07	*5*
125 ROV B11	WIDEAWAKE	14	47	10	78	0.70914	0.23	0.04	*3*
125 ROV-13	WIDEAWAKE	10	49	10	81	0.70913	0.16	0.12	*4*
146 ROV-B1	RED LION	3	52.5	10.6	86.4	0.70914	0.17	0.13	*4*
146 ROV-B9+10	RED LION	65	19	14	67	0.70612	-0.60	0.13	*5*
146 ROV-B11	RED LION	20	43.1	11.8	83.9	0.70840	-0.28	0.08	*5*
146 ROV-B12	RED LION	17	44.9	11.8	84.3	0.70845	-0.12	0.07	*5*
200 ROV-B11+13	LILLIPUT	5	51	10	86	0.70914	0.06	0.05	*5*

*deduced after Mg concentrations

The results of the hydrothermal fluid endmembers are burdened with large uncertainties due to the small number of samples available, enhancing the statistical variability and diminishing thus the confidence interval of the regression line. In order to further constrain the endmember values, analyses of more samples are required. However, the extrapolated endmember values should be considered as preliminary results and a basis for discussing hydrothermal circulation at the MAR 5°S.

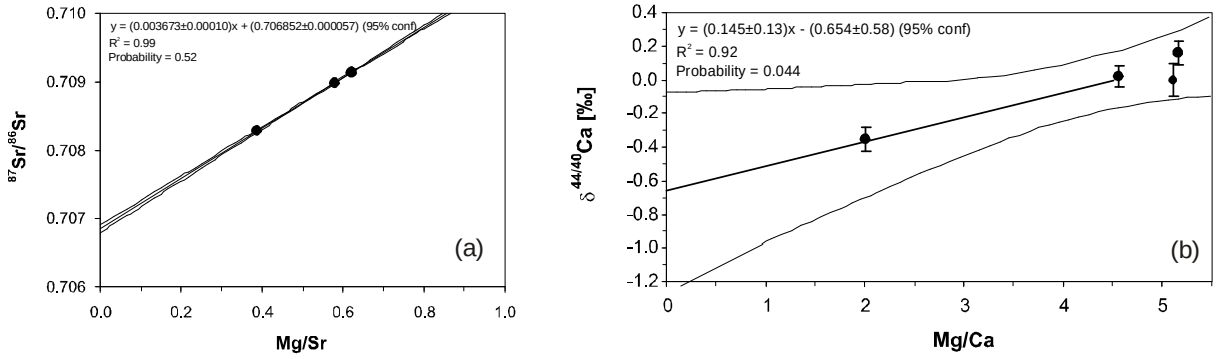

Fig. 3.6, **(a)** Determination of the Sr isotope endmember in fluids from the Turtle Pits vent field. An endmember value of $^{87}Sr/^{86}Sr = 0.70685$ is calculated. **(b)** Preliminary data for the Ca isotope ratios in phase-separated fluids from Turtle Pits at the MAR 5°S indicate a fluid endmember $\delta^{44/40}Ca_{(SW)}$ value of around -0.65‰.

3.2.2 Ca and Sr isotope ratios in anhydrites and basalts

The Ca isotope analyses of the two basaltic glass samples (109 GTV-1 and –2) from Turtle Pits (Tab. 3.5) show an error-weighted average value of -0.97±0.04 ‰ (2sem) being well-consistent with the currently existing average value for MORB ($\delta^{44/40}Ca_{MORB}$ = -0.98±0.07 ‰; Skulan et al., 1997; Zhu & Macdougall, 1998; Richter et al., 2003). Both samples display a Sr isotope composition of 0.70244 as commonly assumed for mid-ocean ridge basalts (MORB).

The anhydrite samples from Turtle Pits show $\delta^{44/40}$Ca values between -0.9 and -1.37 ‰ relative to seawater. Their Sr isotope ratios cover a narrow range of 0.7060 to 0.7079 (Tab. 3.5). The Sr isotope compositions of the anhydrites infer precipitation from solutions containing 50 to 80 % hydrothermal fluid. Interestingly, the $^{87}Sr/^{86}Sr$ values of the samples 123ROV-4A and 130ROV-1C are lower than the endember value determined for the hydrothermal fluids from Turtle Pits.

Tab. 3.5, Results for the Ca and Sr isotopic compositions in rock samples and anhydrites from the Turtle Pits vent field at MAR 5°S, and the anhydrite formation temperatures estimated by isenthalpic mixing using Sr isotopes.

sample ID	T* [°C][1] ($^{87}Sr/^{86}Sr$)	$^{87}Sr/^{86}Sr$	$\delta^{44/40}Ca_{(IAPSO)}$ [‰]	2sem	*n*
MAR 5°S					
anhydrites					
114 ROV-5B	216	0.70737	-0.95	0.07	*4*
123 ROV-4A	310	0.70602	-1.07	0.06	*5*
123 ROV-4C1	156	0.70796	-1.16	0.04	*4*
130 ROV-1C	262	0.70682	-0.90	0.12	*4*
139 GTV-4A3	175	0.70778	-1.37	0.10	*4*
139 GTV-4C3	162	0.70790	-1.14	0.03	*3*
basalts					
109 GTV-1		0.70212	-0.95	0.10	*5*
109 GTV-2		0.70277	-0.98	0.05	*4*

[1]calculated by isenthalpic mixing indicated by Sr isotope ratios (Bach, pers. comm.)

3.3 Compilation of $\delta^{44/40}$Ca in various rock materials

3.3.1 Chemical treatment

Since the spike was added after digestion, the total recovery of Ca during decomposition of silicates is essential for further analytical processing. The two dissolution procedures, $Diss_{HF}$ and $Diss_{HBr}$ were applied in order to monitor the release of Ca from silicate rocks and the effect of chemical pretreatment on the Ca isotope compositions. The results are contrasted in Fig. 3.7 and Tab. A3 in the Appendix.

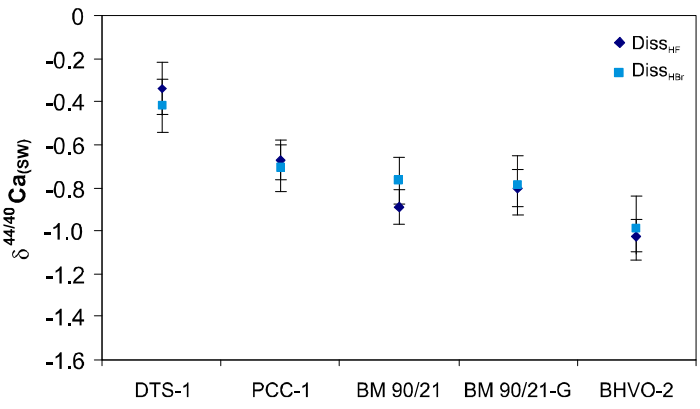

Fig. 3.7, Contrasting two digestion experiments. $Diss_{HF}$ is a commonly used HF/HNO_3 attack used for the decomposition of silicates. In $Diss_{HBr}$ the cations were leached by HBr in prior of the $HF\text{-}HNO_3$ treatment. The results for both procedures overlap within the error limits and show no affection of sample dissolution on the Ca isotope ratios. Error bars indicate 2sem.

The Ca isotopic compositions of both digestion experiments, $Diss_{HF}$ and $Diss_{HBr}$ overlap within 2sem for all of the samples. Because $Diss_{HBr}$ yielded same results as $Diss_{HF}$, artifacts from Ca isotope fractionation during CaF_2-formation can be excluded. The good agreement of the values obtained from $Diss_{HF}$ and $Diss_{HBr}$, (Fig. 3.7) shows that sample dissolution does not contribute significantly to the observed variations of Ca isotope ratios. In addition, the value of $IAPSO_{diss}$ showing the same value as the untreated aliquots of IAPSO (Tab. A3) affirms that no significant isotope effects are evoked by the dissolution procedures used here.

Sparsely soluble minerals in the ultramafic samples (e.g. BM90/21) might not be decomposed entirely. The consistency between the Ca isotope ratios in BM90/21 and its entirely dissolved glassy counterpart BM90/21-G (Fig. 3.7; Tab. A3) shows that accessory refractory minerals such as spinels do not contribute significantly to the Ca content and isotopic composition of the sample.

Since the samples were spiked in prior to chemical separation, reported isotope fractionation during ion exchange chromatography (e.g. Heumann & Lieser, 1972; Russell & Papanastassiou, 1978) can be neglected. A critical point during column chemistry is an appropriate separation of Ca from K and Sr. For each sample the chromatographic element separation was checked by an elution scheme. Although interferences of K^+ and doubly charged Sr ions are improbable in our TIMS measurements, the Ca peak tails were cut generously on both sides in the chromatograms and a relatively pure Ca phase was collected. Thereby, the total Ca yield was diminished to ~80 %. By this proceeding, large overlaps with adjacent elements in particular Mg, K and Sr is obviated.

Tab. 3.6, Two aliquots of the basalt BHVO-2 was dissolved directly by HF-HNO_3 ($Diss_{HF}$) attack and once by a pretreatment with HBr ($Diss_{HBr}$). Aliqouts of the respective dissolved solutions were processed through different column separations (a-c) and the single values for $\delta^{44/40}Ca_{(SW)}$ are compared.

BHVO-2	$\delta^{44/40}Ca_{(SW)}$ ± 2sem		
column batches	**a**	**b**	**c**
$Diss_{HF}$ 1	-1.01 ± 0.15	-1.06 ± 0.17	-1.02 ± 0.21
$Diss_{HF}$ 2	-1.22 ± 0.22	-0.91 ± 0.11	-0.96
$Diss_{HBr}$ *	-1.15 ± 0.27	-0.91 ± 0.02	-1.08

* blank corrected

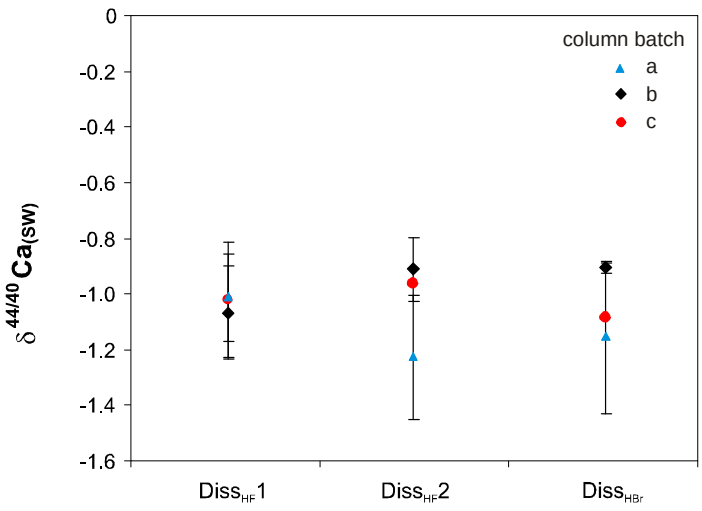

Fig. 3.8, Comparison of different column separation throughputs to test statitstical variability of Ca isotopes. As an example sample BHVO-2 was processed through three different column runs. Intra-column variations are consistent to inter-column variations. Analytical uncertainties are indicated as 2sem.

A minimum of 3 separate elutions for each sample was carried out in order to test reproducibility of the column chemistry. The results deriving from different chromatographic throughputs do not show a systematic variability. Tab. 3.6 lists the single values for the sample BHVO-2 as an example. Subsamples of BHVO-2 were digested twice, once by $Diss_{HF}$ and once by $Diss_{HBr}$ and processed through independent column procedures (Tab. 3.6; Fig. 3.8). Analyses of variance show that variances between the single values do not exceed the reproducibility of the measurements ($p = 0.38$). In addition, as during each procedure IAPSO was processed parallel to the samples, and since all data are normalized to the corresponding IAPSO values, systematic offsets between the individual sessions are largely canceled out. It can be concluded that the chemical processing applied in this study does not significantly affect the Ca isotopic compositions of the samples.

3.3.2 Homogeneity

Tab. 3.7 lists the $\delta^{44/40}Ca_{(SW)}$ of 4 MPI-DING reference glasses and their respective original powders. Except for ML3B, no significant differences can be observed between the $\delta^{44/40}Ca_{(SW)}$ of the sample powders and their quenched products (Fig. 3.9). This is to be expected as no flux agents were used for the fusion of the glasses, except for pure SiO_2 that was added to BM90/21. Therefore, the only potential sources of contamination were the components of the crucible and the furnace consisting of Pt, ZrO_2 and $MoSi_2$ (Jochum et al., 2000).

Tab. 3.7, The MPI-DING reference glasses were analyzed for their Ca isotope compositions and contrasted to their original powders. Disregarding ML3B, no variations caused by the fusion process can be detected within the analytical uncertainties. For ML3B, analysis of variance shows a significant variation at the 98 % level between the reference glass and its original powder.

	MPI-DING glass				original powder				
sample ID	**$\delta^{44/40}Ca_{(SW)}$**	**2sem**	***n***	**variance**	**$\delta^{44/40}Ca_{(SW)}$**	**2sem**	***n***	**variance**	**p-value**
StHs6/80	-1.07	0.09	*16*	0.03	-1.14	0.10	*6*	0.02	0.27
T1	-0.99	0.06	*14*	0.01	-1.10	0.07	*6*	0.01	0.05
KL2	-1.12	0.06	*15*	0.01	-1.17	0.07	*6*	0.01	0.38
ML3B	-1.11	0.07	*17*	0.03	-1.28	0.13	*6*	0.02	0.02
BM 90/21	-0.86	0.18	*16*	0.02	-0.87	0.06	*21*	0.02	0.21

The $\delta^{44/40}Ca_{(SW)}$ values in sample ML3B and its glassy counterpart, however, are significantly different at the 98 % significance level (ANOVA). It should be noted that heterogeneities in ML3B-G have been also reported for Cr isotopes due to the formation of Cr-rich 'islands' during quenching (Jochum et al., 2000). A similar effect has been anticipated for variations of Ca isotope ratios measured by TIMS. During evaporation of the sample on the filament, mixing/unmixing processes lead to the formation of isotopically heterogeneous reservoirs (Hart & Zindler, 1989). This effect might have been occurred during quenching of the MPI-DING glass ML3B-G evoking the exhibited Ca isotope difference to the original material.

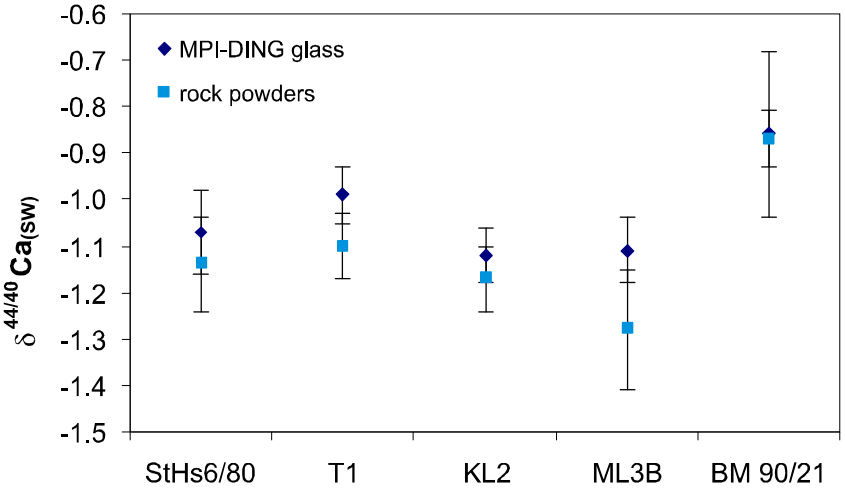

Fig. 3.9, MPI-DING reference glasses are compared to their original rock powders. Except for ML3B, all of the samples are identical within the error limits (2sem) in their Ca isotope compositions. A contamination or a formation of isotope heterogeneities during the fusion process can be excluded. For ML3B a significant difference between the rock powder and its glassy equivalent could be detected by analysis of variance. See text for further explanation.

Homogeneity is an important requirement for geological reference materials. In particular, in situ-microanalytical work demands highly homogeneous reference standards. The suite of the MPI-DING reference glasses was subject to many detailed studies demonstrating that they are homogeneous with regard to most elements and isotope systems in the µm-scale (e.g. Jochum et al., 2000; Jochum et al., 2006). With regard to the above-mentioned potential formation of isotopic reservoirs (Hart & Zindler, 1989), the homogeneous distribution of the Ca isotopes of the samples have been checked in two different mm-sized glass shards.

Both glass splits were digested and prepared independently but measured within the same analytical run, in order to preclude instrumental bias. In order to monitor the chemical preparation, aliquots of the well-established Hawaiian basalt BHVO-2 and the BIR-1 proven to be well-homogenized for their elemental and most isotopic systems (Wilson, 1997; Flanagan, 1984) were processed in addition to the MPI-DING glasses. The resulting $\delta^{44/40}Ca_{(SW)}$ values and the relative standard errors between both splits are reported in Tab. A4 in the Appendix and are illustrated below in Fig. 3.10.

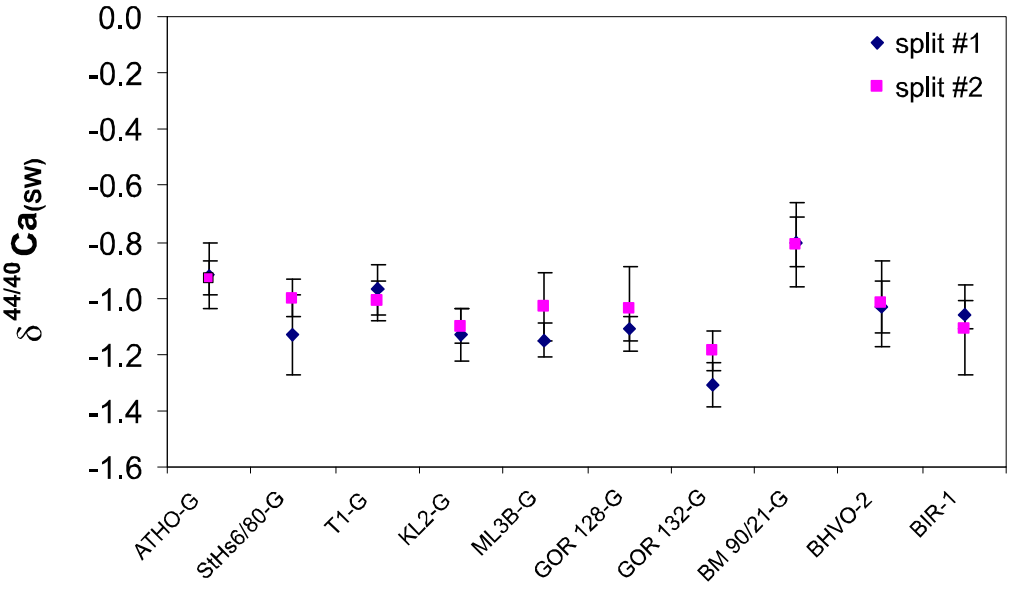

Fig. 3.10, Test for the homogeneity of the MPI-DING reference glasses. $\delta^{44/40}Ca$ of two different glass splits (#1 and #2) were measured independently. Variances between the glass splits are smaller than the analytical uncertainty.

Analyses of variance (ANOVA) were carried out in order to test for the homogeneity of the samples (Tab. A4). Thereby, GOR132-G and ML3B-G show the highest variability between the glass splits, StHs6/80-G is probably homogeneous within the given analytical uncertainty (Fig. 3.10). Generally, it can be shown that the probability for homogeneity exceeds 95 % for all samples (Tab. A4). Hence, it can not be stated that the MPI-DING glasses are inhomogeneous with regard to their Ca isotope compositions. The analytical precision does not allow detecting any Ca isotope variability in the MPI-DING reference glasses.

3.3.3 Leaching experiments

In general, the Ca isotope compositions of the carbonate and silicate fractions of both carbonatite samples range between -0.97 and -1.17 ‰ and are consistent with previously reported whole rock analyses of carbonatites (-1.1± 0.4 ‰; Russell et al., 1978) and the $\delta^{44/40}Ca$ values of basaltic samples (Tab. 3.11; cf. DePaolo, 2004).

However, while the $\delta^{44/40}Ca$ values of the carbonate and silicate phases from the calcio-carbonatite 83HV26 are identical within the analytical error, the magnesio-carbonatite shows a significant difference of 0.2 ‰ between its silicate and carbonate fraction. Thereby, the carbonatic leachate agrees with the calcio-carbonatite. The Ca isotope composition of the silicate residue, however, is ~0.2 ‰ heavier (Tab. 3.11).

3.3.4 Information values

One aim of this study is to provide information on the Ca isotope compositions of various rock materials. This work reports preliminary information values for $\delta^{44/40}Ca_{(SW)}$ of the investigated rock samples. The data are summarized together with the respective $\varepsilon^{44/40}Ca_{(SW)}$, the reference values for the Ca and Mg concentrations, and the K/Ca ratios in Tab. 3.11. The proposed values are calculated by averaging all measured values obtained from the different experiments. Uncertainties are indicated as two standard errors of the mean (2 sem). All of the values were determined with an uncertainty of less than 0.1 ‰ (2 sem), except for StHs6/80 and ML3B. The latter shows with a 2 sem of 0.13 ‰ the largest uncertainty.

Currently existing data about the Ca isotope compositions of volcanic rocks point to a mean $\delta^{44/40}Ca_{(SW)}$ of around -0.95±0.2 ‰ (cf. DePaolo, 2004). The volcanic rocks analyzed in this study fit in this range. The ocean island basalts ML3B and KL2 and the respective MPI-DING glasses (ML3B-G and KL2-G) exhibit $\delta^{44/40}Ca_{(SW)}$ values ranging between -1.28±0.13 ‰ and -1.11±0.07 ‰. They agree with the tholeiitic basalts provided as reference materials by the USGS, BHVO-2, BCR-2 and the Icelandic basalt BIR-1. Confirming previous results (cf. DePaolo, 2004), the Ca isotope compositions of the felsic samples, ATHO-G and StHs6/80 and accordingly StHs6/80-G matches with the $\delta^{44/40}Ca_{(SW)}$ values of the mafic samples. This is also the case for TML, T1 and T1-G, the diabase W-2, the carbonate and the silicate phases of both carbonatites 82LM66A and 83HV26, and the two Cretaceous-Tertiary komatiites from the Gorgona Island GOR128-G and GOR132-G (Tab. 3.11).

In contrast, both Archean komatiites of the Onverwacht group are 0.3 ‰ heavier than their younger counterparts. The Archean komatiites are consistent to the values obtained for the peridotite BM90/21 and its glassy equivalent. While the peridotite PCC-1, with a $\delta^{44/40}Ca_{(SW)}$ value of -0.72±0.07 ‰, is only slightly heavier in its Ca isotope composition, the dunite DTS-1 and the Carrara marble are significantly enriched in ^{44}Ca compared to all other samples analyzed in this study. The value for the Carrara marble agrees reasonably well with the previously reported $\delta^{44/40}Ca_{(SW)}$ of -0.38 ± 0.1 ‰ determined on MC-ICPMS by Halicz et al. (1999) and renormalized to IAPSO with a $\Delta^{44/40}Ca_{(SW-SRM915a)}$ of 1.88 ‰ (Hippler et al., 2003).

The K/Ca ratios and the radiogenic Ca isotope ratios show that none of the samples investigated here are affected by an excess of ^{40}Ca from the decay of ^{40}K (Tab. 3.11). Neither the Archaen komatiites of the Onverwacht group nor sample ATHO-G with a high K/Ca ratio exhibit a detectable ^{40}Ca excess (Tab. 3.11). The data show that the differences in the Ca isotopic compositions between different rock types are intrinsically tied to mass-dependent fractionation.

Tab. 3.11, Preliminary Ca isotope information values for the rock samples analyzed in this study. The Ca, Mg and K contents are taken from GeoReM database (http://georem.mpch-mainz.gwdg.de).

sample	rock type	$\delta^{44/40}Ca_{(SW)}$	2sem	n	$\varepsilon^{40/44}Ca_{(SW)}$	2sem	CaO conc. [wt%]	MgO conc. [wt%]	K/Ca
commonly used references									
NIST SRM 915a	calcium carbonate	-1.82	0.03	143	0.2	1.8			
IAPSO	seawater	0	0.03	135	0.0	1.0			
MPI-DING glasses									
ATHO-G	rhyolite	-0.93	0.07	13	0.6		1.7	0.103	0.901
St. Hs6/80-G	andesitic ash	-1.07	0.09	16	0.3		5.28	1.97	0.142
T1-G	quartz diorite	-0.99	0.06	14	0.3		7.1	3.75	0.160
KL2-G	tholeiite - Kilauea	-1.12	0.06	15	1.1	1.5	10.9	7.34	0.026
ML3B-G	tholeiite - Mauna Loa	-1.11	0.07	17	1.2	1.4	10.5	6.59	0.021
GOR 128-G	komatiite (Cret-Tert)	-1.09	0.08	13	1.5	2.0	6.24	26	0.003
GOR 132-G	komatiite (Cret-Tert)	-1.25	0.06	11	1.9	2.4	8.45	22.4	0.002
BM 90/21-G	peridotite	-0.81	0.06	16	1.2	2.3	2.1	34.3	0.001
original rock powders									
StHs6/80	andesitic ash	-1.16	0.11	6				1.97	
T1	quartz diorite	-1.1	0.07	6				3.75	
KL2	tholeiite - Kilauea	-1.17	0.07	6				7.34	
ML3B	tholeiite - Mauna Loa	-1.28	0.13	6				6.59	
BM 90/21	peridotite	-0.87	0.06	21				34.3	
USGS reference materials									
BHVO-2	tholeiitic basalt	-1.03	0.07	20	1.1	1.6	11.4	7.23	0.026
BIR-1	tholeiitic basalt	-1.08	0.07	14			13.4	9.7	0.001
BCR-2	tholeiitic basalt	-0.99	0.04	6			7.12	3.59	0.146
W-2	diabase	-0.94	0.11	6			10.87	6.37	0.033
DTS-1	dunite	-0.4	0.09	15			0.17	49.59	0.003
PCC-1	peridotite	-0.72	0.07	13			0.54	42.9	0.011
other certified materials									
TML	table mountain latite	-1.14	0.07	6					
IAEA-CO1	Carrara marble	-0.54	0.07	14					
non-certified rock samples									
Onverwacht 5019	komatiite (~3.5 Ga)	-0.87	0.05	6	0.3		2.34	34.96	0.005
Onverwacht 5031	komatiite (~3.5 Ga)	-0.86	0.05	6	0.5		3.37	31.99	0.009
82 LM 66A (Res)[+]	magnesiocarbonatite	-0.97	0.02	6			38.7	9.55	0.000
82 LM 66A (Cc)[†]	Carbonate phase	-1.17	0.05	6					
83 HV 26 (Res)[+]	calciocarbonatite	-1.15	0.04	6			48.6	3.56	0.006
83 HV 26 (Cc)[†]	Carbonate phase	-1.09	0.06	6					

[+] Residue after leaching the material, corresponding to the silicate phase
[†] Carbonate phase after leaching the whole rock powder with HCl

4. Discussion

4.1 $\delta^{44/40}$Ca variations along the hydrothermal pathway of LHF

4.1.1 The Ca isotope compositions of hydrothermal fluids

During its circulation through mid-ocean ridge basement, seawater experiences successive chemical modifications at temperatures of > 400 °C, and pressures of 500 bar (e.g. Von Damm, 1995; Seyfried and Ding, 1995; Fig. 1.3; Fig. 4.1). Ca and Sr contents and isotope compositions, specifically, are changing along the fluid flow path as a result of exchange reactions with the host-rocks and precipitation of hydrothermal minerals such as anhydrite and calcium carbonates.

In the downflow zone, seawater-Mg ($[Mg]_{SW}$) is lost from the fluid to hydrous Mg-silicates forming in the basement. This Mg loss is largely balanced by the continued release of Ca from the basement to the interstitial water (c.f. Mottl & Wheat, 1994; Berner & Berner, 1996; Wetzel & Shock, 2000). If all the $[Mg]_{SW}$-loss were compensated by the release of Ca from the host-rocks, the Ca content ($[Ca]_{initial}$) in the fluid would increase by 54 mM from 10 mM in seawater to 64 mM (Fig. 4.1). Fluid-mineral reactions, however, buffer Ca concentrations in the fluid at elevated temperatures. For instance, at temperatures above ~140 °C, a fraction of the dissolved Ca, and nearly the entire seawater-sulfate $[SO_4^{-2}]_{SW}$, is lost from the fluid due to the precipitation of anhydrite (Fig. 4.1). Secondary Ca-bearing minerals such as amphiboles and Ca-silicates also affect the Ca content of the hydrothermal fluid endmember $[Ca]_{HydEnd}$. The actual $[Ca]_{HydEnd}$ at peak pressure and temperature conditions is hence the result of fluid-mineral phase equilibrium in the rock-dominated part of the hydrothermal fluid path. Coupled to these reactions that control the sizes of the Ca and Sr pools in the fluids and are strongly affected by temperature and water-to-rock ratios is the isotope exchange of Ca and Sr that accompanies the fluid evolution (e.g. Bickle & Teagle, 1992). After passing the recharge and reaction zone the hydrothermal solution shows clear chemical and isotopic characteristics distinctively different from its original seawater composition.

During its ascent in the discharge zone, the hydrothermal fluid cools adiabatically, and potentially also due to conductive cooling (e.g. Seewald & Seyfried, 1990), and/or subseafloor mixing with entrained seawater (e.g. Tivey et al., 1995). Along the fluid flow pathway in the discharge zone $[Ca]_{HydEnd}$ may become further depleted due to precipitation of anhydrite and calcium carbonates. The Sr and Ca isotopic evolution of the hydrothermal solution in the discharge zone may be expected to change along binary mixing lines between seawater and hydrothermal fluid, if continued water-rock interactions in the upflow zone can be neglected.

As a consequence of the entrainment of seawater during sampling, the Sr and Ca isotope systematics determined in this study for the Logatchev hydrothermal field (LHF) indeed reflect binary mixing implying a two-component mixing of seawater (SW) as one and hydrothermal fluid (HydEnd) as the other endmember. The extrapolated hydrothermal fluid endmember is characterized by a low Sr isotope composition ($^{87}Sr/^{86}Sr$ = 0.7034(4); Fig. 3.1b), which closely resembles rocks from reaction and upflow zone sampled by the Ocean Drilling Program (e.g. Alt & Teagle, 2000).

The Ca concentration in the hydrothermal fluid ($[Ca]_{HydEnd}$ = 32 mM) is enriched relative to the original $[Ca]_{SW}$ concentration by about 22 mM achieved from leached host-rocks by an exchange with seawater-Mg ($[Mg]_{SW}$ = 54 mM). The difference of 22 mM to the expected maximum Ca concentration of 54 mM by an equimolar exchange with $Mg]_{SW}$ is mainly due to the precipitation of anhydrite and calcium carbonate during fluid ascent in the discharge zone (Fig. 4.1). For simplicity this approach ignores Ca buffering by fluid-mineral equilibria involving Ca-silicates.

Binary mixing calculations between seawater and the hydrothermal fluid (Fig. 3.1) result in a Ca isotopic composition of $\delta^{44/40}Ca_{HydEnd}$ of -0.95±0.07 ‰ (95 % confidence) for the fluid endmember. This value is in good agreement with the published value of -0.96±0.19 ‰ (2sd) by Schmitt et al. (2003a) implying a homogeneous Ca isotope composition for hydrothermal fluids. The good agreement between the hydrothermal endmember and the commonly assumed value for the Bulk Earth of -0.92 ± 0.18 ‰ (Skulan et al., 1997) and the Ca isotope data available for Mid-Ocean Ridge Basalt (MORB) ($\delta^{44/40}Ca_{MORB}$ = -0.98±0.07 ‰; Skulan et al., 1997; Zhu & Macdougall, 1998; Richter et al., 2003) apparently confirm the common assumption that no significant isotopic fractionation occurs between hydrothermal fluids and oceanic crust (Zhu & Macdougall, 1998; Schmitt et al., 2003a). However, the results for the hydrothermal anhydrites investigated in this study lead to a reconsideration of this assumption.

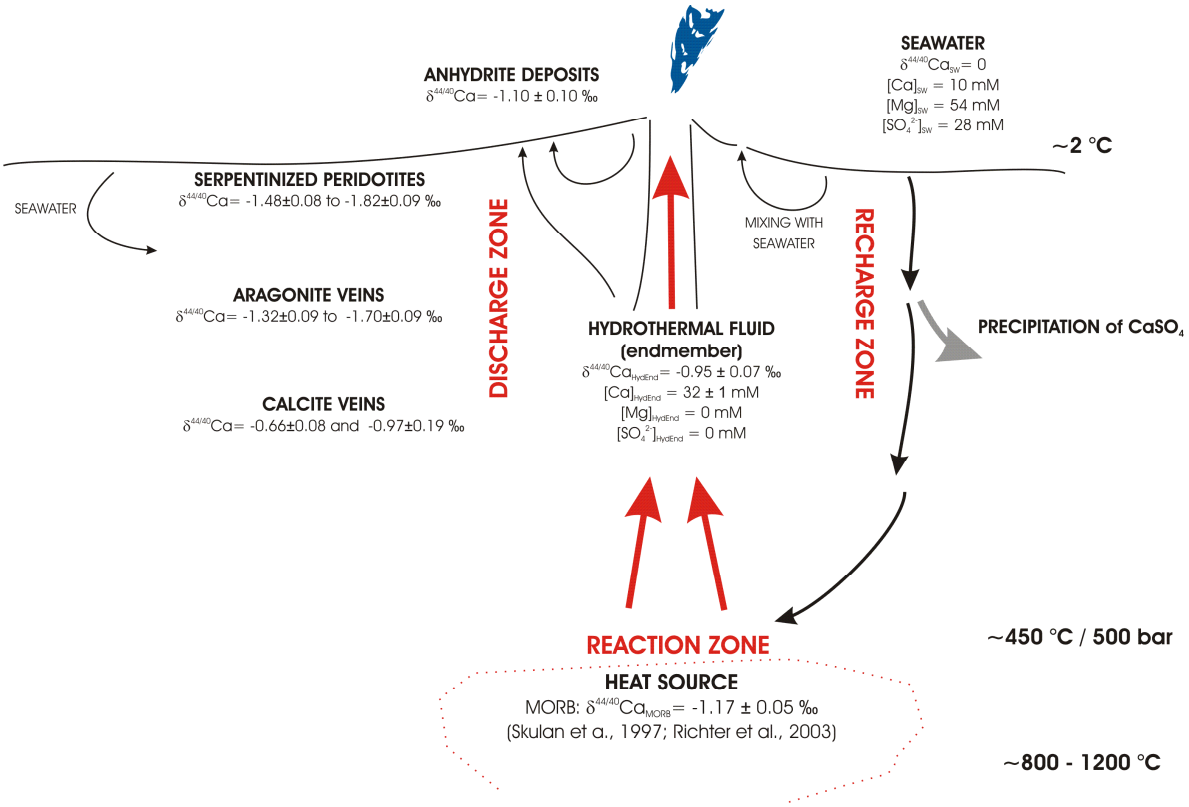

Fig. 4.1, Schematic illustration of the Ca isotope systematic within the Logatchev hydrothermal cell. Seawater entraining the oceanic crust along the recharge zone is chemically modified on the way down to the reaction zone and is then pouring through as hydrothermal fluid along the discharge zone before exciting on the seafloor. Thereby seawater passes various temperature and pressure conditions and interacts with different rock phases most likely MORB. During upwelling the hydrothermal fluid is admixed with ambient seawater in the discharge zone, while anhydrite and calcium carbonate polymorphs are precipitating.

4.1.2 Ca isotope fractionation in hydrothermal anhydrites from LHF

The $^{87}Sr/^{86}Sr$ ratio of 0.7053 for anhydrite sample 35GTV-7/4 reflects precipitation from a mixture of 59 % hydrothermal fluid and 41 % seawater. From the $^{87}Sr/^{86}Sr$-$\delta^{44/40}Ca$ relationship in hydrothermal solutions (Fig. 3.1c) and under the assumption that there is no isotopic difference between hydrothermal solution and anhydrite precipitate the $^{87}Sr/^{86}Sr$ ratio of 0.7053 corresponds to a $\delta^{44/40}Ca_{(SW)}$ value of -0.77±0.08 ‰ for sample 35GTV-7/4 (Fig. 3.1c). The same approach applied to sample 64ROV-10C points to a $\delta^{44/40}Ca_{(SW)}$ value of -0.46±0.04 ‰ for the parental solution (Fig. 3.1c). In contrast, the isotope analyses of the anhydrite samples yielded a $\delta^{44/40}Ca_{(SW)}$ value of -1.10±0.14 ‰ for 35GTV-7/4 and -1.08±0.08 ‰ for 64ROV-10C (Tab. 3.2). Hence, the Ca isotopic composition of sample 35GTV-7/4 is fractionated by $\Delta^{44/40}Ca_{HydFluid\text{-}Anh}$ = -0.33±0.16 ‰ from its parental solution, and sample 64ROV-10C exhibits a $\Delta^{44/40}Ca_{HydFluid\text{-}Anh}$ of -0.62±0.09 ‰. Both values yield an error-weighted mean of $\Delta^{44/40}Ca_{HydFluid\text{-}Anh}$ = -0.55±0.08 ‰ that can be considered as an overall isotope fractionation during anhydrite precipitation within the Logatchev hydrothermal system. However, isotope fractionation depends on information about the magnitude and the physico-chemical conditions of the precipitation process. Therefore, the two samples analyzed here might not be representative for the anhydrite budget of the Logatchev field.

Temperature-dependency of Ca isotope fractionation in anhydrites

Ca isotope fractionation is supposed to be a function of temperature and precipitation rate (Gussone et al., 2003; Lemarchand et al., 2004; Böhm et al., 2006). Up to now, no $\Delta^{44/40}Ca_{Fluid\text{-}Min}$-temperature correlation for anhydrite is reported. The only information about the temperature for the anhydrite samples analyzed in this study is the temperature range of 96-106 °C measured onsite in retrieved mud, where sample 35GTV-7/4 were imbedded (Kuhn et al., 2004). However, a precipitation temperature of ~110 °C is lower than commonly assumed formation temperature of anhydrite from fluids with seawater-like compositions (~140°C).

The formation temperatures of hydrothermally precipitated anhydrite samples can be computed from the mixing proportions between seawater and hydrothermal fluid as indicated by the Sr isotope systematics and assuming that the fluid has conserved enthalpy during its ascent (Bischoff & Rosenbauer, 1985; Humphris & Bach, 2005). Thermodynamic data for 3.2 wt% NaCl solutions and 300 bar from Bischoff and Rosenbauer (1985) yield isenthalpic mixing temperatures (T*) of 234 °C for the anhydrite sample 35GTV-7/4 and 113 °C for 64ROV-10C (Tab. 3.2). The T*-values are positively correlated to the measured Ca isotope fractionations ($\Delta^{44/40}Ca_{HydFluid\text{-}Anh}$) of both samples (Fig. 4.2). Including the $\Delta^{44/40}Ca_{Fluid\text{-}Anh}$ value of -1.0±0.2 ‰ at 40 °C reported by Hensley and Macdougall (2003) and with respect to the subsequent temperature interval of 40°<T<300 °C, the isotope fractionation follows a linear $1/T^2$-relationship and can be described by $1000\ln(\alpha) = -94707/T^2 - 0.0399$ between $\Delta^{44/40}Ca_{Fluid\text{-}Anh}$ and the formation temperatures (Fig. 4.2) following a $1/T^2$–correlation. The linear T*-$\Delta^{44/40}Ca_{HydFluid\text{-}Anh}$ behaviour is also consistent to the fractionation-temperature relationships assumed for aragonite and calcites (Gussone et al., 2003; Marriott et al., 2004) (Fig. 4.3a).

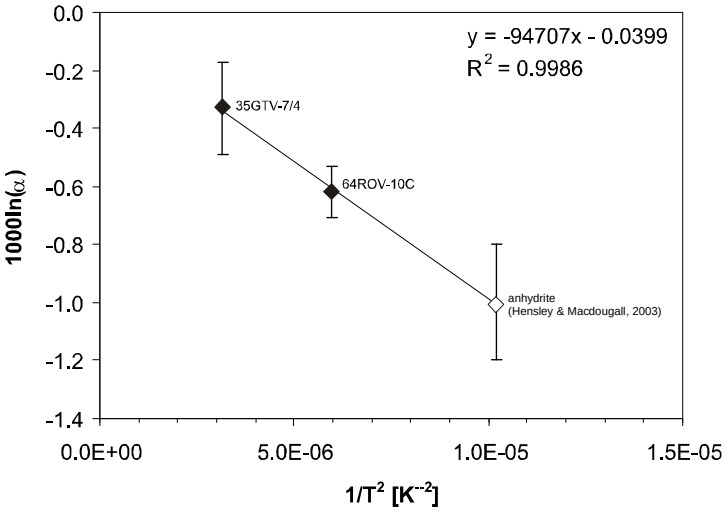

Fig. 4.2, The $\Delta^{44/40}$Ca values of the anhydrite samples 35GTV-7/4 and 64ROV-10C are plotted together with a value from Hensley and Macdougall (2003) as a function of temperature. Precipitation temperatures for the measured anhydrite samples are calculated from the assumption of isenthalpic mixing of seawater with the hydrothermal fluid (Bischoff & Rosenbauer, 1985).

However, it should be noted that isenthalpic based temperatures (T*) also depend on information on conductive cooling of the hydrothermal fluid or conductive heating of seawater in the subseafloor mixing zone, which are not available in detail. Therefore, these T*-values are burdened with larger uncertainties.

As Ca isotope fractionation most likely depends besides temperature in addition on the precipitation rate (Lemarchand et al., 2004; Böhm et al., 2006), the observed temperature-$\Delta^{44/40}Ca_{HydFluid\text{-}Anh}$ relation in the anhydrite samples may also reflect the retrograde solubility of anhydrites, where the formation temperatures are positively correlated to the precipitation rate (Lowell & Yao, 2002). A correlation between decreasing Ca isotope fractionation and increasing precipitation rate has also been stated for aragonites and calcites (Lemarchand et al., 2004; Böhm et al., 2006) (Fig. 4.3b).

Analogies between anhydrite and aragonite such as the same orthorhombic symmetry (2/m 2/m 2/m) and similar Ca coordination numbers with respect to oxygen (anhydrite: [CaO_8]; aragonite: [CaO_9]) leads to the alternative approach of applying the $\Delta^{44/40}Ca_{Fluid\text{-}Min}$-temperature calibration for aragonite to anhydrite. The use of aragonite fractionation data for anhydrite may also be applicable because the $\Delta^{44/40}Ca_{Fluid\text{-}Anh}$ value of -1.0±0.2 ‰ determined by Hensley and Macdougall (2003) for a temperature of 40 °C (Fig. 4.2) is relatively close to the value of -1.30±0.03 ‰ measured by Gussone et al. (2003) for aragonite. Following this approximation a precipitation temperature of about 110 °C from the $\Delta^{44/40}Ca_{HydFluid\text{-}Anh}$ value of -0.33 ‰ (35GTV-7/4) and a temperature of about 88 °C from -0.62 ‰ (64ROV-10C) can be estimated from the Gussone et al. (2003) calibration curve. This temperature is in general accordance with the temperature range of 96-106 °C measured onsite in the sediments at station 35GTV (Kuhn et al., 2004). The T*-values are much higher than the temperature determined by the $\Delta^{44/40}Ca_{Fluid\text{-}Min}$-temperature calibration for aragonite. This large difference challenges the assumption implying that the $\Delta^{44/40}Ca_{Fluid\text{-}Min}$-temperature relationship for aragonite can simply be transferred to anhydrite. Given that the $\Delta^{44/40}$Ca-temperature relationship for aragonite underestimates common precipitation temperatures for anhydrite (~140 °C), the interpretation of the predicted values of 88 °C and 110 °C based on comparison with aragonite fractionation would either reflect minimum temperatures necessary for anhydrite precipitation or imply that Ca isotope exchange during recrystallization processes has played a role.

In addition, these temperature estimates are burdened with large uncertainties because the $\Delta^{44/40}Ca_{Fluid\text{-}Min}$-temperature relationship for aragonite is calibrated only for a temperature interval from 10 °C to 50 °C and it is not known, whether $\Delta^{44/40}$Ca-temperature relationship remains linear above this temperature interval or may change to a non-linear behaviour. Therefore, more inferences are pending on a future $\Delta^{44/40}Ca_{Fluid\text{-}Min}$-temperature calibration for anhydrite as well as for aragonite about 50 °C.

4.1.3 High- and Low-Temperature calcium carbonates

High-temperature calcites

According to their $^{87}Sr/^{86}Sr$ isotope composition the only calcium carbonate polymorphs supposed to be derived directly from hydrothermal fluid are the two calcite samples from ODP hole 1271A showing $\Delta^{44/40}Ca_{HydFluid\text{-}Cal}$ values of -0.02±0.21 ‰ (1271A 1R2) and +0.29±0.12 ‰ (1271A 5R1), respectively (Tab. 3.2). The isotopic composition of sample 1271A 1R2 implies that there was no isotope fractionation between hydrothermal fluid and precipitate. In this case, the precipitation rate and temperature must have been sufficiently high in order to inhibit any Ca isotope fractionation between hydrothermal solution and precipitate (Gussone et al., 2003; Marriott et al., 2004; Lemarchand et al., 2004; Böhm et al., 2006). This is consistent with the formation temperature of 130 °C as inferred from δ^{18}O-thermometry (Tab. 3.2).

The significant positive fractionation of sample 1271A 5R1 (Fig. 4.3a) may point to its formation in a closed system where ongoing precipitation causes an enrichment of ^{44}Ca in the fluid and hence in the subsequent precipitates. Similar processes were recently observed by Teichert et al. (2005) who found a systematic variation in the Ca isotope compositions of various gas hydrate carbonates, where ^{44}Ca was systematically enriched in samples of greater distance to the potential reservoir. Teichert et al. (2005) explained their findings by successive changes in the isotopic signature of the fluid from which the carbonates precipitated due to simple Rayleigh effect. Plotting the Ca isotope fractionatiọn as a function of temperature (Fig. 4.3a) shows that the values are not consistent with the $\delta^{44/40}$Ca-temperature calibrations for calcite (Gussone et al., 2003; Marriott et al., 2004) extrapolated linearly to higher temperature. Apparently, the calcite values are even falling along the extrapolated $\delta^{44/40}$Ca-temperature calibration curve for aragonite. The latter discrepancy can be reconciled because $\delta^{44/40}$Ca values depend besides temperature on the precipitation rate (Lemarchand et al., 2004). Usually it cannot be distinguished between temperature and precipitation rate as the possible origin for Ca isotope fractionation because higher temperatures are often also associated with higher precipitation rates. At higher precipitation rates, normally also related to higher temperatures, the Ca isotope fractionation trends of calcite and aragonite are non-linearly approaching $\Delta^{44/40}Ca_{luid\text{-}Min} = 0$ at high rates (Fig. 4.3b) (Böhm et al., 2006). From the current correlation between Ca isotope fractionation and precipitation rate in calcium carbonates (Fig. 4.3b) it can be deduced that the calcite values correspond to a precipitation rate of at least $10^{4.5}$ µmol*m^{-2}h^{-1}. Therefore, the shift of the calcite samples away from the extrapolated $\delta^{44/40}$Ca-calibration for calcite may be related to higher temperatures and respective precipitation rates, to precipitation in a closed system or to high CO_3^{2-}-concentrations in the hydrothermal fluid that will be discussed below.

The hydrothermal CO_2 system

As mentioned above precipitation temperature and rate are commonly correlated during Ca carbonate formation. However, temperature and precipitation rate may be decoupled because in systems with a high Calcium-to-carbonate ratio ([Ca] / [CO_3^{2-}]), the CO_3^{2-}-concentration in the solution is the main controlling factor on $CaCO_3$ precipitation. Therefore, changes of the CO_3^{2-} abundance in the hydrothermal fluid can trigger distinct changes of the Ca isotope fractionation. However, high CO_3^{2-}-concentrations would be expected in brucite-saturated solutions (i.e. pH ~11) like those venting at the off-axis Lost City Vent Field at MAR 30°N (Kelley et al., 2005). Logatchev vent fluids, however, have pH values that are much smaller (pH of 4.5 to 5 at 350 °C) than the pK_2 (see below) of carbonic acid at 350 °C (about 11.6), suggesting extremely low carbonate activities. Carbonate ions (CO_3^{2-}) are interconnected to dissolved carbon dioxide (CO_2(aq)) and bicarbonate (HCO_3^-) by the simplified equilibria characterizing the carbonate system in aqueous solutions:

$$CO_2(aq) + H_2O \overset{K_1}{\leftrightarrow} HCO_3^- + H^+ \overset{K_2}{\leftrightarrow} CO_3^{2-} + 2H^+$$

where K_1 and K_2 are the first and second dissociation constants of carbonic acid (the true carbonic acid H_2CO_3 is almost entirely given by CO_2(aq)). The first and second dissociation constants of carbonic acid K_1 and K_2 are required for calculating the carbonate ion abundance from a combination of any two of the measurable parameters of the marine CO_2 system that are TA, DIC, pH and fCO_2. The carbonate system in seawater is described by the stoichiometric or apparent equilibrium constants that are related to concentrations instead of activities. Stoichiometric constants vary with temperature, pressure and the composition of the solution. As the salinity of the hydrothermal fluids are close to seawater salinity and in addition as it has been shown that small modification in the composition of the solution will not affect the apparent dissociation constants of the carbonic acid system by any significant degree (Ben-Yaakov & Goldhaber, 1973), the application of dissociation constants determined for seawater to hydrothermal solutions are justified. Speciation of the carbonate system was calculated from the measured total alkalinity (TA) being the amount of H^+ required to neutralize the proton acceptors and by dissolved inorganic carbon (DIC) defined as the sum of the dissolved carbon species CO_2(aq), HCO_3^- and CO_3^{2-} (Tab. 3.3). Hence, carbonate ion concentrations and in addition the solubility product of calcite (K_{sp}^{CC}) are obtained (Tab. 3.3). Knowledge of the solubility of calcite in the system $CaCO_3$-CO_2-H_2O is crucial for understanding calcite deposition from hydrothermal waters. The formation of calcite depends on their solubility product K_{sp}^{CC} that defines the calcite saturation state (Ω):

$$\Omega = [Ca^{2+}] * [CO_3^{2-}] / K_{sp}^{CC}$$

with K_{sp}^{CC} as the stoichiometric or apparent solubility product for calcite. The stoichiometric or apparent solubility product K_{sp} is related to concentrations. This is sinplistic as saturation state is properly calculated in terms of activities rather than concentrations. The precipitation of calcium carbonate occurs only above the saturation horizon ($\Omega > 1$). The extent of dissolution is controlled by the carbonate ion concentration as the Ca contents are only slightly variable in the hydrothermal fluid of the Logatchev field (Douville et al., 2002;

Schmidt et al., in press). K_{sp} varies primarily as a function of temperature and salinity (Mucci, 1983). Thermodnamic solubility of calcite and aragonite were determined by Mucci (1983) at various salinitites and temperatures up to 40 °C. Due to the much higher fluid temperatures given here the obtained K_{sp}^{CC} represent the lower limit (Tab. 3.3) and should be considered as first order approximation.

The TA and DIC values measured in the LHF fluid samples result in a CO_3^{2-} concentrations ($[CO_3^{2-}]$) that are much higher than or at least equal to the respective K_{sp}^{CC} indicating a remarkably high saturation level of the hydrothermal fluids. Hence, the hydrothermal fluids are supersaturated with respect to calcite. This oversaturation serves as an explanation for the occurrence of the high-temperature calcites despite of the low pH and low alkalinity, respectively. Normally, $CaCO_3$ precipitates in response to increase in alkalinity. The calcite overaturation and thus calcite precipitation is based on a decrease of dissolved carbon dioxide with increasing temperatures in fluid-dominated systems. The reason why calcite is precipitated from hydrothermal fluid rather than aragonite is due to the higher stability of calcite in highly supersaturated seawater solutions (Mucci et al., 1989).

Aragonite veins

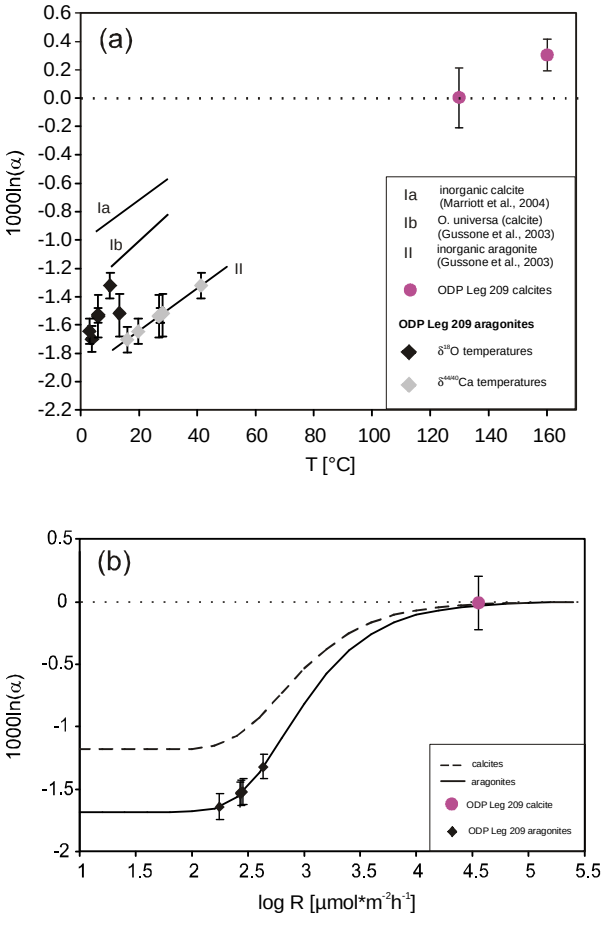

Fig. 4.3, (**a)** The $\Delta^{44/40}$Ca values of calcite and aragonite samples are plotted as a function of their corresponding independently determined temperatures (black symbols). In addition, the previously established $\Delta^{44/40}$Ca-temperature relationships for calcite and aragonite (Ia, Ib, II) (Gussone et al., 2003; Marriott et al., 2004) and the $\Delta^{44/40}$Ca-temperatures for the aragonites (grey diamonds) are also seen in this diagram. Apparently the ODP calcite samples fall along the linear extrapolated line for the $\Delta^{44/40}$Ca-temperature calibration. This might be an accidental artifact of the non-linear behavior of the $\Delta^{44/40}$Ca-temperature calibration for calcite at higher temperatures. The positive value of sample 1271A 5R1 may reflect a reservoir effect where ongoing precipitation in a closed system caused an enrichment of the heavy isotope relative to the parental solution. The $\Delta^{44/40}$Ca-temperature values for the measured aragonites are consistent with the low-temperature calibration of Gussone et al. (2003).
(b) Model for the dependency between the Ca isotope difference between precipitate and parental solution ($\Delta^{44/40}$Ca) and their precipitation rate (Böhm et al., 2006). At higher precipitation rates the fractionation lines of aragonite and calcite converge approaching zero. According to this dependency calcite sample 1271A 1R2 must be precipitated at a rate of at least $10^{4.5}$ µmol*m^{2}h^{-1}. The $\Delta^{44/40}$Ca of the aragonites from the ODP Leg 209 correspond to two order of magnitude lower precipitation rates in the order of $10^{2.5}$ µmol*m^{-2}h^{-1}.

The Ca isotope compositions of the aragonites from the ODP drill cores range between -1.32 ‰ and -1.70 ‰ and correspond to precipitation temperatures between 15 °C and 40 °C according to Gussone et al. (2003) (Tab. 3.2; Fig. 4.3a). These temperature estimates are slightly higher than those based on oxygen isotopes predicting precipitation temperatures ranging between 0 °C and 15 °C (Tab. 3.2), probably due to varying precipitation rates. The aragonites are supposed to be precipitated at rates of $10^{2.2}$ to $10^{2.6}$ µmol*$m^{-2}h^{-1}$ (Böhm et al., 2006). Nonetheless the deduced $\delta^{44/40}$Ca-temperatures are in line with low-temperature ocean crust alteration (e.g. Staudigel et al., 1981; Alt & Teagle, 1999, 2003).

Ca Isotope Fractionation during late-stage seafloor weathering

The recovered peridotites from the Logatchev hydrothermal field are strongly serpentinized and weathered. As obvious from their Sr isotope compositions (Tab. 3.2), all of the samples are significantly affected by seawater. During seafloor weathering of uplifted blocks of peridotites, extensional aragonite veins form as a late-stage product by circulation of cold, oxygenated seawater (e.g. Bonatti et al., 1980; Rosner et al., 2006). Because the Ca and Sr budget of the altered peridotites is mainly controlled by the aragonite veins, the Ca and Sr isotope compositions of the leached serpentinites overlaps the range determined for the aragonite veins (Tab. 3.2) implying a preferential uptake of the lighter Ca isotope during seafloor weathering at low temperatures. Applying the temperature-dependency of inorganic aragonite precipitation (Gussone et al., 2003), the fractionation of Δ = -1.82±0.09 ‰ to -1.48±0.08 ‰ corresponds to precipitation temperatures of 8±7 °C to 31±5 °C consistent with cold conditions at the seafloor and in the shallow subseafloor. The low Ca isotope compositions of the leached serpentinites as well as in the aragonite veins from the ODP drill cores are of particular importance as aragonites formed by low-temperature weathering of oceanic crust are a significant Ca sink representing about 10 % of the marine Ca output (Alt & Teagle, 1999; Berner & Berner, 1996).

4.1.4 The Ca isotope budget of the Logatchev hydrothermal system (LHF)

With respect to the seawater-like Sr isotope signature of the leachates and of the aragonite veins described above, the exhibited fractionation in these late-stage carbonates does not contribute to $\Delta_{HydFluid\text{-}Min}$ in the hydrothermal isotope budget as will be discussed below. This is also the case for the the calcite veins that are derived from hydrothermal fluid but do not exhibit a Ca isotope fractionation. Consequently, the overall Ca isotope fractionation between hydrothermally precipitated minerals and hydrothermal fluid has to be assigned mainly to anhydrite precipitation. This is consistent with the earlier considerations of Berner and Berner (1996) ascribing the removal of Ca exclusively to anhydrite precipitation. Hence, the Ca isotope budget of the hydrothermal cell at the Logatchev field (LHF) is characterized by a hydrothermal fluid with a $\delta^{44/40}Ca_{HydEnd}$ of -0.95±0.07 ‰ and anhydrite precipitates showing an average isotope fractionation of $\Delta^{44/40}Ca_{HydFluid\text{-}Anh}$ = -0.55±0.08 ‰. The isotopic difference between anhydrite and the parental hydrothermal solution clearly revises the earlier assumption of no significant Ca isotope fractionation effects during hydrothermal circulation (Zhu & Macdougall, 1998; Schmitt et al., 2003a). Instead, either a Ca isotope

fractionation during the leaching of Ca from the bedrock and/or a Ca isotope composition of the basement different from the currently assumed values for Bulk Earth (-0.92 ± 0.18 ‰; Skulan et al., 1997) and MORB (-0.98±0.08 ‰; Skulan et al., 1997; Zhu & Macdougall, 1998; Richter et al., 2003) must be taken into account. The latter assumption can be likely the case, as the Logatchev field is underlain by a versatile lithology composed of different rocks, mainly ultramafics (~80 %; Lackschewitz et al., 2005). In addition, LHF is supposed to be a mature and stable system for a long-time period (cf. Chapter 1.2.2), so that the host-rocks of LHF must be considerably altered. Due to the recovery of only strongly altered rocks from the Logatchev field and the lack of Ca isotope data in silicate rocks especially in ultramafics, the Ca isotope composition of the bedrock at LHF and thus the initial composition of the hydrothermal fluid prior to anhydrite precipitation will be deduced theoretically by two approaches.

Mass balance approach

Generally, the Ca isotope budget of the LHF system in steady state can be written as:

$$N_{SW}*\delta_{SW} + N_{initial}*\delta_{initial} = N_{HydEnd}*\delta_{HydEnd} + N_{Min}*\delta_{Min} \quad \text{(Eq. 41)}$$

where N_{SW} is the molar fraction ($[Ca]_{SW}$) entraining the oceanic crust, $N_{initial}$ represents the fraction ($[Ca]_{initial}$) leached from the bedrock (of unknown isotopic composition). N_{HydEnd} is the Ca content in the hydrothermal fluid endmember ($[Ca]_{HydEnd}$), and N_{Min} refers to the moles of Ca precipitated in the hydrothermal upflow and subseafloor mixing zone. The deltas indicate the respective Ca isotope compositions. The demanded term $\delta_{initial}$ is then deduced simply by converting Eq. 4.1 to:

$$\delta_{initial} = (N_{HydEnd}*\delta_{HydEnd} + N_{Min}*\delta_{Min} - N_{SW}*\delta_{SW}) / N_{initial} \quad \text{(Eq. 4.2)}$$

All of the parameters are either known or can be assumed and are listed in Tab. 4.1. δ_{Min} can be described by δ_{HydEnd} and a characteristic value $\Delta_{HydFluid\text{-}Min}$ representing the suggested isotopic difference between the fluid and the precipitated mineral:

$$\delta_{Min} = \delta_{HydEnd} + \Delta_{HydFluid\text{-}Min} \quad \text{(Eq. 4.3)}$$

For the Logatchev hydrothermal field $\Delta_{HydFluid\text{-}Min}$ is approached by the error-weighted average $\Delta^{44/40}Ca_{HydFluid\text{-}Anh}$ = -0.55±0.08 ‰ determined by the Ca isotope differences in the analyzed anhydrite samples 35GTV-7/4 and 64ROV-10C (Fig. 3.1c). For $N_{initial}$ and N_{Min} two scenarios can be discussed. In the first scenario that will be denoted in the following as 'MC' (Mg-controlled) (Tab. 4.1), $N_{initial}$ is approached by the commonly accepted assumption that the amount of Ca ($[Ca]_{initial}$) leached from the bedrock equals the moles of Mg lost from seawater ($[Mg^{2+}]_{SW}$ = 54 mM) (e.g. Seyfried & Bischoff, 1979; Von Damm, 1990; Elderfield & Schultz, 1996). With a Ca content of 32 mM determined for the hydrothermal fluid (N_{HydEnd}) mass balance calculations lead then to a total Ca amount of 22 mM inherent in mineral precipitates (N_{Min}) (Tab. 4.1).

In a second approach indicated as 'SC' (SO_4^{2-}-controlled) N_{Min} is given, while $N_{initial}$ will be deduced from. As shown above and in general agreement to Berner and Berner (1996), the lack of Ca in the hydrothermal budget can be inferred directly from the consumption of sulfate. Therefore, N_{Min} that is the fraction of Ca sequestered in mineral precipitates is adopted to the original $[SO_4^{2-}]_{SW}$ concentration of 28 mM. With respect to the the Ca content in the hydrothermal fluid endmember ($[Ca]_{HydEnd}$) and taken the original $[Ca]_{SW}$ of 10 mM into account, consequently an amount of 50 mM is computed for $N_{initial}$ ($[Ca]_{initial}$) (Tab. 4.1).

Resolving Eq. 4.2 by the numerical parameters of MC yields a $\delta_{initial}$ of -1.17±0.04 ‰ representing the initial Ca isotope composition of the hydrothermal fluid ($\delta^{44/40}Ca_{initial}$) prior to anhydrite precipitation. This is somewhat lower as the determined $\delta^{44/40}Ca_{HydEnd}$ -0.95±0.07 ‰ as well as of the Bulk Earth value of -0.92 ± 0.18 ‰ (Skulan et al., 1997) and an average MORB value ($\delta^{44/40}Ca_{MORB}$ = -0.98±0.07 ‰; Skulan et al., 1997; Zhu & Macdougall, 1998; Richter et al., 2003). The isotopic difference between $\delta^{44/40}Ca_{initial}$ and $\delta^{44/40}Ca_{HydEnd}$ results from the Ca isotope fractionation occurring during the precipitation of anhydrite from the hydrothermal fluid. The deviation between $\delta^{44/40}Ca_{initial}$ from the proposed bedrock signatures, Bulk Earth or MORB points to a lower Ca isotope composition of the bedrock at LHF, if the hydrothermal fluid adopts the $\delta^{44/40}Ca_{initial}$ value without any fractionation. In MC the contribution of $[Ca]_{SW}$ is equal to zero assuming that $[Ca]_{SW}$ has already completely been lost in the recharge zone before exchange of Mg for Ca between fluid and rocks begins, mainly in the reaction zone. Therefore, the hydrothermal solution has most likely equilibrated with the isotopic signature of fresh MORB supposed to be the dominant bedrock in the reaction zone (Fig. 4.1). Note that, the values measured by Skulan et al (1997) and Richter et al. (2003) for MORB average to a $\delta^{44/40}Ca$ of -1.14±0.09 ‰ disregarding the very high results of $\delta^{44/40}Ca_{(SW)}$ = -0.61±0.12 ‰ for the isotope compositions of MORB glasses reported by Zhu & Macdougall (1998). It has been previously suggested (DePaolo, 2004) that the $^{44}Ca/^{40}Ca$ ratios of the mantle is slightly lower than the Bulk Earth value as currently analyzed typical terrestrial volcanic rocks average to a slightly lower value than the currently assumed Bulk Earth value of -0.92±0.18 ‰.

Tab. 4.1, Ca mass balance calculations for the determination of the fractionation during hydrothermal precipitation. See text for further explanation.

	$[Ca]_{SW}$ [mM]	$[Ca]_{initial}$ [mM]	$[Ca]_{Min}$ [mM]	$[Ca]_{HydEnd}$ [mM]	$\delta^{44/40}Ca_{SW}$ [‰]	$\delta^{44/40}Ca_{HydEnd}$ [‰]	$\Delta_{HydFluid-Min}$ [‰]	α	f_{remain} [%]	$\delta^{44/40}Ca_{initial}$ [1] [‰]	$\delta^{44/40}Ca_{initial}$ [2] [‰]
MC	0	54	22	32	0	-0.95±0.07	-0.55±0.08	0.99945	60	-1.17±0.04	-1.23±0.10
SC	10	50	28	32	0	-0.95±0.07	-0.55±0.08	0.99945	53	-1.45±0.05	-1.56±0.18

[1] calculated by mass balance calculations (after Eq. 4.2)
[2] calculated assuming Rayleigh precipitation (after Eq. 4.4)

While the MC-$\delta^{44/40}Ca_{initial}$ lies well within the range of volcanic rocks, the model assumption made in SC, in contrast, result in a $\delta^{44/40}Ca_{initial}$ value of -1.45±0.05 ‰ that is ~0.4 ‰ lower than the average value for terrestrial igneous rocks (cf. DePaolo, 2004). The interpretation of this value would be that in SC there is no specific loss of Ca in the recharge zone and the hydrothermal solution has interacted with all occurring rock phases through the whole hydrothermal pathway from the recharge zone, via the reaction zone to the discharge zone (Fig. 4.1). As a consequence of integrating over the entire hydrothermal cell, $\delta^{44/40}Ca_{initial}$ is composed of different rock types including alteration products and mineral precipitates.

It should be noted that Fantle and DePaolo (2005) recently obtained a $\delta^{44/40}Ca$ of -1.45±0.07 ‰ (converted to seawater scale by subtracting -0.95 ‰ after the authors' suggestion) for the average Ca isotope compositions of marine carbonates. These carbonates are considered to represent the Ca removal from the ocean over the past 20 Ma. Over such a long time scale that widely exceeds the residence time of Ca in the ocean, the marine Ca output expectedly should equal the Ca input commonly assumed to be represented by volcanic rock composition. Fantle & DePaolo (2005) proposed several explanations for this discrepancy, one that volcanic rocks analyzed to date may not be representative for continental rocks exposed to weathering. Likewise, it may be argued for the $\delta^{44/40}Ca_{initial}$ obtained by SC. The Ca isotope composition of ultramafic and altered rocks in the oceanic crust might not be represented adequately by the currently investigated volcanic rocks.

Both models, MC and SC are burdend with some uncertainties. MC is simplistic in that it does not address Ca-buffering by mineral-fluid reactions invoking plagioclase, amphibole and Ca-silicates and the compensation of Mg-loss by a proton flux that can be of importance in Ca-poor, ultramafic-hosted systems as given here (Bach et al., 2004). Whereas SC does not account for imbalances due to potential reduction of seawater-sulfate to sulfide and/or additional oxidation of released sulfide from the substratum. In addition, $\Delta_{HydFluid\text{-}Min}$ approached by the determined value of $\Delta^{44/40}Ca_{HydFluid\text{-}Anh}$ = -0.55±0.08 ‰ is a mean value from the analyses of two anhydrites that precipitated at specific conditions, precipitation rates and temperatures. It is unclear whether both anhydrite samples are representative for overall anhydrite precipitation at the Logatchev hydrothermal system and whether the proportion and conditions remain constant over space and time. However, in the absence of data for the net mass balance of the Logatchev system, both models serve as a useful first-order approximation of the hydrothermal Ca isotope budget at the Logatchev field.

Rayleigh fractionation approach

In an alternative approach the isotopic composition of the initial fluid will be deduced by the assumption that the precipitation process of hydrothermal minerals might be approximated by Rayleigh type fractionation (e.g. Rayleigh, 1896; Bigeleisen & Wolfsberg, 1958). In the above-described mass balance considerations (MC and SC) $[Ca]_{HydEnd}$ represents only 60 % (MC) or 53 % (SC) (f_{remain}, Tab. 4.1) of the total initial Ca amount ($[Ca]_{initial}$), respectively. Furthermore, following the model approaches and using an average isotope difference $\Delta^{44/40}Ca_{HydFluid\text{-}Min}$ of about -0.55 ‰ between hydrothermal fluid and mineral precipitate a $\delta^{44/40}Ca_{initial}$ of -1.17±0.04 ‰ and -1.45±0.05 ‰ is calculated, respectiviely. Both observations can be reconciled by the assumption of a Rayleigh type isotope fractionation effect causing an enrichment of the heavier isotope in the fluid and the lighter isotope in the precipitate.

Assuming Rayleigh fractionation and using the values of the mass balance approach as described above (f_{remain}, $\Delta^{44/40}Ca_{HydFluid\text{-}Min}$), the expected Ca isotope signature of the initial fluid in prior to mineral precipitation ($\delta^{44/40}Ca_{initial}$) may then be calculated. This theoretically determined value can be compared with those obtained from the mass balance calculations above. The degree of consistency between the calculated Rayleigh values and the mass balance data is a measure of the semi-closed system behaviour for hydrothermal mineral precipitation, because a precondition for Rayleigh fractionation is that along the path of the reservoir material may precipitate from but no further material is added to the reservoir. Given that the hydrothermal fluid is closely following this precondition, the calculated value is expected to be relatively close to the above-deduced values. However, if there is major material and isotope exchange between the hydrothermal reservoir and the host-rocks of the discharge zone where precipitation mainly occurs, a larger discrepancy between both values must be expected. $\delta^{44/40}Ca_{initial}$ can be computed by:

$$\delta_{remain} - \delta_{initial} = 1000 * (f_{remain}^{\alpha-1} - 1) \quad \Rightarrow \quad \delta_{initial} = \delta_{remain} - 1000 * (f_{remain}^{\alpha-1} - 1) \qquad \text{(Eq. 4.4)}$$

where f_{remain} is the fraction of Ca remaining in the hydrothermal fluid and α is the fractionation between fluid and precipitate. Note that α is deduced by $\Delta^{44/40}Ca_{HydFluid\text{-}Min} = 1000\ln(\alpha)$ (Tab. 4.1). Inserting the values of MC with $\delta_{remain} = \delta^{44/40}Ca_{HydEnd} = -0.95\pm0.07$ ‰, $f_{remain} = 0.6$ and $\alpha = 0.99945$ (Tab. 4.1), a $\delta^{44/40}Ca_{initial}$ of -1.23±0.10 ‰ is calculated (Fig. 4.4). In case of SC, a theoretical value of -1.30±0.18 ‰ for the Ca isotope composition of the remaining fluid is obtained by assuming a $f_{remain} = 0.53$ and $\alpha = 0.99945$ (Tab. 4.1). Note that the calculated value for SC is not simply equal to $\delta^{44/40}Ca_{initial}$. The relative contribution of $[Ca]_{SW} = 10$ mM and its isotopic signature enhances the intrinsic $\delta^{44/40}Ca_{initial}$ and must be retracted. Hence, a $\delta^{44/40}Ca_{initial}$ of -1.56±0.18 ‰ is achieved for the model assumptions of SC.

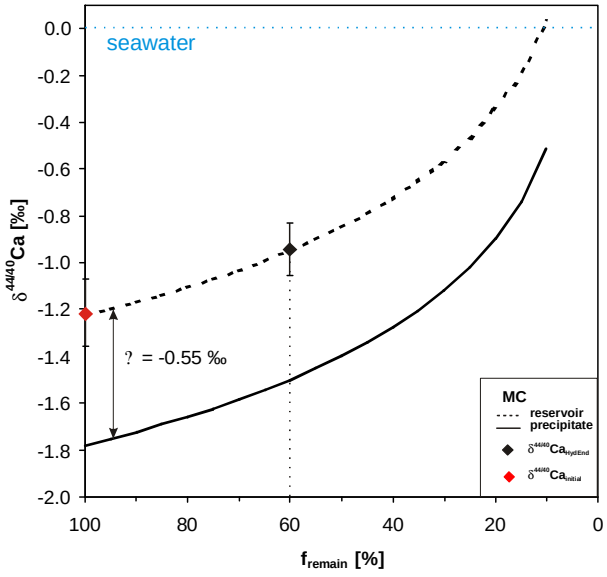

Fig. 4.4, Assuming Rayleigh fractionation of Ca isotopes during mineral formation and applying the values of the mass balance calculations for MC ($\Delta_{HydFluid\text{-}Min}$ = -0.55 ‰; 60 % remaining fraction) results in a $\delta^{44/40}Ca_{initial}$ that is consistent to the values deduced by mass balance calculations.

Both calculated values of $\delta_{initial}$, -1.23±0.10 ‰ (MC) and -1.56±0.18 ‰ (SC) are within the statistical uncertainties indistinguishable from the $\delta^{44/40}Ca_{initial}$ values deduced by mass balance approach (-1.14±0.09 ‰ and -1.45±0.05 ‰) (Tab. 4.1). The very good agreement of both approaches, mass balance calculations and Rayleigh type fractionation, indicate that mineral precipitation in hydrothermal systems, at least in the discharge zone, is well described by a semi-closed system behaviour where minerals are precipitated from but no material is added to during hydrothermal fluid ascent. This is consistent with the assumption of a self-sealing process in the channel ways of the upper part of the discharge zone by the precipitation and deposition of minerals (Bischoff, 1980; Lowell & Yao, 2002).

4.1.5 U, Mg, and B isotopes in hydrothermal fluids of LHF

$^{234}U/^{238}U$

The concentration and isotopic composition of Uranium (U) in hydrothermal fluid samples from the Logatchev field were measured in order to investigate the nature and where applicable also the chronology of exchange processes between seawater and crust and the source of U. Uranium is besides Mg and SO_4^{2-} one of the few chemical species that is quantitatively removed from seawater during hydrothermal circulation. Uranium is a redox sensitive element and easily mobilized during water-rock interactions. In oxidizing environments, U occurs in solution as the uranyl ion UO_2^{2+} that forms complexes such as $(UO_2)(CO_3)_3^{4-}$ in the ocean. During hydrothermal processes U is reduced to the insoluble oxide UO_2 and removed from seawater both by adsorption onto rock surfaces or grain boundaries, and by incorporation into authigenic minerals, such as calcium carbonates and palagonite. This is reflected by the results showing that U is removed from seawater coherently with Mg displaying the fluid amount (Tab. 3.1; Fig. 3.2). The U concentrations range from a seawater value of ~3.15 ng/g (ppb) to about 0.7 ppb in the samples with the highest fluid amounts (Tab. 3.1; Fig. 3.2). This indicates that U was quantitatively removed from seawater and deposited to the crust during hydrothermal circulation. Typically, U concentration in unaltered MORB range from 42 to ~85 ppb (Bacon, 1978; Hertogen et al., 1980), while average U contents of highly altered basalt is elevated up to 600 ppb (Macdougall, 1977).

For modern seawater the activity ratio of $^{234}U/^{238}U$ = 1.146±0.002 (Anderson et al., 2004). U in freshly crystallized ocean basalt is expected to be in secular equilibrium with $^{234}U/^{238}U$ = 1.00 (Somayajulu et al., 1966). A sample which contains U from seawater will have activity ratios >1 and if it were isolated fom exchange with seawater would evolve toward equilibrium with a half-life of $2.445*10^5$ years ($t_{1/2}$ of ^{234}U; Lounsburg & Durham, 1971; De Bievre et al., 1971). Additionally, $^{234}U/^{238}U$ activity ratio in seawater may change during weathering (Cherdyntsev, 1955). ^{234}U is suggested to be preferentially leached out from host-rocks and added to the seawater/hydrothermal fluid (Chen & Wasserburg, 1986) from which it is incorporated in authigenic minerals. Hence, an enrichment of ^{234}U in the carbonate vein may be a result of precipitation from an enriched fluid. However, the data of this study indicate that $^{234}U/^{238}U$ in the the hydrothermal fluids is constant within ±3 %. There are no variations in $^{234}U/^{238}U$ being consistent to previous studies (Chen & Wasserburg, 1986). Most U in the hydrothermal solutions has the signature of seawater-U and the U contribution from the oceanic crust to the hydrothermal solutions seems to be insignificant.

Mg isotopes

Mg is the second major cation in seawater and is removed from the ocean mainly by hydrothermal exchange processes at mid-ocean ridges. The hydrothermal sink in the modern Mg budget is estimated to range between 60 and 100 % of the total flux (Spencer & Hardie, 1990; Holland, 2005). In high-temperature hydrothermal fluids the Mg removal is nearly quantitative. This fact is used for the determination of endmember compositions as in this study, where fluid amounts are deduced by the extrapolation to zero Mg concentration (Schmidt et al., in press). Hence, in Fig. 3.3 the fluid amounts are reflected by the Mg concentrations (Tab. 3.1; Fig. 3.3). If seawater-Mg is not completely sequestered in the basement, as it could be expected for high-Mg host-rocks such as at LHF, then the reflux might be accompanied by an isotope fractionation. The analyses of selected fluid samples (Tab. 3.1) do not show significant and systematic variations of the Mg isotope ratios displaying all seawater composition. Either the total removal of Mg during hydrothermal circulation is confirmed, or the investigated hydrothermal solutions are too strongly diluted by seawater as a potential fractionation could be resolved. More investigations are required on samples with higher fluid amounts in order to test for potential fractionation processes during hydrothermal exchange of Mg. In addition, there are presently no Mg isotope analyses for off-axis diffuse outflows, where only small amount of Mg is removed, and the reflux may be associated with an isotope fractionation. However, as shown by the results above the resolution of this potential fractioanation will be challenging analytical precision due to the larger admixture with seawater in the subsurface and its subsequent isotopic imprint.

B isotope ratios

Boron (B) is a highly mobile element in submarine hydrothermal systems. Previous studies (Palmer, 1996) showed that up to 50 % of seawater-B is removed from circulating vent fluids at the Mid-Atlantic Ridge (MAR). Boron and B isotope systematics of vent fluids from hydrothermal systems are sensitive tracers of water-rock interaction and controlled by the amount of seawater passing through the convection cell. Thereby, B is taken up by the oceanic crust at temperatures < 150 °C, while it is leached from oceanic crust by hot (>200 °C) vent fluids. Uptake of B from circulating seawater is accompanied by hydration of the oceanic crust including serpentinization of the upper mantle (e.g. Bonatti et al., 1984). Serpentinites generally have higher concentrations of B than the alteration products of the upper oceanic crust (MORB). In addition, serpentinization is commonly considered to induce a fractionation of the boron isotopes during the incorporation of boron into the alteration products with a preferential uptake of ^{10}B (e.g. Palmer, 1996; James et al., 1999). Serpentinization takes place over a temperature range of 0-500 °C, while boron uptake ceases at 150 °C. The average isotope fractionation factor during incorporation into low-temperature alteration products is considered to range between 0.969 at ambient seafloor temperatures to up to 1 with increasing temperatures. The boron isotope compositions ($\delta^{11}B$) of silicates has been determined to range between -6.7 and -1.2 ‰ (Chaussidon & Jambon, 1994). For the hydrothermal fluids of the Logatchev field an endmember value of 20.2±3.6 ‰ could be determined by B concentrations (Fig. 3.4a). This is much higher than an average oceanic crust composition (-5 ‰) and indicates that the boron isotope systematics at the Logatchev field are not described by simple binary mixing between oceanic crust and seawater such as observed for the East Pacific Rise (Palmer, 1996). This has been observed

previously for the TAG site and is generally assumed for hydrothermal systems along the slow-spreading MAR (Palmer, 1996), where seawater interacts to a greater extent with the bedrock than at shallow, fast-spreading systems such as the EPR (Palmer, 1996). The concentration values for the fluids (Koschinsky et al., 2006) clearly indicate an uptake of boron consistent to the ultramafic and strongly serpentinized bedrock at the Logatchev hydrothermal field (Kuhn et al., 2004; Lackschewitz et al., 2006).

As hydrothermal activity at LHF seems to have been long-lived, the interplay between leaching and serpentinization as well as re-dissolution of secondary alteration minerals is complicated and might be monitored by an independent tracer. This could be represented by the Ca isotope systematics. The positive correlation between B and Ca isotope ratios (Fig. 3.4b) provides not only confirmation of the respective endmember values but also reveal isotope effects that are independent from the concentrations. Hence, via Ca isotopes a $\delta^{11}B_{HydEnd}$ for the hydrothermal endmember of 20.9±4.3 ‰ can be computed being well-consistent within error to the endmember determined by B contents. Vice versa, the Ca isotope composition of the hydrothermal endmember can be deduced via boron isotopes and yield a $\delta^{44/40}Ca_{HydEnd}$ of -0.94±0.13 being in good agreement to the above determined endmember values using Ca contents and/or Sr isotopes. Additionally, the relation between Ca and B isotopes show for the sample 53ROV-2 and partly also for 73ROV-4 a deviation from the trend line and indicate an additional process shifting their isotope signatures towards seawater value. This might be based either to re-dissolution processes of alteration minerals or to leaching of B from the host-rocks with a preferential release of the heavier isotope due to high temperatures exceeding 150 °C. Indeed, at site IRINA II where sample 53ROV-2 was withdrawn the highest temperatures of about 350 °C at LHF were measured (Schmidt et al., in press). Hydrothermal fluids rising up from the basement might have interacted geochemically with the overlying sediments. However, because of the weak database at this time no further inferences can yet be made from the boron isotope analyses.

4.2 Ca isotope systematics during phase separation

4.2.1 Comparison of the different hydrothermal vent fields

The recently discovered hydrothermal vent fields (Turtle Pits and Red Lion) in the neovolcanic zone of the Mid-Atlantic Ridge at 5°S (MAR 5°S) (German et al., 2005) provides a direct comparison of the hydrothermal pathway of Ca at two different hydrothermal systems on a slow-spreading ridge. The Logatchev field (LHF) provides a tectonically controlled, ultramafic-hosted hydrothermal system with constant fluid supply and chemistry. In contrast, the post-eruptive, basaltic-hosted high-temperature Turtle Pits field at MAR 5°S is highly influenced by phase separation (Koschinsky et al., 2006) due to low chlorinity of the fluids (Fig. 4.5), their high exit temperatures and the magmatic activity that has so far only been observed along fast- and intermediate-spreading centers (Lilley et al., 2003; Von Damm et al., 1995).

From the diffusive outflows from Lilliput and Wideawake inferences can as yet not be made. The Ca isotope ratios of vent fluids from Wideawake being apparently higher than seawater (Tab. 3.4) may be most likely due to analytical artifacts, but may also indicate a fluid phase being enriched in ^{44}Ca. However, these data requires further investigations. It should be mentioned a priori that due to small sample numbers available, generally the data for all of the vent fields at the MAR°S are burdened with large statistical uncertainties. However, the present preliminary results for the Red Lion and Turtle Pits site may point to fundamentally different processes being active in the respective hydrothermal cells and will be discussed in the following.

Despite of their spatial proximity, the fluid compositions of the Turtle Pits and the Red Lion vent fields suggests that the influence of recent volcanic activity on the hydrothermal systems is confined to the Turtle Pits vent field leading to venting of vapor-type fluids, but is not affecting the nearby Red Lion field located about 2 km to the North. The Red Lion vent field is characterized by fluid supply of normal seawater salinity and much lower vent fluid exit temperatures without visible boiling (Haase et al., submitted). There is also less clear evidence for phase separation at the Logatchev field (Koschinsky et al., 2006). Due to the different geologic settings of the ultramafic-hosted LHF and the basaltic Turtle Pits vent field their vent fluid compositions differ significantly. On the other hand, fluids from the basaltic-hosted Red Lion field have been shown to be similar in their chemical and isotopic compositions to those from the Logatchev field (Tab. 3.1) but quite different to Turtle Pits fluids (Fig. 4.5). In particular, the fluids from LHF and Red Lion are enriched in Ca (~32 mM and ~16 mM, respectively) compared to Turtle Pits (~10 mM) and to seawater (~11 mM). Remarkably, the Ca content in the Turtle Pits fluid endmember seems to be depleted in Ca relative to seawater and compared to Red Lion and LHF. Significant differences between the vent fields are also mirrored in their Ca and Sr isotope compositions, where the LHF and Red Lion exhibit a $\delta^{44/40}Ca_{(SW)}$ of about -0.95 ‰ for the hydrothermal endmember with an average crustal $^{87}Sr/^{86}Sr$ (Fig. 3.1). In contrast, the Ca and Sr isotope compositions of the fluid endmember from Turtle Pits seems to be much higher (-0.65 ‰; 0.7069) (Fig. 3.6). The loss of Ca and the enrichment in the heavier isotope in the fluid endmember of the Turtle Pits field may be a result of high water-to-rock ratio and the relative size and reactivity of the Ca pool as indicated also by Sr. The Sr isotope data of the vent fluids from MAR 5°S indicate that the fluids from Turtle Pits contain significant amounts of radiogenic seawater showing an incomplete equilibration of the hydrothermal fluid with the basement represented by the two basaltic samples (Tab. 3.5). This is indicated also by the Ca isotope ratios that are much heavier than the bedrock.

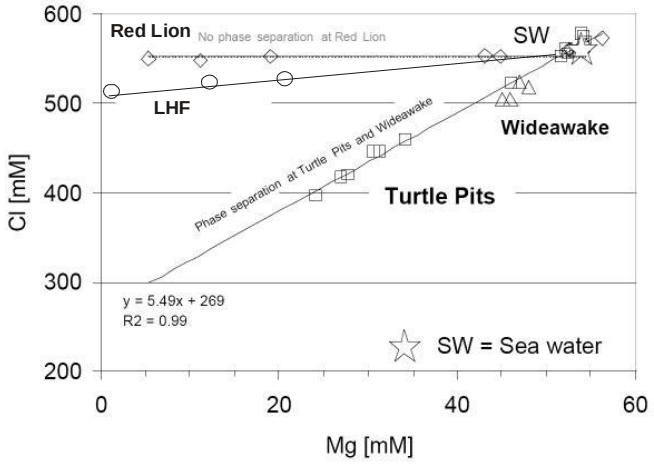

Fig. 4.5, Mg versus Cl concentrations in hydrothermal fluids. In contrast to Red Lion and LHF, Turtle Pits and Wideawake fluids show strong evidence to be phase-separated. From Koschinsky et al. (2006).

However, high exit temperatures and the lack of Mg in the hydrothermal solutions indicate an extensive reaction between seawater and oceanic crust. A rough estimation of the water-rock ratios by the Sr isotope systematic may clarify the question, whether high water-to-rock ratio solely causes a shift in the Ca isotopic signature of Turtle Pits fluids. The water-to-rock ratios may be calculated by the following relationship after Faure (1986):

$$W / R = [C_{initial} * (I_{initial} - I_{HydEnd})] / [C_{SW} * (I_{HydEnd} - I_{SW})] \quad \text{(Eq. 4.5)}$$

With W and R as water and rock masses respectively, C and I as the concentrations and isotopic compositions of the bedrock (initial), the hydrothermal fluid endmember (HydEnd) and seawater (SW), respectively. Inserting the Sr values of the samples from Turtle Pits, a water-to-rock ratio of 48 is deduced (Tab. 4.2). From this ratio a resulting $\delta^{44/40}$Ca of the hydrothermal endmember can be computed. Converting Eq. 4.5 yields a Ca isotopic composition of -0.77 ‰ relative to seawater. The measured value of -0.65 ‰ for $\delta^{44/40}Ca_{HydEnd}$, on the other hand, requires a W/R of 93 (Tab. 4.2).

Tab. 4.2, Determination of the water-to-rock ratio using Sr and Ca isotope ratios at the Turtle Pits hydrothermal field.

	C_{SW}	$C_{initial}$	C_{HydEnd}		I_{SW}	$I_{initial}$	I_{HydEnd}	W / R
Sr [µM]	87	2270	31	**$^{87}Sr/^{86}Sr$**	0.7092	0.7025	0.7069	48
Ca [mM]	10.55	2000	9.8	**$\delta^{44/40}$Ca [‰]**	0	-0.65	-0.95	93

Hence, it may be stated that the measured $\delta^{44/40}Ca_{HydEnd}$ for the hydrothermal fluid at the Turtle Pits vent site may not be explained exclusively by a high water-rock ratio, but further processes have led to a an enrichment of the heavier Ca isotope in the fluid. Ca loss and isotopic fractionation may be caused by the formation of mineral precipitates with a related Ca isotope fractionation as reported for LHF. In particular, extensive anhydrite formation may result in a hydrothermal fluid with heavier isotopic signature. As shown for the Logatchev field, anyhydrite precipitation exhibits large fractionation effects incorporating preferentially the lighter isotope while shifting the parental solutions towards higher values. An alternative or additional explanation to anhydrite precipitation might be phase separation, wherein the lighter Ca isotopes become relatively enriched in the brine and the heavier one in the vapor phase. Both suggestions will be reconciled in the following, although the analytical uncertainties hamper clear implications, and more investigations are required, in order to test the statistical signifcance of the isotopic compositions of the fluid endmembers.

4.2.2 Ca isotope fractionation during anhydrite precipitation at Turtle Pits

As shown for the Logatchev hydrothermal system, anhydrites significantly affect the hydrothermal Ca budget. The high temperatures at the Turtle Pits vent field provide the formation of a considerable amount of anhydrites, because the solubility of anhydrite decrease rapidly at temperatures >150 °C (Bischoff & Seyfried, 1978). With respect to the importance of anhydrite precipitation for the Ca isotope budget in hydrothermal systems (Berner & Berner, 1996; Ch. 4.1.2), a set of hydrothermal anhydrite samples from the Turtle Pits vent field were investigated for their Sr and Ca isotopic compositions.

The Ca isotopic compositions of the anhydrites range between -0.9 and -1.4 ‰ (Tab. 3.5). From their Sr isotope ratios an emanation of hydrothermal solutions must be assumed. Although the Ca isotope systematics in the hydrothermal fluids from the Turtle Pits is not clearly constrained, Ca isotope fractionations were determined using the preliminary endmember value for the Turtle Pits hydrothermal fluid of about -0.65 ‰ (Fig. 4.6). The two samples 123ROV-4A and 130ROV-1C might be derived from a different source as their Sr isotopic compositions are lower than the endmember value determined for the hydrothermal fluid from Turtle Pits (Fig. 3.6; Tab. 3.5). Except for these both samples a Ca isotope fractionation $\Delta^{44/40}Ca_{Fluid\text{-}Anh}$ of up to -0.9 ‰ is determined (Fig. 4.6) confirming former suggestions of a large isotope fractionation during anhydrite precipitation (Hensley, 2006; Ch. 4.1). Hensley (2006) reports very low $\delta^{44/40}Ca_{(SW)}$ values of around -2 ‰ for hydrothermal chimney anhydrites. Unfortunately, Hensley (2006) did comment neither on formation temperatures nor on the Ca isotope composition of the parental solution of these anhydrites. However, with respect to an average $\delta^{44/40}Ca_{HydEnd}$ of around -0.95 ‰ (this work; Schmitt et al., 2003), a Ca isotope fractionation of at least -1 ‰ can be assumed for the samples measured by Hensley (2006).

Assuming that the anhydrite samples recovered here are representative for the physico-chemical conditions of the precipitation process at Turtle Pits, an overall Ca isotope fractionation for anhydrite precipitation within the Turtle Pits hydrothermal cell can be deduced by the average $\Delta^{44/40}Ca_{Fluid\text{-}Anh}$ of around -0.65 ‰ being close to the overall fractionation value $\Delta^{44/40}Ca_{Fluid\text{-}Anh}$ of about -0.55 ‰ determined for the Logatchev hydrothermal system (Ch. 4.1). Whether this isotopic difference suffices to explain the $\delta^{44/40}Ca_{HydEnd}$ of -0.65 ‰ for the Turtle Pits fluid endmember will be discussed in detail below.

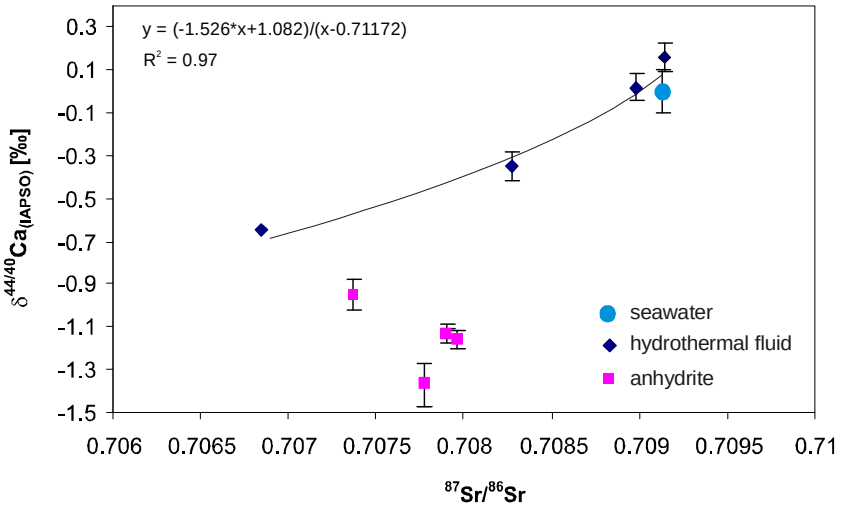

Fig. 4.6, Ca isotope fractionation in anhydrite samples precipitated from hydrothermal solution at Turtle Pits.

Temperature-dependency of Ca isotope fractionation in anhydrites

The Ca isotope fractionation inherent in the anhydrites from the Turtle Pits field show strong evidence for a temperature-dependency confirming the suggestions made by the two anhydrite samples from the Logatchev field (Ch. 4.1.2). Likewise as for the LHF anhydrites, the formation temperatures of the Turtle Pits anhydrites are estimated by isenthalpic mixing using Sr isotopes (Bischoff & Rosenbauer, 1985; Humphris & Bach, 2005). Thereby, thermodynamic data for 3.2 wt% NaCl solutions and 300 bar from Bischoff and Rosenbauer (1985) and, because of the lack of heat capacity data at the critical point, a fluid endmember at 360 °C with $[Sr]_{HydEnd}$ = 88µM and $^{87}Sr/^{86}Sr$ of 0.7035 were used (Bach, pers. comm.). These presumptions provide an absolute lower limit for the formation temperatures of the anhydrites. In addition, larger uncertainties are due to conductive cooling of the hydrothermal solutions or heating of seawater in the subseafloor prior to exciting. However, this method can be considered as a first order approximation to obtain a rough estimate of the formation temperatures of these anhydrites. Hence, isenthalpic mixing temperatures (T*) from 150 °C up to 310 °C are calculated (Bach, pers. comm.) (Tab. 3.5). As for the both anhydrites from the LHF, the T*-values of the Turtle Pits-anhydrites are positively correlated to the measured Ca isotope fractionations ($\Delta^{44/40}Ca_{HydFluid-Anh}$) and with regard to the high uncertainity level of T* (assumed to be ~50 °C) agree well with the $\Delta^{44/40}Ca_{HydFluid-Anh}$-temperature relationship of the LHF anhydrites (Ch. 4.1.2; Fig. 4.7a). The linear T*-$\Delta^{44/40}Ca_{HydFluid-Anh}$ behaviour is also consistent to the fractionation-temperature relationships assumed for aragonites and calcites (Gussone et al., 2003; Marriott et al., 2004) (Fig. 4.7a), but the temperature sensitivity of Ca isotopes in anhydrites is apparently a factor of ~5 lower than in the calcium carbonate polymporphs (Fig. 4.7a). This might be due to differing physico-chemical factors controlling mineral precipitation of calcium carbonates and sulfates, such as solution chemistry, solubilities, crystal structure and bonding character that result in different precipitation rates and temperatures favoring different fractionation mechanisms. With respect to the wide temperature interval of > 150 °C, the isotope fractionation in the Turtle Pits anhydrites defines a linear relationship to $1/T^2$ of $1000\ln(\alpha) = -18769/T^2 - 0.0203$ (Fig. 4.7b).

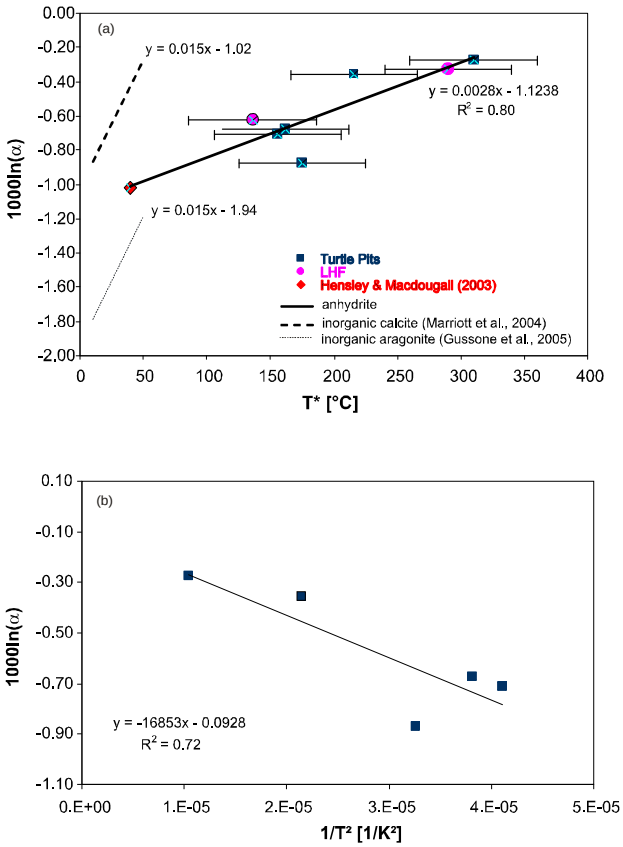

Fig. 4.7, Temperature-dependency of Ca isotope fractionation in anhydrites.
(a) Ca isotope fractionation in anhydrites analyzed in this study are positively correlated to temperature consisitent to calcite and aragonite.
(b) $1/T^2$-relationship between Ca isotope fractionation and temperature in the Turtle Pits anhydrite samples.

Because of the high values and its positive correlation of $\Delta^{44/40}Ca_{HydFluid\text{-}Anh}$ in these anhydrites, a chemically induced kinetic fractionation mechanism is unlikely. Chemical kinetic fractionation results in an increase of fractionation with temperature. This is clearly not given here. In contrast, physical kinetic fractionation is not temperature-dependent and may serve as an underlying fractionation mechanism rather than equilibrium fractionation that is supposed to become negligibly small at high temperatures. However, constraints on the mechanism for Ca isotope fractionation in anhydrites on the basis of this study is critical and certainly beyond the scope of this study. More detailed investigations have to be undertaken in order to make inferences upon that. An appropriate correlation between Ca isotope fractionation and temperature in anhydrites require systematic investigations such as experimentally controlled anhydrite precipitation and/or the more accurate determination of formation temperatures as by fluid inclusion (microscopic globules of parental fluid trapped during crystal formation) microthermometry. In summary, the pertinent data clearly indicate a temperature-dependency of Ca isotope fractionation in anhydrites at high temperatures >100 °C and imply that Ca isotope fractionation in anhydrite has in principle the potential to be a proxy for the reconstruction of precipitation temperatures for anhydrites in hydrothermal cells as soon as a $\Delta^{44/40}Ca_{Fluid\text{-}Anh}$-temperature calibration is established.

4.2.3 The Ca isotope budget of the Turtle Pits hydrothermal system

In order to assess the Ca isotope budget of the phase-separated hydrothermal system at Turtle Pits, a similar model approach as discussed for the LHF (Ch. 4.1; Eq. 4.1) will be considered:

$$N_{SW}*\delta_{SW} + N_{initial}*\delta_{initial} = N_{HydEnd}*\delta_{HydEnd} + N_{Anh}*(\delta_{HydEnd} + \Delta_{HydFluid\text{-}Anh}) \quad \text{(Eq. 4.6)}$$

Thereby, the average Ca isotope fractionation of $\Delta^{44/40}Ca_{Fluid\text{-}Anh}$ = -0.65 ‰ represents the overall Ca isotope fractionation of the anhydrites $\Delta_{HydFluid\text{-}Anh}$ from the Turtle Pits vent field. In contrast to the Logatchev field, the isotopic signature of the basement at Turtle Pits, and hence $\delta_{initial}$, is well-determined by the analyses of the two basaltic samples averageing to a value of -0.97±0.04 ‰ (Tab. 3.5). Further distinctions to the model assumptions made for LHF are that due to the high temperatures predominate at the Turtle Pits hydrothermal field, the quantitative removal of seawater-SO_4^{2-} by anhydrite precipitation is given by a sulfate concentration for the fluid endmember $[SO_4^{2-}]_{HydEnd}$ of ~ 0 determined for Turtle Pits (Schmidt, pers. comm.). This is to be expected as anhydrite is precipitating quantitatively at temperatures >150 °C. In addition, a total exchange of Mg for Ca must be presumed as an equimolar exchange of Mg and Ca during water-rock interaction can only be doubted for low temperatures (< 150 °C) and Ca-poor host-rocks (e.g. Seyfried & Bischoff, 1979; Bischoff & Dickson, 1975), both definitely not given here. These preconditions exhibit that the Ca input into the hydrothermal cell overbalances the output to about 16 mM ($\boldsymbol{N_{PS}}$). N_{PS} must be sequestered either in mineral precipitates different than anhydrite such as calcium carbonates or is sequestered by a brine phase in the subsurface as a consequence of phase separation. Hence, N_{PS} has to be included in the mass balance equation with its respective isotopic composition $\boldsymbol{\delta_{PS}}$ in order to provide steady state.

$$N_{SW}*\delta_{SW} + N_{initial}*\delta_{initial} = N_{HydEnd}*\delta_{HydEnd} + N_{Anh}*(\delta_{HydEnd} + \Delta_{HydFluid\text{-}Anh}) + \mathbf{N_{PS}*(\delta_{HydEnd} + \Delta_{HydFluid\text{-}PS})} \quad \text{(Eq. 4.7)}$$

Except for $\Delta_{H\psi\delta Ev\delta-PS}$ all of the parameters are known or can be assumed (Tab. 4.3). $\Delta_{H\psi\delta Ev\delta-PS}$ can be deduced by converting Eq. 4.7 to:

$$\Delta_{H\psi\delta Ev\delta-PS} = N_{SW}*\delta_{SW} + N_{initial}*\delta_{initial} - N_{HydEnd}*\delta_{HydEnd} - N_{Anh}*(\delta_{HydEnd} + \Delta_{HydFluid\text{-}Anh}) - N_{PS}*\delta_{HydEnd} / N_{PS} \quad \text{(Eq. 4.8)}$$

Two scenarios can be considered in order to assess the value of δ_{PS} (Tab. 4.3). Ignoring the high water-rock ratios of ~ 48 as deduced above and inserting the empirically determined $\delta^{44/40}Ca_{HydEnd}$ of -0.65 ‰, a $\delta^{44/40}Ca$ of -0.36 ‰ is calculated for δ_{PS} (scenario I). On the other hand, if the high water-to-rock ratio at Turtle Pits leading to an endmember value of -0.77 ‰ is taken into account, then a value of -0.19 ‰ is calculated for δ_{PS}. δ_{PS} describes the isotopic composition of an additional fraction N_{PS} = 16 mM that is not inherent in anhydrites or issued by hydrothermal fluid. Both results for δ_{PS} being lighter than seawater in their Ca isotopic compositions show that N_{PS} must be isotopically fractionationated when removed from the hydrothermal pathway.

Tab. 4.3, Ca mass balance calculations for the determination of Ca isotope fractionation during phase separation. See text for further explanation.

	$[Ca]_{SW}$ [mM]	$[Ca]_{initial}$ [mM]	$[Ca]_{Min}$ [mM]	$[Ca]_{HydEnd}$ [mM]	N_{PS} [mM]	$\delta^{44/40}Ca_{SW}$ [‰]	$\delta^{44/40}Ca_{initial}$ [1] [‰]	$\delta^{44/40}Ca_{HydEnd}$ [‰]	$\Delta_{H\psi\delta Ev\delta-PS}$ [‰]
I	10	54	28	10	26	0	-0.97±0.04	-0.65	-0.37
II	10	54	28	10	26	0	-0.97±0.04	-0.77[2]	-0.19

[1] determined by two basaltic samples
[2] Endmember value when taking a water-rock-ratio of 48 as deduced by Sr isotopes into account

It should be emphasized once again that these mass balance calculations are based on the very weakly determined hydrothermal endmember value for the Turtle Pits and should only be considered as hypothetical predictions awaiting confirmation as soon as the hydrothermal fluid endmember for Turtle Pits is further constrained. On the basis of these suggestions the mass balance approach shows that the higher Ca isotope composition of the fluid endmember value from Turtle Pits compared to the Red Lion and LHF may be best explained by an interplay of high water-to-rock ratio, extensive anhydrite precipitation and an additional process that sequesters preferentially the lighter isotope leading to an increase of the Ca isotope composition of the hydothermal effluent. This process is lacking in the both hydrothermal systems of Red Lion and LHF. As described above the additional Ca isotope fractionation is most likely to ascribe to phase separation as this process distinguishes hydrothermal circulation at Turtle Pits from that at Red Lion and LHF. Little is known about the chemical behavior of Ca in sub- or supercritical conditions and nothing is known about Ca isotopes during phase separation. With respect to the likelihood of Ca isotope fractionation implied above, some theoretical suggestions about a fractionation mechanism of Ca isotopes during phase separation will be presented in the following chapter.

4.2.4 Ca isotope fractionation during phase separation

The increase of Ca in high-chlorinity solutions strongly suggests that Cl-complexing plays an important role in the mobility of Ca in these solutions (Bowers et al., 1988). The Ca mass transport in high-Cl solutions have been subject to experimental investigations (e.g. William-Jones & Seward, 1989; Roselle & Baumgartner. 1995). In order to model Ca speciation at hydrothermal conditions the three components HCl, CaO, H_2O were considered in these studies. These studies determined species of the forms $Ca_mCl_n^{2m-n}$, comprising Ca^{2+}, $Ca(OH)^+$, $CaCl^+$, $CaCl_2^0$ complexes with the latter becoming dominant close to the critical point (Fig. 1.4) (William-Jones & Seward, 1989). Additionally, in contrast to other metals Ca form higher order chloride complexes such as $CaCl_3^-$ also leading to a greater solubility of Ca compared to other metal chloride species in high-Cl solutions (Roselle & Baumgartner, 1995). The importance of the $CaCl_3^-$ species expands with increasing total chlorine concentration, while the $Ca(OH)^+$ species becomes dominant under low chloride contents.

As Ca forms stable aquo-chloro complexes and the Ca concentrations of hydrothermal fluids vary positively with chlorinity, it seems possible that Ca isotope fractionation takes place during phase separation and segregation of vapor from brine, and during water-rock reactions. Fractionation of the stable O- and H-isotopes during phase transformation and water-rock interaction was previously reported (Driesner et al., 2000) and implies that isotope fractionation related to the hydration of ions, ion clusters or neutral species may play a significant role in high-temperature aqueous solutions and vapors in hydrothermal systems (Driesner et al., 2000). Ionic hydration is considered to influence not only stable isotope fractionation at phase transitions but also the rate and magnitude of many other important geochemical processes such as the dissolution and precipitation of minerals and the mass transport in hydrothermal fluids (Driesner et al., 2000). Hence, Ca isotope fractionation has been proposed to occur due to different speciations such as the hydration shell or mass differences affecting diffusional mass transport effects (cf. Ch. 1.2.1).

The compositions of phase-separated fluids provide new insights into the process of the chemical behavior of metal cations, in particular Ca and Ca isotopes and the overall controls on the elemental and isotopic compositions of the hydrothermal fluids. Circulating seawater at Turtle Pits is supposed to underlie phase separation and the emanating hydrothermal fluid represents the vapor phase (Koschinsky et al., 2006; Haase et al., submitted). In addition, the very low Ca content of the Turtle Pits fluid endmember being even less than seawater-Ca and the fact that the Ca and Sr systematics from the Red Lion field resembles rather LHF than the Turtle Pits vent field suggests phase separation to be a controlling factor. Phase separation may lead to a sequestration of Ca with an enrichment of the lighter Ca isotopes in the brine phase and the heavier one in the vapor phase exciting on the seafloor. This might be based on that lighter isotopes form more readily chloro-complexes than the heavier isotopes. The latter inferences are similar to the findings for the REE, where the LREE become enriched in the brine and the HREE in the vapor phase. Although further studies including experiments of aqueous solutions at high temperatures are requested in order to constrain the chemical and isotopic behaviour of Ca at sub- and supercritical conditions and to manifest the hypothetical inferences made above, generally it can be stated that despite of the high temperatures and exceptional physico-chemical conditions phase separation has theoretically the potential to induce Ca isotope fractionation.

4.3 The Ca isotope compostions of various rock materials

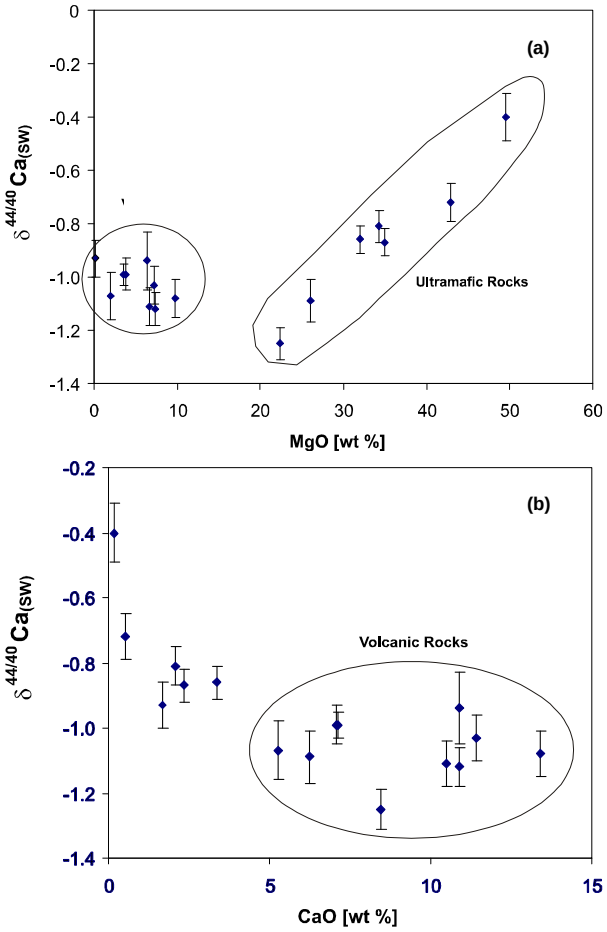

Fig. 4.8, (a) Ca isotope ratios in different rock types vs. their MgO contents. In contrast to all other rock types, the ultramafic rocks show a positive correlation between MgO concentrations and $\delta^{44/40}$Ca. See text for further explanation.
(b) There is no correlation between the Ca content and the Ca isotope compositions. This might indicate that Ca isotopes do not fractionate during fractional crystallization.

The Ca isotope compositions of various rock materials were investigated with regard to the above-demonstrated necessity for Ca isotope data in silicate rocks and the occurrence for Ca isotope fractionation at higher temperatures as demonstrated for anhydrite and assumed for phase separation processes. The currently available data do not provide a representative range of the different rock types (cf. DePaolo, 2004). Most samples investigated are volcanic and relatively common rock types. As their $\delta^{44/40}Ca_{(SW)}$ are similar, typically of about -1 ‰ and statistically indistinguishable, potential Ca isotope variations were disregarded suggesting that they are too small to be resolved by the currently used analytical techniques (DePaolo, 2004). However, Ca isotope variations of up to 7 ‰ between a basaltic and a rhyolitic melt at ambient mantle temperatures could be experimentally demonstrated (Richter et al., 2003). The rock compilation presented in this work constitutes a broader range of geological reservoirs from different settings and rock types of ultramafic to highly silicous compositions (Tab. 2.1). As yet, no data existed for Ca in mantle rocks such as peridotites, although stable isotope fractionation in ultramafic rocks has been detected for Li, and Mg, with the latter considered as a chemical analog for Ca (e.g. Lundstrom et al., 2005; Pearson et al., 2006).

For the ultramafic samples, there is a clear positive relation between the MgO content and $\delta^{44/40}$Ca (Fig. 4.8a). Variations in the MgO content of mafic melts are indicative for either a breakdown of magnesian phases during partial melting or their removal during fractional crystallization. As no correlation exist between Ca isotope ratios and the MgO content of the felsic and mafic rocks (Fig. 4.8a), and in addition, although the analyzed volcanic rocks cover a wide range of Ca concentrations no systematic relation to the Ca isotopes (Fig. 4.8b) can be observed, it must be assumed that the processes inducing Ca isotope fractionation will be based rather on partial melting than on fractional crystallization.

Interestingly, likewise no significant Li isotope variability as a result of magmatic differentiation could be detected (Tomascak et al., 1999), while large variations in the Li isotope ratios between dunites and peridotites within an ophiolite complex were found (Lundstrom et al., 2005). Lundstrom et al. (2005) suggested melt extraction being the important factor for diffusive isotope fractionation of Li between dunites and harzburgites. Considering Ca isotope fractionation during partial melting, there are two processes providing variations in $^{44}Ca/^{40}Ca$. Ca isotopes may fractionate as a consequence of different melting degrees, and/or chromatographic isotope effects during melt segregation evoke variances in the Ca isotope compositions. Melt extraction processes have also been suggested to involve Mg isotope fractionation (Pearson et al., 2006). Notably, Pearson et al. (2006) report in their work a positive correlation between Mg isotope ratios ($\delta^{26}Mg$) and Ca contents in olivines. And although this complementary behavior between Ca and Mg isotopes and contents had been stated also in previous studies (Russell et al., 1978; Lee et al., 1978), an appropriate explanation is still outstanding. On the basis of the present data set, as yet it can not be assessed, which mechanism causes the variations in $\delta^{44/40}Ca$ and the correlation between Ca isotope ratios and MgO contents in ultramafic rocks. A closer consideration of the petrogenesis of the different rock types and their comparison, however, may provide some hints for the underlying mechanism.

4.3.1 Comparison of different rock types

An argument for the Ca isotope fractionation during partial melting is the heavy isotope signature of the dunite DTS-1. Dunites are supposed to be residues of extensive melt extraction of harzburgitic source. Thereby, the harzburgite is further depleted in most of the elements such as Ca due to interaction with ascending melt and is left as a restite almost entirely composed of olivine. According to the experiments of Richter et al. (2003), the higher $\delta^{44/40}Ca$ of the DTS-1 is consistent to a preferential diffusion of the lighter isotope in magmatic melts and an enrichment of the heavier isotopes in the residue caused by a physical kinetic isotope fractionation. Whether the diffusivity of Ca isotopes and the fraction of melt producing a dunite from a harzburgite can explain a fractionation of ~0.3 ‰ as found between DTS-1 and the peridotites analyzed in this study require further detailed investigation.

The two komatiite types, from Gorgona Island and the Onverwacht group, differ significantly. This has been stated earlier for many geochemical parameters (e.g. Echeverria, 1980; Révillon et al., 2000) and is here extended to Ca isotopes. Komatiites in general are derived from high-magnesian melts with MgO content of the parental magma of > 20 wt% (Révillon et al., 2000). Despite of their ultramafic compositions, the two Gorgona komatiites (GOR128-G and GOR132-G) display a $\delta^{44/40}Ca$ that is 0.3 ‰ lighter than the value for the Onverwacht komatiites. An enrichment of the lighter Ca isotope during secondary processes can be excluded, because based on the presence of fresh glass and the absence of secondary minerals such as carbonates, Gorgona komatiites were assessed to be virtually unaltered (Echeverria, 1980). A characteristic of the Gorgona komatiites are their high Ca/Al ratios. Compared to the Onverwacht komatiites, they display a three times higher Ca concentration (Tab. 3.11), most probably because of the presence of plagioclase with a high amount of normative anorthite that has not been reported for the Onverwacht komatiites.

Plagioclase is the last phase to crystallize in komatiitic melts. Dietrich et al. (1981) suggested that komatiites from the Gorgona Island result from rapid uplift and growth such that the rate of crystallization exceeded the diffusion rate of Ca. In addition, this indicates that there was not much interaction with the matrix during melt extraction and a potential isotope effect (Heumann, 1972; Russell & Papanastassiou, 1978; Navon & Stolper, 1986) during melt percolation was diminished.

An additional significant difference between komatiites from the Gorgona Island and those from the Onverwacht Group, or generally Archean type komatiites, is the typical high Mg content of the latter. This difference has been explained by either an addition of secondary Mg, higher melting degree or a more refractory source for Archean komatiites compared to those from the Gorgona Island. Remarkably, the Ca isotope ratios are strictly following the Mg trend (Fig. 4.8a) indicating a strong correlation between $\delta^{44/40}$Ca and melting degree.

With regard to the similar Ca isotope compositions of the Gorgona komatiites and the oceanic island basalts (OIB) (Tab. 3.11) as well as mid-ocean ridge basalts (MORB) (Skulan et al., 1997; Richter et al., 2003), it should be noted that Gorgona komatiites are supposed to be derived from melting of oceanic mantle domains, which have undergone depletion of incompatible elements similar to MORB (Echeverria, 1980). In addition, Gorgona Island is part of the Carribean oceanic plateau (Hauff et al., 2000) that is assumed to have formed through partial melting within a mantle plume similar to OIBs (Duncan & Hargraves, 1984).

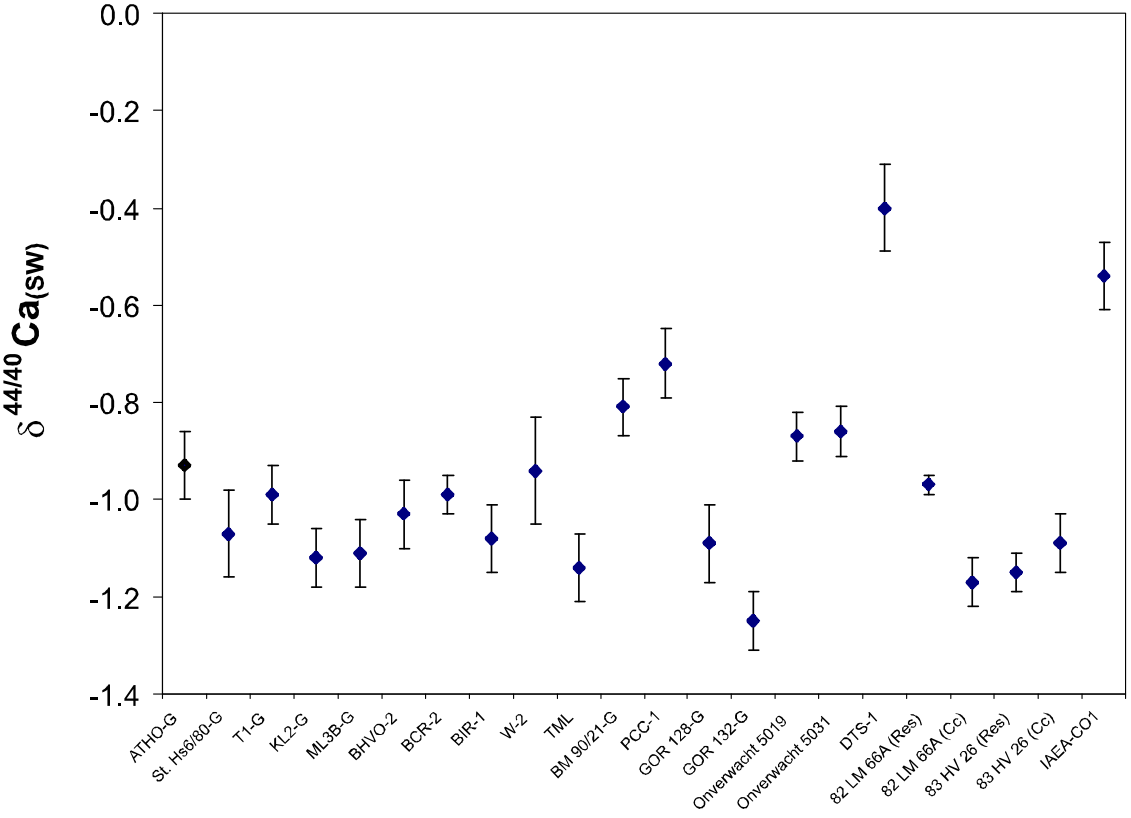

Fig. 4.9, Overview of the Ca isotope compositions in various rock samples. The different rock types show differences in their $\delta^{44/40}$Ca isotopic compositions. In particular, ultramafic rocks are significantly heavier than mafic rock samples. The results provide preliminary information values that await confirmation. Analytical uncertainties are given as 2sem.

Another unique characteristic distinguishing Gorgona komatiites from those of the Onverwacht group is the fact that former are unmetamorphosed. With regard to the Ca isotope systematic this might be insofar of importance as the Carrara marble (IAEA-CO1) investigated in this study display a strikingly high $\delta^{44/40}$Ca (Tab. 3.11; Fig. 4.9) indicating that fractionation of Ca isotopes may also occur during metamorphic processes. The Carrara marble formed during the Tertiary greenschist facies metamorphosis of a former Liassic carbonate platform. A Ca isotope composition of about -0.5 ‰ relative to seawater as displayed by the Carrara marble is unlikely for Jurassic sedimentary carbonates. The $\delta^{44/40}Ca_{(SW)}$ of Jurassic chalks was determined to be around -1.1 ‰ (Skulan et al., 1997). Farkas et al. (2007) measured $\delta^{44/40}Ca_{(SW)}$ of -1.2 to -1.8 ‰ for Jurassic belemnites and brachiopods. In addition, Böhm et al. (pers. comm.) determined for a Liassic cement in an alpine limestone a $\delta^{44/40}Ca_{(SW)}$ of -1.1 ‰. It must be therefore suggested that the intrinsic Ca isotope signature of the pristine carbonates was shifted towards higher values during the metamorphic formation of the Carrara marble. Characteristic fractures and joint systems (Ottria & Molli, 2000) are indicative for an extensive fluid circulation that potentially have caused a Ca isotope fractionation.

An interlinkage between carbonates and silicates are carbonatites. Carbonatites are carbonate-rich igneous rocks supposed to be derived directly from a mantle source. Their radiogenic Sr, Nd, and Pb isotope compositions resemble that of ocean island basalts suggesting a similar source for both rock types (Hoernle and Tilton, 1991). Carbonatites offer the possibility to investigate differences in the Ca isotope compositions of carbonates and silicates with the same evolutionary history. First insights are given here by leaching experiments, where the Ca isotope compositions of the leachates in the calcio- and the magnesio-carbonatites 83HV26 and 82LM66A (Hoernle et al., 2002) are analyzed separately from their silicate fraction (Tab. 3.11). In general, the Ca isotope compositions of the carbonate and silicate fractions of both carbonatite samples ranging between -0.97 and -1.17 ‰ are consistent with previously reported whole rock analyses of carbonatites (-1.1± 0.4 ‰; Russell et al., 1978) and the $\delta^{44/40}$Ca values of basaltic samples (Tab. 3.11; Fig. 4.9; cf. DePaolo, 2004). Notably, carbonatites seem also to resemble basalts (MORB, OIBs) in their Li isotope compositions (Halama et al., 2007).

While the $\delta^{44/40}$Ca values of the carbonate and silicate phases from the calcio-carbonatite 83HV26 are identical within the analytical error, the magnesio-carbonatite shows a significant difference of 0.2 ‰ between its silicate and carbonate fraction. Thereby, the carbonatic leachate agrees with the calcio-carbonatite. The Ca isotope composition of the silicate residue, however, is ~0.2 ‰ heavier. Previous studies are proposing that the magnesio-carbonatites are formed through the melting of carbonate-bearing peridotites at greater depth (e.g. Wallace & Green, 1988). The $\delta^{44/40}$Ca of the peridotites BM90/21/BM90/21-G and PCC-1 analyzed in our study are in average 0.2 ‰ heavier than the basaltic samples (Tab. 3.11; Fig. 4.9). The derivation of the magnesio-carbonatite from such an isotopically heavy source may explain the heavier Ca isotope composition of the silicate phase in the magnesio-carbonatite.

In contrast, similarities in Sr-Nd-Pb isotopic compositions in the calcio-carbonatite 83HV26 and associated silicate rocks indicate a genetic relationship between its silicate and carbonate phase (Gerlach et al., 1988; Hoernle and Tilton, 1991; Kokfelt, 1998). The consistency between the Ca isotope compositions of the silicate and carbonate phase of the calcio-carbonatite analyzed here is in good agreement to this assumption.

Generally, the data indicate the potential importance of diffusion-related (kinetic) processes for controlling Ca isotope fractionation at high temperatures. However, equilibrium fractionation may play a role when comparing modal mineralogy. Systematic differences between the Li isotope compositions of olivine, orthopyroxene and clinopyroxene was recently observed (Seitz et al., 2004) and may also be the case for Ca. Net changes in modal mineral assemblages may thus evoke isotope variability. For further constraints, systematic and elaborated investigations such as analyses of mineral separates are required. In summary, a more comprehensive and coherent data set must be addressed, in order to draw conclusions on Ca isotope variations as a consequence of petrogenesis and magma evolution.

4.3.2 Reconsideration of the Ca isotope compostion of Bulk Earth

The variances between the Ca isotope compositions of different rock types as outlined above should be taken into account for defining a $\delta^{44/40}$Ca value of Bulk Earth. This is of particular importance as the use of Bulk Earth as a reference for Ca isotope studies is common (Skulan et al., 1997; DePaolo, 2004; Fantle & DePaolo, 2005) and reasonable because of its assumed temporal constancy and the integration over the Earth's inventory of Ca (DePaolo, 2004). The Ca isotopic composition of the Bulk Earth is presently approached by an ultrapure $CaCO_3$ standard (Skulan et al., 1997; DePaolo, 2004; Fantle & DePaolo, 2005) being closely adjusted to the average Ca isotope composition of terrestrial igneous rocks measured to date. However, previous data did not provide a representative range of the different rock types (cf. DePaolo, 2004). Most samples investigated were volcanic and relatively common rock types. As their $\delta^{44/40}Ca_{(SW)}$ are similar, typically of about -0.9 ‰ and statistically indistinguishable, the Bulk Earth value is considered to be homogenous around -0.9 ‰. However, in addition to the experiments of Richter et al. (2003), the results of this work show strong evidence that the Ca isotope compositions between mafic and ultramafic rocks differ significantly by up to -0.6 ‰ (Tab. 3.11; Fig. 4.9) likewise demonstrating that Ca isotope fractionation does occur during the differentiation of silicates.

These findings imply that there is most likely not a single value for the Ca isotope composition of the oceanic crust (~ -0.9 ‰, Skulan et al., 1997). Rather a more inhomogeneous distribution of the Ca isotope composition of the oceanic crust as a function of the regional and local geological settings has to be assumed. Furthermore, the significant deviation between the Ca isotope compositions of mafic and ultramafic and also metamorphic rocks of up to 0.6 ‰ (Tab. 3.11; Fig. 4.9) requires a closer consideration and a potential refinement of the isotopic composition of Bulk Earth. Since Bulk Earth is constituted by > 99 % of the mantle, which is dominated by ultramafic rocks, specifically peridotites, it seems that the recently assumed Bulk Earth value has to be reconciled towards the higher values obtained for the peridotites analyzed in this study or even higher when taken the much heavier Ca isotope composition of the dunite (Tab. 3.11; Fig. 4.9) into account. However, the peridotites investigated in this work might be affected by secondary processes not reflecting the isotopic composition of the mantle. In order to make reliable inferences on the Bulk Earth value further detailed investigation, for instance of mantle xenoliths and/or eclogites assumed to provide insights into deep mantle composition are required.

4.4 Implications for the oceanic Ca budget

It may be stated that the findings of this study not only imply a reconsideration of the Bulk Earth value but might have also an impact on the marine Ca mass balance. The findings for the three working points in this study, hydrothermal solutions, anhydrite precipitation and low-temperature carbonate formation challenges the marine Ca isotope budget.

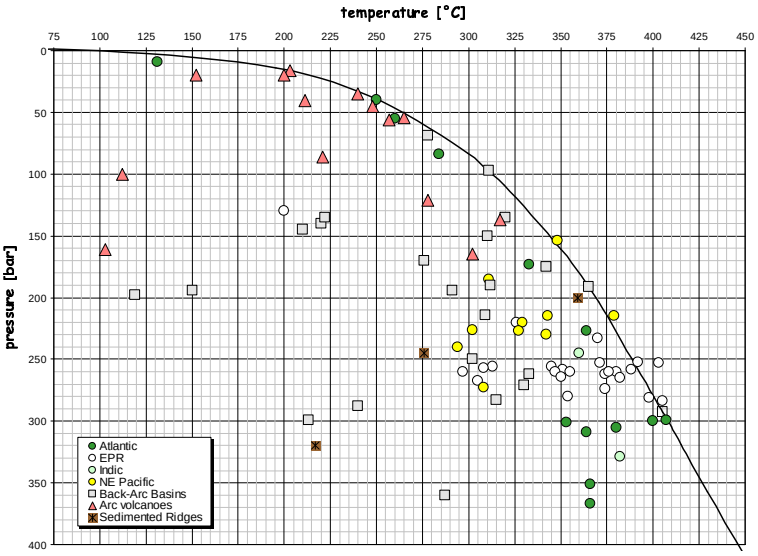

Fig. 4.10, Two-phase curve showing the distribution of known hydrothermal vent fields. The vent fields along or close to the two-phase boundary are boiling systems with evidence for phase separation. The sites are distinguished by their geologic settings. From S. Petersen (pers. comm.).

The investigation of hydrothermal fluids from different vent fields exhibits differences due to the physico-chemical conditions of the respective hydrothermal systems. The apparent deviation between the hydrothermal influx of Turtle Pits and Red Lion and LHF as well as the previously reported values of Schmitt et al. (2003a) points to variabilities in the hydrothermal Ca influx into the ocean. If phase separation indeed leads to the supply of heavier hydrothermal effluents as outlined above, then the global Ca influx from hydrothermal activity must be adapted. As yet, the global distribution of hydrothermal vent fields is assumed to be composed of about 70 % of non-boiling systems and 30 % of phase-separated systems such as Turtle Pits (Fig. 4.10; Petersen, pers. comm.). If the net fluxes are assumed to be equal in both systems, then the hydrothermal contribution to the Ca mass balance will be shifted to higher values than the presently assumed of about -1.0 ‰ (Fig. 4.11).

On the basis of the present dataset, model calculations for the oceanic mass balance would be too speculative and will be therefore disregarded. Nonetheless, the already existing data enables to postulate as a matter of fact a discrepancy between the Ca isotope composition of the oceanic crust and the hydrothermal effluent based on Ca isotope fractionation during anhydrite formation. The deviation between basement and hydrothermal fluid seems to be even higher in boiling systems due to potential Ca isotope fractionation during phase separation. Hence, the common assumption of a correspondence between the Ca isotope composition of the oceanic crust and the hydrothermal flux (e.g. Zhu & Macdougall, 1998; Schmitt et al., 2003a) appears to be at least over short time scales untenable. Integration over longer time periods may equalize this discrepany due to off-ridge dissolution of the fractionated anhydrites. The time frame and the magnitude to which extent the differentiation between oceanic crust and hydrothermal flux can be compensated has to be tested by the investigation of off-axis anhydrite deposits. To date, the sequestration of Ca in anhydrites and consequently the related Ca isotope fractionation is not considered in the currently existing models for the oceanic Ca budget.

Likewise, seafloor weathering inducing the formation of low-temperature alteration carbonates is barely considered, although carbonates formed by low-temperature weathering of oceanic crust are a significant Ca sink representing about 10 % of the marine Ca output (Fig. 1.1/4.11; Alt & Teagle, 1999). As outlined in this work, these carbonates seem to be substantially fractionated in their Ca isotope compositions. An average value of -1.70±0.06 ‰ (2sd) is deduced for the carbonate fraction of serpentinized peridoties from the seafloor and -1.54±0.08 ‰ for aragonite veins within the crust. The good agreement between both values and, in addition the consistency to the Ca isotopic compositions of carbonate veins in peridotites from the Gakkel Ridge recovered during the cruise AMORE in 2001 (unpublished values; Thiede et al., 2001) that averages to a value of -1.53±0.11 ‰, indicate a value of about -1.60 ‰ to be representative for low-temperature ocean crust alteration (Fig. 4.11). In summary, the results of this study suggest that the marine Ca sinks are isotopically significantly lighter than the Ca input into the ocean. This would imply that the ocean becomes in terms of Ca isotopes heavier through time, if there is no reflux of the primary sinks, hydrothermal anhydrite and low-temperature alteration carbonates.

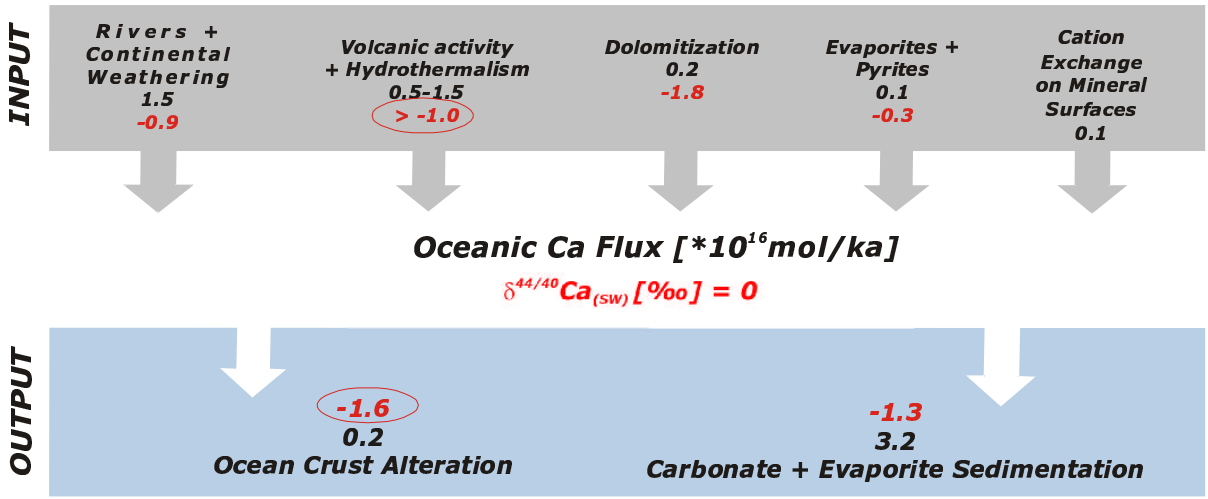

Fig. 4.11, Model currently assumed for the modern oceanic Ca budget with flux rates (dark numbers) and the known isotopic compositions relative to seawater (red numbers) modified after the findings of this work (encircled). Compare also Fig. 1.1.

5. Summary and Conclusion

High- and low-temperature ocean crust alteration plays an important role for the oceanic Ca budget representing a major source as well as a significant sink for marine Ca. Seawater-Ca is altered during convective circulation of seawater through oceanic crust at mid-ocean ridges. The chemical composition of hydrothermal solutions and mineral precipitates from different hydrothermal vent fields constrain the processes of hydrothermal fluid flow, mineral precipitation, and water-rock interactions at various physico-chemical conditions. The Logatchev hydrothermal field (LHF) and the vent fields at the MAR 5°S offer the possibility of a direct comparison between differing hydrothermal vent fields.

At LHF and the Red Lion field at the MAR 5°S seawater is chemically transformed to a hydrothermal fluid in the recharge and reaction zone, where seawater-Mg ($[Mg]_{SW}$) is sequestered and the Ca content in the hydrothermal fluid ($[Ca]_{HydFluid}$) is released from the bedrock. The expected initial Ca content of around 50 mM in the fluid drops to a $[Ca]_{HydEnd}$ of about 32 mM for LHF and ~16 mM for Red Lion with a $\delta^{44/40}Ca_{HydEnd}$ of -0.95±0.07 ‰ and -0.90±0.44 ‰, respectively. The decrease of the Ca concentration in the hydrothermal fluid and the increase of $\delta^{44/40}Ca_{HydEnd}$ compared to $\delta^{44/40}Ca_{initial}$ of the basement are best explained by the Rayleigh type precipitation of anhydrite. An overall isotopic difference of $\Delta^{44/40}Ca_{HydFluid\text{-}Min}$ = -0.55±0.08 ‰ is determined for the precipitation of anhydrite at the Logatchev field. With regard to the Ca isotope fractionation during anhydrite precipitation the Ca isotope composition of the basement is approximated either by -1.17±0.04 ‰ for the bedrock in the reaction zone or by -1.45±0.05 ‰ for the entire hydrothermal cell. U and Mg isotope ratios in the hydrothermal solutions of LHF do not show a systematic correlation with fluid amounts. Both isotope systems seem not to be significantly discriminated during water-rock interaction as the hydrothermal solutions display seawater composition. In contrast to LHF and the Red Lion field, a $\delta^{44/40}Ca_{HydEnd}$ of -0.65 ‰ was determined for the boiling hydrothermal system at the Turtle Pits field. Although not significant, the high value can be explained theoretically by an interplay between anhydrite precipitation, high water-to-rock ratios and an additional process sequestering light Ca isotopes, most likely phase separation. Ca isotopes may be discriminated during phase separation due to Cl^--complexation, in that the lighter Ca isotopes are more readily complexed than the heavier isotopes and hence retained in the brine phase.

Extensive anhydrite precipitation was observed at Turtle Pits. Likewise to LHF, the anhydrites are highly fractionated up to -0.9 ‰ in their Ca isotopic compositions. Ca isotope fractionation in anhydrites shows strong evidence for a temperature-dependency. Formation temperatures as deduced by isenthalpic mixing using Sr isotopes are positively correlated to the exhibited Ca isotope fractionation being consistent to the temperature-dependent Ca isotope fractionation in the calcium carbonate polymorphs aragonite and calcite. The temperature-dependency of anhydrite is apparently less sensitive than in calcium carbonates, emphasizing the necessity of a $\Delta^{44/40}Ca_{HydFluid\text{-}Min}$ –temperature calibration for anhydrite for future applications.

Investigated calcium carbonates from LHF and surrounding area are not affecting the Ca isotope budget of the hydrothermal cell. Calcites analyzed in this study precipitated at high temperatures above 100 °C and show therefore no Ca isotope fractionation. The calcites are precipitated despite of low pH and carbonate ion contents due to the high temperatures and the hence increased saturation state of the hydrothermal solutions.

Seafloor weathering is characterized by the formation of aragonite directly from seawater with a Ca isotope fractionation of up to -1.82 ‰. Both calcium carbonate polymorphs do not contribute to the Ca isotope budget of the hydrothermal fluid venting at Logatchev because $\Delta^{44/40}Ca_{HydroFluid\text{-}Min}$ is zero for the calcites and the Ca in aragonites originates from seawater rather than from a hydrothermal solution. However, as carbonates formed by low-temperature ocean crust alteration represent a significant Ca sink in the ocean, the strong Ca isotope fractionation for aragonite indicates a major influence on the ocean's Ca isotopic composition and has to be constrained in future studies.

In order to further constrain Ca isotope fractionation at high temperatures and due to the lack of data for silicate rocks, the Ca isotope compositions of various rock materials comprising several reference materials such as the MPI-DING glasses and USGS reference rock materials were investigated in this study. Different experimental methods were applied to assure that no analytical artifacts are obscuring the results. The experiments show that conventional chemical procedures seem not to affect the Ca isotope compositions within the statistical uncertainties. Analytical resolution allows attesting homogeneity on mm-scale for the MPI-DING glasses. Except for the Hawaiian tholeiitic basalt ML3B, no deviations can be detected between the MPI-DING glasses and their original rock powders. This study affirms that the MPI-DING reference glasses are not only homogeneous in their major element and most trace element distributions from the µm- to the cm-scale (Jochum et al., 2000; 2006) but also for their Ca isotopic compositions. Hence, the MPI-DING glasses are a suitable set of reference materials for Ca isotope measurements providing the advantage of simple sample dissolution and various matrices. In addition, they offer the possibility for Ca isotope in situ-microanalysis (Vigier et al., 2006). The reported values for the isotopic composition of the reference materials should be considered as proposing information values and a base for future studies on silicate rocks. A validation of these data by an interlaboratory check and the application of independent analytical techniques are desirable.

The Ca isotope compositions of the volcanic rocks are similar to previously reported values of around -1 ‰ relative to seawater. In contrast, the ultramafic rocks tend to be enriched in the heavier isotope. The $^{44}Ca/^{40}Ca$ ratios in the ultramafic rocks show a strong positive correlation to MgO contents evoking a Ca isotope fractionation during partial melting and/or melt segregation rather than through fractional crystallization, as no Ca isotope variations can be detected in the volcanic rocks. There is no correlation between the Ca content and $\delta^{44/40}Ca$, which would be expected for fractional crystallization. Hence, Ca isotope fractionation might occur as a result of either different melting degree and/or chromatographic effect during melt percolation. Further constraints on crystal chemical, mineralogical and melt structural controls on the Ca isotope variations require a systematic study of a coherent sample assemblage including the analyses of mineral separates. Ca isotopes may also vary during metamorphic processes as shown by the high $\delta^{44/40}Ca$ value for the Carrara marble. The results for the rock materials confirm experimental findings of a Ca isotope fractionation at high temperatures in natural systems. It should be noted that a remarkable variability of Ca isotope ratios in igneous and metamorphic rocks, in particular ultramafics, demands a reconsideration of the proposed value for Bulk Earth. In conclusion, the oceanic Ca budget has to be reconsidered for its currently assumed hydrothermal influx and ocean crust alteration output due to large variabilities in hydrothermal solutions and alteration products exhibited in this study.

References

Alt, J.C., Teagle, D.A.H., 1999. The uptake of carbon during alteration of ocean crust. *Geochim. Cosmochim. Acta* **63**(10), 1527-1535(9).

Alt, J.C., Teagle, D.A.H., 2000. Hydrothermal alteration and fluid fluxes in ophiolites and oceanic crust. In *Ophiolites and Oceanic Crust: New insights from field studies and the Ocean Drilling Program*, Vol. 349 (ed. Y. Dilek, E. M. Moores, D. Elthon, and A. Nicolas), pp. 273-282. Geological Society of America, Special Paper.

Alt J.C., Davidson G.J., Teagle D.A.H., Karson J.A., 2003. Isotopic composition of gypsum in the Macquarie Island ophiolite: Implications for the sulfur cycle and the subsurface biosphere in oceanic crust. Geology, **31**, 549-552.

Anderson, L.G., Wedborg, M.,1985. Comparison of potentiometric titration methods for the determination of alkalinity and total carbonate in seawater. *Oceanologica acta.* Paris. Vol. **8**, no. 4. 479-483.

Anderson, R.F., Chase, Z., Fleisher, M.Q., Sachs, J.P., 2002. The Southern Ocean's biological pump during the last glacial maximum. *Deep Sea Res.II*. **49**,1909-1938.

Anderson, L.G., Jutterström, S., Kaltin, S., Jones, E.P., 2004. Variability in river runoff distribution in the Eurasian Vasin of the Arctic Ocean. *J Geophys Res.* **109.** doi:10.1029/2003JC001773.

Bach, W., Garrido, C.J., Paulick, H., Harvey, J., Rosner, M., 2004. Seawater-peridotite interactions: First insights from ODP Leg 209, MAR 15°N. *Geochem. Geophys. Geosys.* **5**(9): doi:1029/2004GC000744.

Bacon, M.P., 1978. Radioactive disequilibrium in altered mid-oceanic basalts. *Earth Planet. Sci. Lett*. **39,** 250-254..

Ben-Yaakov, S., Goldhaber, M.B., 1973. The influence of seawater composition on the apparent constants of the carbonate system. *Deep Sea Res* **20**, 87-99.

Berner, E.K., Berner, R.A., 1987. Global Water Cycle: Geochemistry and Environment*. Englewood Cliffs N.J*., Prentice Hall.

Berner, E.K., Berner, R.A., 1996. Global Environment: Water, Air and Geochemical Cycles. *Englewood Cliffs N.J*., Prentice Hall.

Berner, R.A., (2004). A model for calcium, magnesium and sulfate in seawater over Phanerozoic time. Amer. J. Sci., **304**, 438-453.

Bickle, M.J., Teagle, D.A.H., 1992. Strontium alteration in the Trodoos ophiolite: implications for fluid-fluxes and geochemical transport in mid-ocean ridge hydrothermal systems. *Earth Planet. Sci. Lett*. **113,** 219-137.

Bigeleisen, J., Wolfsberg, M., 1958. Theoretical and experimental aspects of isotope effects in chemical kinetics. *Adv. Chem. Phys.* **1**, 15-76.

Bischoff, J.L., Dickson, W.E., 1975. Seawater-basalt interaction at 200°C and 500 bars: Implications for origin of sea-floor heavy-metal deposits and regulation of seawater chemistry. *Earth Planet. Sci. Lett*. **25,** 385..

Bischoff, J.L., Seyfried, W.E., 1978. Hydrothermal chemistry of seawater from 25°C to 350°C. *Am. J. Sci.* **278,** 838-860.

Bischoff, J.L., 1980. Geothermal system at 21°N, East Pacific Rise: Physical limits on geothermal fluid and role of adiabatic expansion. *Sciene* **207,** 1465-1469.

Bischoff, J.L., Rosenbauer, R.J., 1985. An empirical equation of state for hydrothermal seawater (3.2 percent NaCl). *Am. J. Sci.* **285,** 725-763.

Böhm, F., Joachimski, M.M., Dullo, W.-C., Eisenhauer, A., Lehnert, H., Reitner, J., Wörheide, G., 2000. Oxygen isotope fractionation in marine aragonite of coralline sponges. *Geochim. Cosmochim. Acta* **64**, 1695-1703.

Böhm F. Eisenhauer A., Heuser A., Kiessling W., Wallmann K. 2005. Calcium isotope fractionation during dolomitization (Abstract). Schriftenr. Deutsch. Ges. Geowiss. **39**, 39.

Böhm, F., Gussone, N., Eisenhauer, A., Dullo, W.-C., Reynaud, S., Paytan, A., 2006. Ca Isotope fractionation in modern corals, *Geochim. Cosmochim. Acta* **70**, 4452-4462.

Böhm, F., Amini, M., Blenkinsop, J., Buhl, D., Eisenhauer, A., Farkas, J., V. Geldern, R., Gussone, N., Heuser, A., Munnecke, A., Veizer, J., Voigt, S., Wallmann, K., 2007. Calcium Isotope Budget of the Phanerozoic Ocean, *Geochim. Cosmochim. Acta* **71** *Suppl.1*.

Bonatti, E., Lawrence, J.R., Hamlyn, P.R., Breger, D., 1980. Aragonite from deep sea ultramafic rocks. *Geochim. Cosmochim. Acta* **44**, 1207-1215.

Bonatti, E., Lawrence, J.R., Morandi, N., 1984. Serpentinization of oceanic peridotites: temperature dependence of mineralogy and boron content. *Earth Planet. Sci. Lett*. **70 (1),** 88-94.

Bonifacie, M. ,Charlou, J.L., Jendrzejewski, N., Agrinier, P., Donval, J.P., 2005. Chlorine isotopic compositions of high temperature hydrothermal vent fluids over ridge axes. *Chem. Geol*. **221**, 279-288.

Bowers, T.S., Campbell, A.C.,Measures, C.I., Spivack, A.J., Khadem, M., Edmond, J.M., 1988. Chemical controls on the composition of vent fluids at 13°-11°N and 21°N, East Pacific Rise. *J. Geophys.Res.* **93**, 4522-4536.

Broecker, W.S., Peng, T.H., 1982. *Tracers in the sea*.Lamont-Doherty Geol. Obs., Palisades, NY, 690 pp.

Butterfield, D.A., Jonasson, I.R., Massoth, G.J., Feely, R.A., Roe, K.K., Embley, R.E., Holden, J.F., McDuff, R.E., Lilley, M.D., Delaney, J.R., 1997. Seafloor eruptions and evolution of hydrothermal fluid chemistry. *Phil. Trans. R. Soc. Lond. A* **355**, 369-386.

Caldeira K. (1995): Long-term control of atmospheric carbon dioxide: low-temperature seafloor alteration or terrestrial silicate-rock weathering? Amer. J. Sci., **295**, 1077-1114.

Chang, V.T.-C., Williams, R.J.P., Makishima, A., Belshawl, N.S., O'Nions, R.K., 2004. Mg and Ca isotope fractionation during CaCO3 biomineralisation, *Biochem. Biophys. Res. Comm.,* **323**, 79-85.

Chaussidon, M., Jambon, A., 1994. Boron content and isotopic composition of ocean basalts: Geochemical and cosmochemical implications. *Earth Planet. Sci. Lett*. **121,** 277-291.

Chen J.H., Lawrence Edwards, R., Wasserburg, G.J., 1986. ^{238}U, ^{234}U and ^{232}Th in seawater. *Earth Planet. Sci. Lett*. **80,** 241-251.

Cherdyntsev, V.V., 1955. Transaction of the third session of the commission for the determining the absolute age of geological formations. *Izv Akad Nauk SSSR* **175**, Moscow.

De Bievre, P., Lauer, K.F., Le Duigon, Y., Moret, H., Muschenborn, G., Spaepen, J., Spernol, A., Vaninbroukx, R., Verdingh, V., 1971. The half life of ^{234}U. In *Proc. Int. Conf. Chem. Nucl.. Data, Measurements and Applications*. Canterbury (ed. M.L. Hurrell), pp. 215-219. Inst. Civil Engineers, London.

De LaRocha, C.L., DePaolo, D.J., 2000. Isotopic Evidence for Variations in the Marine Calcium Cycle over the Cenozoic. *Science* **289**, 1176-1177.

Demicco, R.V., Lowenstein, T.K., Hardie, L.A., 2003. Atmospheric pCO_2 since 60 Ma from records of seawater pH, calcium, and primary carbonate mineralogy. *Geology* **31**, 793-796.

DePaolo, D.J., 2004. Calcium isotopic variations produced by biological, kinetic, radiogenic and nucleosynthetic processes. *Rev. Mineral. Geochem.* **55,** 255-288.

Devey, C.W., Lackschewitz, K.S., Baker, E., on behalf of METEOR 62/5 scientific party, 2005. Hydrothermal and Volcanic activity found on the southern Mid-Atlantic Ridge. *EOS* **86(22),** 209-212.

De Villiers, S., Dickson, J.A.D., Ellam, R.M., 2005. The composition of the continental river weathering flux deduced from seawater Mg isotopes. *Chem Geol*. **216,** 133-142.

Dickson, J.A.D., 1990. Carbonate mineralogy and chemistry. *Carbonate Sedimentology.* Oxford, UK, Blackwell Science.

Dietrich, V.J., Gansser, A., Sommerauer, J., Cameron, W.E., 1981. Palaeocene komatiites from Gorgona Isalnd, east Pacific; a primary magma ocean floor basalt. *Geochem J* **15**, 141-161.

Dingwell D., Bagdassarov N., Bussod N., Webb S.L., 1993. et al., 1993. Magma Rheology. *Mineralogical Association of Canada Short Course on Experiments at High Pressure and Applications to the Earth's Mantle*, 131-196.

DOE, 1994. Handbook of Methods for the Analysis of the Various Parameters of the Carbon Dioxide System in Seawater, Version 2: Dickson, A.G., Goyet, C. (eds.), *Report ORNL/CDIAC-74*, Oak Rodge National Laboratory, Oak Ridge, TN, USA.

Douville, E., Bienvenue, P., Charlou, J.L., Donval, J.P., Fouquet, Y., Appriou, P., Gamo, T., 1999. Yttrium and rare earth elements in fluids from various deep-sea hydrothermal systems.ermal fluids, *Geochim. Cosmochim. Acta* **63 (5)**, 627-643.

Douville, E., Charlou, J.L., Oelkers, E.H., Bienvenu, P., Jove Colon, C.F., Donval, J.P., Fouquet, Y., Prieur, D., Appriou, P., 2002. The rainbow vent fluids (36°14'N, MAR): the influence of ultramafic rocks and phase separation on trace metal content in Mid-Atlantic Ridge hydrothermal fluids, *Chem. Geol.* **184**, 37-48.

Driesner, T., Ha, T.-K., Sewald, T.M., 2000. Oxygen and hydrogen isotope fractionation by hydration complexes of Li^+, Na^+, K^+, Mg^{2+}, F^-, Cl^-, and Br^-: A theoretical studydge hydrothermal fluids, *Geochim. Cosmochim. Acta* **64 (17)**, 3007-3033..

Duncan, R.A., Hargraves, R.B., 1984. Plate tectonic evolution of the Carribean region in the mantle reference frame. in: Bonini W.E., Hargraves, R.B., Shagam, R. (eds.) The Caribbean-South American plate boundary and regional tectonics. *Bull. Geol. Soc. Am.***162,** 81-84.

Echeverria, L.M., 1980. Tertiary or Mesozoic Komatiites from Gorgona Island, Colombia: Field Relations and Geochemistry. *Contrib. Mineral. Petrol.* **73**, 253-266.

Edmonds, H.N., Edmond, J.M. 1995. A three-component mixing model for ridge-crest hydrothermal fluids. *Earth Planet. Sci. Lett*. **134,** 53-67.

Eisenhauer, A., Nägler, T., Stille, P., Kramers, J., Gussone, N., Bock, B., Fietzke, J., Hippler, D., Schmitt, A.-D., 2004. Proposal for an international agreement on Ca notation as result of the discussions from the workshops on stable isotope measurements in Davos (Goldschmidt 2002) and Nice (EGS-AGU-EUG 2003), *Geostandards and Geoanalytical Research* **28,** 149-151.

Elderfield, H., Schultz, A., 1996. Mid-Ocean ridge hydrothermal fluxes and the chemical composition of the ocean. *Annu Rev Earth Planet Sci* **24,** 191-224.

Escartin, J., Cannat, M., 1999. Ultramafic exposuresand the gravity signature of the lithosphere near the Fifteen-twenty Fracture zone (Mid-Atlantic Ridge, 14°-16,5°N). *Earth Planet. Sci*. **171,** 411-424.

Fantle, M.S., DePaolo, D.J., 2005. Variations in the marine Ca cycle over the past 20 million years. *Earth Planet. Sci. Lett*. **237,** 102-117.

Farkas J., Buhl D., Blenkinsop J., Veizer J., 2007. Evolution of the oceanic calcium cycle during the late Mesozoic: Evidence from $\delta^{44/40}Ca$ of marine skeletal carbonates. *Earth Planet. Sci. Lett.*, **253**, 96-111.

Faure, G. 1986. Principles of Isotope Geology. Jon Wiley & Sons, New York.

Fietzke, J., Liebetrau, V., Eisenhauer, A., Dullo C., 2004. Determination of uranium isotope ratios by multi-static MIC-ICP-MS: method and implementation for precise U- and Th-series isotope measurements. *J. Anal. At. Spectrom.* **20**, 395-401.

Fietzke, J., Eisenhauer, A., Gussone, N., Bock, B., Liebetrau, V., Nägler, Th.F., Spero, H.J., Bijma, J., Dullo C., 2004. Direct measurement of $^{44}Ca/^{40}Ca$ ratios by MC-ICP-MS using the cool-plasma-techniq,ue, Chemical Geology,**206**, 11-20.

Fietzke, J., Eisenhauer, A., 2006. Determination of temperature-dependent stable strontium isotope ($^{88}Sr/^{86}Sr$) fractionation via bracketing standard MC-ICP-MS. *Geochem. Geophys. Geosys.* **7**(8), doi:10.1029/2006GC001243.

Flanagan F.J., 1984. Three USGS mafic rock reference samples, W-2, DNC-1, and BIR-1. *U.S. Geological Survey Bulletin 1623* [1984] 1-54

Friedman, I., O'Neill, J.R., 1977. Compilation of stable isotope fractionationfactors of geochemical interest. *Geol. Surv. Prof. Pap.* **440-KK.** US Govt. Printing Office.

Fujiwara, T., Lin, J., Matsumoto, T., Kelemen, P.B., Tucholke, B.E., Casey J.F., 2003. Crustal evolution of the Mid-Atlantic Ridge near the Fifteen-Twenty Fracture Zone in the last 5 Ma. *Geochem. Geophys. Geosys.* **4**(3), doi:10.1029/2002GC000364.

Galy, A., Belshaw, N.S., Halicz, L., O'Nions, R.K., 2001. High-precision measurements of magnesium isotopes by multiple-collector inductively coupled plasma mass spectrometry (MC-ICPMS). *Int. J. Mass. Spectrom. Ion. Proc..***208**, 89-98.

Garbe-Schönberg, D., Koschinsky, A., Ratmeyer, V., Jähmlich, H., Westernströer, U., 2005. KIPS - A new Multiport Valve-based all--Teflon-Fluid Sampling Systems for ROVs. EGU06-A-07032.

Gerlach, D.C., Cliff, R.A., Davies, G.R., Norry, M., Hodgson, N., 1988. Magma sources of the Cape Verdes archipelago: isotopic and trace element constraints. *Geochim. Cosmochim. Acta* **52,** 2979-2992.

German, C.R., Parson, L.M., Murton, B.J., Bennett, D.P., S.A., Connelly, D.P., Evans, A.J., Prien, R.D., Rmirez,-Llodra, E.Z., Shank, T.M., Yoerger, D.R., Jakuba, M., Bradley, A.M., Baker, E.T., Nakamura, K., 2005. Hydrothermal activity on the Sothern Mid-Atlantic-Ridge: Tectonicall- and Volcanically-hosted high Temperature Venting at 2-7°S. *EOS Trans AGU Fall Meet. Suppl.* **86**, Abstract OS21C-04.

Goldstein, S.L., Rudnick, R.L., Deines, P., Walter L.M., Oelkers, E.H., 2003. Standards for publication of isotope ratio and chemical data in *Chemical Geology. Chem. Geol.,***202**, 1-4.

Gopalan, K., Macdougall, D., Macisaac, C., 2006. Evaluation of a ^{42}Ca-^{43}Ca double spike for high precision Ca isotope analysis.*Int. J. Mass. Spectr.* **248**, 9-16.

Gussone, N., Eisenhauer, A., Heuser, A., Dietzel, M., Bock, B., Böhm, F., Spero, H.J., Lea, D.W., Bijma J., Nägler, T.F. 2003. Model for kinetic effects on calcium isotope fractionation (d^{44}Ca) in inorganic aragonite and cultured planktonic foraminifera. *Geochim. Cosmochim. Acta* **67**(7), 2375-1382.

Gussone, N., Böhm, F., Eisenhauer, A., Dietzel, M., Heuser, A., Teichert, B.M.A., Reitner, J., Wörheide, G., Dullo, W.-C. 2005. Calcium isotope fractionation in calcite and aragonite. *Geochim. Cosmochim. Acta* **69**(7), 4485-4494.

Haase K. Shipboard Scientific Party, 2005. Mid-Atlantic-Ridge Expedition 2005. In: Haase K. and Lackschewitz K. S., 2005. Mid-Atlantic Expedition 2005, Cruise No. 64, 2 April 2005 - 3 Mai 2005. METEOR-Berichte, Universität Hamburg, in press.

Haase, K.M., S. Petersen, A. Koschinsky, R. Seifert, C. Devey, N. Dubilier, S. Fretzdorff, D. Garbe-Schönberg, C.R. German, O. Giere, R. Keir, J. Kuever, Lackschewitz, K.S., J. Mawick, H. Marbler, B. Melchert, C. Mertens, H. Paulick, M. Perner, M. Peters, S. Sander, O. Schmale, J. Stecher, H. Strauss, J. Süling, U. Stöber, M. Walter, S. Weber, U. Westernströer, D. Yoerger, and F. Zielinski, Young volcanism and related hydrothermal activity at 5°S on the slow-spreading southern Mid-Atlantic Ridge. Submitted for publication in *Geochemistry Geophysics Geosystems*

Habfast K., 1983. Fractionation in the Thermal Ionization source, *Int. J. Mass Spectrom. Ion Phys.* **51**, 165-189.

Halama, R., McDonough, W.M., Rudnick, R.L., Keller, J., Klaudius, J., 2007. The Li isotopic composition of the Oldoinyo Lengai: Nature of the mantle source and lack of isotopic fractionation during carbonatite petrogenesis. *Earth Planet. Sci. Lett.* **254**, 77-89.

Halicz, L., A. Galy, N.S. Belshaw, R.K. O'Nions,1999. High-precision measurement of calcium isotopes in carbonates and related materials by multiple collector inductively coupled plasma mass spectrometry (MC-ICPMS),*J. Anal. At. Spectrom.,* **14***,* 1835-1838.9

Hannigton, N., Herzig, P., Stoffers, P., 2001. First observation high-temperature submarine hydrothermal vents and massive anhydrite. *Marine Geoy* **177.** 199-220.

Hardie, L.A., 1996. Secular variation in seawater chemistry: An explanation for the coupled secular variations in the mineralogies of marine limestones and potash evaporites over the past 600 m.y. *Geology* **24,** 279-283.

Hart, R., 1973. A model for chemical exchange in the basalt-seawater system of oceanic layer II. *Can. J. Earth Sci*., 799-816.

Hart, S.R., Zindler, A., 1989. Isiotope Fractionation Laws: A test using Calcium. *Int. J. Mass Spectrom. Ion Phys.* **89**, 287-301.

Hauff, F., K. Hoernle, G. Tilton, D.W. Graham, A.C. Kerr, 2000. Large volume recycling of oceanic lithosphere over short time scales: geochemical constraints from the Carribean Large Igneous Province. *Earth Planet. Sci. Lett.* **174**, 247-263.

Henderson, G.M., 2002. New oceanic proxies for paleoclimate. *Earth Planet. Sci. Lett*. **203,** 1-13.

Hensley, T.M., MacDougall, J.D., 2003. Calcium isotope fractionation in Ca-bearing phases of Marine evaporites. *EOS Trans. AGU* **84***(46)*.

Hensley, T.M., 2006. Calcium Isotopes in the Marine Environment, *Dissertation thesis*

Hertogen, J., Janssens, M.-J., Palme, H., 1981. Trace elements in ocean ridge basalt glasses: implications for fractionation dutring mantle evolution and petrogenesis. *Geochim. Cosmochim. Acta* **44**, 2125-2143.

Heumann, K.G., 1972. Untersuchung von Calciumisotopieeffekten bei heterogenen Austauschgleichgewichten, *Zeitschrifgt für Naturforschung* **27b**(2), 126-133.

Heumann, K.G., 1988. Isotope dilution mass spectrometry, in: *Mass spectrometry (eds. Adams, F., Gijbels, R., van Grieken, R.),* Wiley*,* New York, 301-376.

Heuser, A., Eisenhauer, A., Gussone, N., Bock, B., Hansen, B.T., Nägler, T.F., 2002. Measurement of calcium isotopes ($\delta^{44}Ca$) using a multiccollector TIMS technique. *International J Mass Spectrometry* **220,** 385-397.

Heuser, A., Eisenhauer, A., Böhm, F., Wallmann, K., Gussone, N., Pearson, P.N., Nägler, T.F., Dullo, W.-C., 2005. Calcium isotope ($\delta^{44/40}Ca$) variaitons of Neogene Planctonic Foraminifer. *Paleaocenography* **20**. PA2013. doi:10.1029/2004PA001048.

Hirt, B., Epstein, S., 1964. A search for isotopic variations in some terrestrial and meteoritic calcium. *Trans. Am. Geophys U* **45**, 113.

Hippler, D., Schmitt, A.-D., Gussone, N., Heuser, A., Stille, P., Eisenhauer, A., Nägler, T.F., 2003. Calcium isotopic composition of various reference materials and seawater. *Geostandards* **27**(1), 13-19.

Hoernle, K., Tilton, G., 1991. Sr-Nd-Pb isotope data for Fuerteventura (Canary Island) basal complex and subaerial volcanics : application to magma genesis and evolution. *Schweiz. Mineral. Petrogr. Mitt.* **71**, 3-18.

Hoernle, K., Tilton, G., Le Bas, M.J., Duggen, S., Garbe-Schönberg, D. 2002. Geochemistry of oceanic carbonates compared with continental carbonatites : mantle recycling of oceanic crustal carbonate. *Contrib. Mineral. Petrol.* **142**, 520-542.

Holland, H.D., Horita J., Seyfried, W.E., 1996. On the secular variations in the composition of Phanerozoic marine potash evaporites. Geology, **24**, 993-996.

Holland H. H. and H. Zimmermann (2000), The dolomite problem revisited, *International Geology Review,* **42**, 481-490.

Holland H.D., 2005. Sea level, sediments and the composition of seawater. Amer. J. Sci., **305**, 220-239.

Horita, J., H. Zimmermann and H.D. Holland 2002. Chemical evolution of seawater during the Phanerozoic: Implications from the record of marine evaporites, *Geochim. Cosmochim. Acta,* **66**, 3733-3756.

Humphris, S.E., Bach, W., 2005. On Sr isotope and REE compositions of anhydrite from the TAG seafloor hydrothermal system. *Geochim. Cosmochim. Acta* **6**(22), 4665-4678.

Jackson, M.G., Hart, S.R., 2006. Strontium isotopes in melt inclusions from Samoan basalts: Implications for heterogeneity in the Samoan plume. *Earth Planet. Sci. Lett.*, **245**, 260-277.

James, R.H., Elderfield, H., 1996. Chemistry of ore-forming fluids and mineral formation rates in an active hydrothermal sulfide deposit on the Mid-Atlantic Ridge. *Geology* **24** 1147-1150

James, R.H., Rudnicki, M.D., Palmer, M.R., 1999. The alkali element and boron geochemistry of the Escanaba Through sediment- hosted hydrothermal system. *Earth Planet. Sci. Lett.*, **171 (1)**, 157-169.

Jochum, K.P., Arndt, N.T., Hofmann, A.W., 1991. Nb-Th-La in komatiites and basalts : constraints on komatiite petrogenesis and mantle evolution. *Earth. Planet. Sci. Lett.* **107**, 272-289.

Jochum, K.P. et al., 2000. The preparation and preliminary characterization of eight geological MPI-DING reference glasses for in-situ microanalysis. *Geostand. Newsl.* **24**, 87-133.

Jochum, K.P. et al., 2006. MPI-DING reference glasses for in-situ microanalysis: New reference values for element concentrations and isotope ratios. *Geochem. Geophys. Geosys.* **7(2)**, pp. 44. doi: 10.1029/2005GC001060.

Johnson, K.M., King, A.E., Sieburth, J.M., 1985. *Marine Chem.* **16**, 61.

Johnson, K.M., Wills, K.D., Butler, D.B., Wong, C.S., 1993. Coulometric total carbon dioxide analysis for marine studies: maximizing the performance of an automated gas extraction system and coulometric detector. *Marine Chem.* **44**, 167.-187.

Kelemen, P.B., Kikawa, E., Miller, D.J., et al. 2004. Proc. ODP Init. Repts., 209 [online] (www.odp.tamu.edu/publications/209_IR/209ir.HTM)

Kelley, D.S., Karson, J.A., Früh-Green, G.L., Yoerger, D.R., 2005. A serpentinite-hosted ecosystem: The Lost City Hydrothermal Field. *Science* **307** (5714), 1428-1434.

Kokfelt, T., 1998. A geochemical and isotopic study of the island of Fogo, the Cape Verde Islands. *PhD Thesis.* University Copenhagen.

Koschinsky, A., Billings, A., Devey, C.W., Dubilier, N., Duester, A., Edge, D., Garbe-schönberg, D., German, C., Giere, O., Keir, R., Lackschewitz, K.S., Melchert, B., Mertens, C., Stöber, C., Suck, I., Walter, M., Weber, S., Yoerger, D., Zarrouk, M., Zielinski, F., 2006. Discovery of new hydrothermal vents on the southern Mid-Atlantic Ridge (4°S-10°S) during cruise M68/1. *InterRidge* News. **15**, 9-15.

Krolikowska-Ciaglo, S., Hauff, F., 2005. Sr-Nd isotope systematics in 14-28 Ma low-temperature altered mid-ocean ridge basalt from the Australian Antarctic discordance, Ocean Drilling Program Leg 187. *Geochem. Geophys. Geosys.* **6**(1), doi:10.1029/2004GC000802.

Kuhn, T., Shipboard Scientific Party, 2004. Mineralogical, geochemical, and biological investigations of hydrothermal systems on the Mid-Atlantic Ridge between 14°45'W and 15°05'N (HYDROMAR I). In: Christiansen B., Morgan J. P., Kuhn T., Send U. and Wallace D. W. R., 2004. Mid-Atlantic Expedition 2003/2004, Cruise No. 60, 11 November 2003 - 15 April 2004. METEOR-Berichte, Universität Hamburg, in press.

Lackschewitz, K.S., Shipboard Scientific Party, 2005. Longterm study of Hydrothermalism and biology at the Logatchev field, Mid-Atlantic Ridge at 14°45' (revisit 2005) (HYDROMAR II). In: Haase K. and Lackschewitz K. S., 2005. Mid-Atlantic Expedition 2005, Cruise No. 64, 1 April 2005 - 7 Juni 2005. METEOR-Berichte, Universität Hamburg, in press.

Lee, T., Papanastassiou, D.A., Wasserburg, G.J., 1978. Calcium anomalies in the Allende meteorite.*Ap. J. Lett.***220,** L21-L25.

Lemarchand, D., Wasserburg, G.J., Papanastassiou, D.A., 2004. Rate-controlled Calcium isotope fractionation in synthetic calcite. *Geochim. Cosmochim. Acta* **67**(7), 2375-1382.

Lilley, M.D., Butterfield, D.A., Lupton, J.E., Olson E.J., 2003. Magmatic events can produce rapid changes in hydrothermal vent chemistry, *Nature* **422**, 878-881.

Lounsburg, M., Durham, R.W., 1971. The alpha half-life of ^{234}U. In *Proc. Int. Conf. Chem. Nucl.. Data, Measurements and Applications*. Canterbury (ed. M.L. Hurrell), pp. 215-219. Inst. Civil Engineers, London.

Lowell, R.P., Yao, Y., 2002. Anhydrite precipitation and the extent of hydrothermal recharge zones at ocean ridge crests. *J. Geophys. Res.* **107**, 2183-2192.

Lowenstein T.K., Hardie L.A., Timofeeff M.N., Demicco R.M., (2003): Secular variation in seawater chemistry and the origin of calcium chloride basinal brines. *Geology*, **31**, 857-860.

Lundstrom, C.C., Chaussidon, M., Hsiu, A.T., Kelemen, P., Zimmermann, M. 2005. Observation of Li isotopic variations in the Trinity Ophiolite: Evidence for isotopic fractionation by diffusion during mantle melting. *Geochim. Cosmochim. Acta* **69**(3), 735-751.

MacDougall, J.D., 1977. Uranium in marine basalts: concentration, distribution and implications. *Earth Planet. Sci. Lett*. **35,** 65-70.

Marriott, C.S., Henderson, G.M., Belshaw, N.S., Tudhope, A.W., 2004. Temperature dependence of $d^{44}Ca$ and Li/Ca during growth of calcium carbonate. *Earth Planet. Sci. Lett*. **222,** 615-624.

Marshall, B.D., DePaolo, D.J., 1982. Precise age determinations and petrogenetic studies using the K-Ca method. *Geochim. Cosmochim. Acta* **46**, 2537-2545.

McArthur, J.M., Howarth, R.J., 2004. Strontium isotope stratigraphy. In Gradstein F., Ogg J., Smith A. (Eds.), *A Geologic Time Scale* (2004), 96-105, Cambridge Universitiy Press, Cambridge.

Metz, S., Trefry, J.H., 2000. Chemical and mineralogical influences on concentrations of trace metals in hydrothermal fluids. *Geochim. Cosmochim. Acta* **58**(10), 2225-2237.

Millero, F.J., 1995. Thermodynamics of the carbon dioxide system in the oceans. *Geochim. Cosmochim. Acta* **59**(4), 661-677.

Millero, F.J., Graham, T.B., Fen Huang, Bustos-Serrano, H., Pierrot, D., 2006. Dissociation constants of carbonic acid in seawater as a function of salinity and temperature. *Marine Chemistry* **100(1),** 80-94.

Milliman, J.D., 1993. Production and accumulation of calcium carbonate in the ocean: budget of a nonsteady state. Global Biogeochem. Cycles, **7**, 927-957.

Milliman, J.D., Droxler, 1996. Production and accumulation of calcium carbonate in the ocean: budget of a nonsteady state. Global Biogeochem. Cycles, **7**, 927-957.

Mintrop, L., Pérez, F.F., González-Dávila, M., Santana-Casiano, J.M., Körtzinger, A., 2000. Alkalinity determination by potentiometry: Intercalibration using three different methods, *Ciencias Marinas* **26(1)**, 23-37.

Mottl, M.J., Wheat, C.G., 1994. Hydrothermal circulation through mid-ocean ridge flanks: Fluxes of heat and magnesium. *Geochim. Cosmochim. Acta* **58**(10), 2225-2237.

Mucci, A.,1983. The solubility of calcite and aragonite in seawater at various salinities, temperatures, and one atmosphere total pressure. *Am J Sci* **283**, 780-799.

Mucci, A., Canuel, R., Shaojun Zhong, 1989. The solubility of calcite and aragonite in sulfate-free seawater and the seeded growth kinetics and composition of the precipitates at 25°C. *Chem Geol.* **74,** 309-320.

Nägler, Th.F. and Kamber, B.S. 1996. A new silicate dissolution procedure for isotope studies on garnet and other rock forming minerals. *Schweiz. Mineral. Petrogr. Mitt.* **76**, 75-80.

Navon, O., Stolper, E., 1987. Geochemical consequences of melt percolation: The upper mantle as a chromatographic column. *J. Geol.* **95 (3)**, 285-307.

Nehlig, P., 1993. Interaction between magma chambers and hydrothermal systems: Oceanic and ophiolitic constraints. *J Geophys Res* **98**, 19,621-19,633.

Nesbitt, R.W., Sun, S.S., Purvis, A.C., 1979. Komatiites : geochemistry and genesis. *Can. Mineral.*, **17**, 165-186.

Niederer, F.R., Papanastassiou, D.A., 1984. Ca isotopes in refractory inclusions. *Lunar Planet.Sci X*, 913-915.

O'Hanley, D.S., 1996. Serpentinites. *Oxford University Press In*, New York.

O'Neill, J.R., Clayton, R.N., Mayeda, T.K., 1969. Oxygen isotope fractionation in divalent metal carbonates. *J. Chem. Phys.* **51,** 5547-558.

Ottria, G., Molli, G., 2000. Superimposed brittle structures in the late-orogenic extension of the Northern Appennine: results from the Carrara area (Alpi Apuane, NW Tuscany). *Terra Nova* **12 (2)**, 52-59.

Palmer, M.R., 1996. Hydration and uplift of the oceanic crust on the Mid-Atlantic Ridge associated with hydrothermal activity: Evidence from boron isotopes. *Geophys Res Lett***23 (23)**, 3479-3482.

Pearson, N.J., Griffin, W.L., Alard., O., O'Reilly, S.Y., 2006. The isotopic composition of magnesium in mantle olivine: Records of depletion and metasomatism. *Chem. Geol*. **226**, 115-133.

Rayleigh, J.W.S., 1896. Theoretical considerations respective the separation of gases diffusion and similar processes. *Philos. Mag.* **42,** pp. 493.

Reagan, M.K., Sims, K.W.W., Erich, J., Thomas, R.B., Cheng, H., Edwards R.L., Layne, G.D., Ball, L., 2003. Time-scales of differentiation from mafic parents to rhyolite in North American continental arcs. *J Petrol* **44(9)**, 1703-1726.

Révillon, S., Arndt, N.T., Chauvel, C., Hallot, E., 2000. Geochemical Study of Ultramafic volcanic and Plutonic Rocks from Gorgona Island, Colombia: the Plumbing System of an Oceanic Plateau. *J Petrol* **41 (7),** 1127-1153.

Richter, F.M., Davies A.M., DePaolo, D.J., Watson E.B., 2003. Isotope fractionation by chemical diffusion between molten basalt and rhyolite. *Geochim. Cosmochim. Acta* **67,** 3905-3923.

Roselle, G., Baumgartner, L., 1995. Experimental determination of anorthite solubility and calcium speciation in supercritical chloride solutions at 2kb from 400 to 600°C. *Geochim. Cosmochim. Acta* **59 (8)**, 1539-1549.

Rosner, M., Bach, W., Paulick, H., Erzinger, J., 2006. Carbonate veins from oceanic core complexes: Tracing different stages of sub-seafloor alteration. Extended abstract German ODP-ICDP Meeting 2006 (27. - 29. 03. 2006), Greifswald, Germany.

Russell W.A., and Papanastassiou D.A., 1978. Calcium Isotope Fractionation in Ion-Exchange Chromatography, *Analytical Chemistry* **50**(8), 1151-1154.

Russell, W.A., Papanastassiou, D.A., Tombrello, T.A., 1978. Ca isotope fractionation on the Earth and other solar system materials. *Geochim. Cosmochim. Acta* **42**, 1075-1090.

Schmidt, K., Koschinsky-Fritsche, A., Garbe-Schönber, D.,De Carvalho, L.M.,Seifert, R., 2007. Geochemistry of hydrothermal fluids from the ultramfic-hosted Logatchev field, 15°N on the Mid-Atlantic Ridge *Geochim. Cosmochim. Acta*. in press.

Schmitt, A.-D., Chabeaux, F., Stille, P., 2003a. The calcium riverine and hydrothermal isotopic fluxes and the oceanic calcium mass balance. *Earth Planet. Sci. Lett*. **6731,** 1-16.

Schmitt, A.-D., Stille, P., Vennemannn, T., 2003b. Variations of the $^{44}Ca/^{40}Ca$ ratio in seawater during the past 24 million years: evidence from $\delta^{44}Ca$ and $\delta^{18}O$ in Miocene phosphates. *Geochim. Cosmochim. Acta* **67**(12), 2607-2614.

Schmitt, A.-D., Stille P., 2005. The source of calcium in wet atmospheric deposits: Ca-Sr isotope evidence.10 *Geochim. Cosmochim. Acta*, **69**, 3463-3468.

Seewald, J.S., Seyfried, W.E., Jr., 1990. The effect of temperature on metal mobility in subseafloor hydrothermal systems: constraints from basalt alteration experiments. *Earth Planet. Sci. Lett.* **101**, 388-403.

Seitz, H.-M., Brey, G.P., Lahaye, Y., Durali, S., Weyer, S. 2004. Lithium isotopic structures of peridotite xenoliths and isotopic fractionation at high temperature between olivine and pyroxenes. *Chem. Geol*. **212**, 163-177.

Seyfried, W.E., Bischoff, 1979. Experimental and theoretical constraints on hydrothermal alteration processes at mid-ocean ridges. *Ann. Rev. Earth Sci.* **15**, 317-335.

Seyfried, W.E., 1987. Experimental and theoretical constraints on hydrothermal alteration processes at mid-ocean ridges. *Ann. Rev. Earth Sci.* **15**, 317-335.

Seyfried, W.E., Ding, K., 1995. Phase equilibria in subseafloor hydrothermal systems: a review of the role of redox, temperature, pH and dissolved Cl on the chemistry of hot spring fluids on mid-ocean ridges. In Seafloor hydrothermal systems, *Geophysical Monograph* **91** (ed. S. E. Humphris, R. A. Zierenberg, L. S. Mullineaux, and R. E. Thomson), pp. 248-272. American Geophysical Union.

Shmulovich, K., Heinrich, W., Möller, P., Dulski, P. 2002. Experimental determination of REE fractionation between liquid and vapor in the systems NaCl-H_2O and $CaCl_2$-H_2O up to 450°C. *Cont. Mineral. Petrol.* **144**, 257-273.

Skulan, J., DePaolo, D.J., Owens, T.L., 1997. Biological control of calcium isotopic abundances in the global calcium cycle. *Geochim. Cosmochim. Acta* **61**(12), 2505-2510.

Skulan, J., D.J. DePaolo, 1999. Calcium isotope fractionation between soft and mineralized tissues as a monitor of calcium use in vertebrates, *Proc. Nat. Acad. Sci.,* **96**, 13709-13713.

Somayajulu, B.L.K., Goldberg, E.D., 1966. Thorium and Uranium isotopes in seawater and sediments. *Earth Planet. Sci. Lett.* **1**, 102-106..

Spencer, R.J., Hardie, L.A., 1990. Control of seawater composition by mixing of river waters and mid-ocean ridge hydrothermal brines. in: *Spencer, R.j., and Chou, I.-M., eds.,* Fluid-mineral interactions: A tribute to H.P. Eugster, Geochemical Society Special Publication **19**, 409-419.

Stanley, S.M., Hardie, L.A., 1998, Secular oscillations in the carbonate mineralogy of reef-building and sediment-producing organisms driven by tectonically forced shifts in seawater chemistry, *Palaeogeogr. Palaeoclimatol. Palaeoecol.,* **144**, 3-19.

Staudigel, H., Hart, S.R., Richardson, S.H., 1981. Alteration of the oceanic crust: Processes and timing. *Earth Planet. Sci. Lett.* **52,** 311-327.

Teichert, B.M.A., Gussone, N., Eisenhauer, A., Bohrmann, G., 2005. Clathrites: Archives of near-seafloor pore-fluid evolution on ($\delta^{44/40}Ca$, $\delta^{13}C$, $\delta^{18}O$) in gas hydrate environments. *Geology* **33** (3), 213-216.

Thiede, J., Shipboard Scientific Party, 2001. Cruise report, AMORE 2001 Arctic Mid-Ocean Ridge Expedition. *Reports on Polar and marine Research.*

Thompson, G., 1983. Hydrothermal fluxes in the Ocean. *Chemical Ocanography*, London Academic Press**,** 271-337.

Tipper E.T., Galy A., Bickle M.J., 2006. Riverine evidence for a fractionated reservoir of Ca and Mg on the continents: Implications for the oceanic Ca cycle. *Earth Planet. Sci. Lett*., **247**, 267-279.

Tivey, M.K., Humphris, S.E., Thompson, G., Hannington, M.D., Rona, P.A., 1995. Deducing patterns of fluid flow and mixing within the active TAG mound using mineralogical and geochemical data. *J. Geophys. Res.* **100**, 12,527-12,555.

Tomascak, P.B., Tera, F., Helz, R.T., Walker, R.J., 1999. The absence of lithium isotope fractionation during basalt differentiation: New measruments by multicollector sector ICP-MS. *Geochim. Cosmochim. Acta* **63** (6), 907-910.

Turner, S., Black, S., Berlo, K., 2004. ^{210}Pb-^{226}Ra and ^{228}Ra-^{232}Th systematic in young arc lavas: implications for magma degassing and ascent rates. *Earth Planet. Sci. Lett.* **227**, 1-16.

Urey, H.C., 1947. The thermodynamic properties of isotopic substances. *J. Chem. Soc.*562-87.

Vigier, N., Rollion-Bard, C., Spezzaferri, S., 2006. In-situ Ca isotope measurements in foraminifera. *Geochim. Cosmochim. Acta* **71** *Suppl.1*. *Geochim. Cosmochim. Acta* **70** *Suppl.1*.

Von Damm, K.L., Edmond, J.M., Grant B., Measures, C.I., Walden, B., Weiss, R.F., 1985. Chemistry of submarine hydrothermal solutions at 21°N, East Pacific Rise. *Geochim. Cosmochim. Acta* **49**, 2197-2220.

Von Damm, K.L., 1990. Seafloor hydrothermal activity: Black smoker chemistry and chimneys. *Ann. Rev. Earth Planet Sci* **18**, 173-204.

Von Damm, K.L., Buttermore, L.G., Oosting, S.E., Bray, A.M., Fornari, D.J., Lilley, M.D., Shanks, W.C., 1997. Direct observation of the evolution of a seafloor 'black smoker' from vapor to brine. *Earth Planet. Sci. Lett.* **149,** 101-111.

Von Damm, K.L., 1995. Controls on the chemistry and temporal variability of seafloor hydrothermal fluids. Seafloor Hydrothermal Systems: Physical, Chemical, Biological, and Geological Interactions, *AGU. Geophys Monogr* **91,** 222-247.

Von Damm, K.L., Lilley, M.D., Shanks, W.C., Brockington, M., Bray, A.M., O'Grady, K.M., Olson, E., Graham, A., Proskurowski, G., the SouEPR Science Party, 2003. Extraordinary phase separation and segregation in vent fluids from the southern East Pacific Rise. *Earth Planet. Sci. Lett.* **206,** 365-378.

Wallace, M.E., Green, D.H., 1988. An experimental determination of primary carbonatite magma composition. *Nature* **335, 343-346.**

Wallmann, K., 2001. Controls on the Cretaceous and Cenozoic evolution of seawater composition, atmospheric CO2 and climate, *Geochim. Cosmochim. Acta,* **65**, 3005-3025.

Ware, J.R., Smith, S.V., Reaka-Kudla, M.L.,1991. Coral reefs: Sources or sinks of atmosphereric CO_2?. *Coral Reefs* **11**, 127-130.

Wetzel, L.R., Shock, E.L., 2000. Distinguishing ultramfic- from basalt-hosted submarine hydrothermal systems by comparing calculated vent fluid compositions. *J. Geophys. Res.* **105**, 8319-8340.

White, W.M., Patchett, J., 1983. Hf-Nd-Sr isotopes and incompatible element abundances in island arcs - Implication for magma origins and crust-mantle evolution. *Earth Planet. Sci. Lett.* **67,** 167-185.

Williams, R., Collerson, K., Gill, J., Deniel, C., 1992. High Th/U ratio in subcontinental lithospheric mantle: mass spectrometric measurement of Th isotopes in Gaussberg lamproites. *Earth Planet. Sci. Lett.* **111**, 257-268.

Wilson S.A. 1997. Data compilation for USGS reference material BHVO-2,Hawaiian Basalt. U.S. Geological Survey Open-File.Report [1997]

Wombacher, F., Eisenhauer, A., Böhm, F., Gussone, N., Kinkel, H., Lezius, J., Noé, S., Regenberg, M., Rüggeberg, A., 2006. Magnesium Stable isotope Compositions in biogenic CaCO3. *Geophys Res Abs **8.***

Young E.D., Galy, A., 2004. The Isotope Geochemistry and Cosmochemistry of Magnesium. *Rev. Min. Geochem.***55**(1), 197-230.

Zhu, P., Macdougall, J.D., 1998. Calcium isotopes in the marine environment and the oceanic calcium cycle. *Geochim. Cosmochim. Acta* **62**(10), 1691-1698.

Acknowledgements

The present dissertation was supported by grants from the priority program 1144 of the "Deutsche Forschungsgemeinschaft, DFG: "From Mantle to Ocean: Energy-, Material- and Life-cycles at Spreading Axes". Furthermore, this study was supported by the EUROclimate program of the European Science Foundation, ESF in the frame of the CASIOPEIA project (Ei272/21-1).

This work could not have been accomplished without the commitments of many people. To mention all of the persons who helped to fulfil this work would probably exceed the extent of the intrinsic manuscript. Some persons, however, being directly related to this work shall be pointed out and particularly thanked; others not mentioned in the following can be sure of my tacit gratitude.

Directly indebted for this work, I'm certainly to my advisor Prof. Dr. A. Eisenhauer, whom I'd like to thank for the initiation of this very interesting project and his confidence providing me the chance to be in charge of it. I greatly acknowledge his commitment conceding maximum of freedom and autonomy to me not only for the accomplishment of the pertinent study, but in addition to pursue my interests, to experiment and letting my mind wander, although driving him to the limits of his patience with some 'awkward' practices. In particular, I'd like to thank him for thoughening and teaching me defending my own statements. Likewise, I'd like to thank the co-initiators of this project, Folkmar Hauff and Klas Lackschewitz. It was not at least the well-maintained TIMS lab and his non-restrictive availability (even on Christmas) by Folkmar that addicted me to continuously conduct measurements as many as possible. In this regard, Ana Kolevica is thanked for the maintenance of the clean lab, for providing sufficient beakers and her patience in QS. Klas Lackschewitz and Nico Augustin were my first contact persons keeping me informed about the logistics and the science around the SPP. Nico is particularly thanked for providing working materials such as samples and maps and for pleasant chats on shore as well as onboard. I appreciate the unhesitant aid of Prof. Dr. W. Bach providing data, much improving my understanding of hydrothermalism and helping to write a scientific paper. I wish to thank Dieter Garbe-Schönberg and Karin Kissling for their assistance in ICP-OES analyses and Jutta Heinze for urgent XRD analyses. Andrea Koschinsky, Katja Schmidt, Sven Petersen and Thomas Kuhn are thanked for providing sample material and valuable hints.

I'd like to express my gratitude for my working group, that are/were Barbara Bock who instructed me in Ca isotope analyses at the beginning, Frank Wombacher for giving insights into Mg isotope analyses, Alexander Heuser for resolving computer problems, Volker Liebetrau for being the utility man, Reini alias Reinhard Kozdon for bearing with me and my moods that long in one office and leaving it in good times. In particular, this work benefited much from the support of Florian Böhm. I'd like to thank him for enhancing my enthusiasm for scientific work, for broadening my mind, for many genial and fruitful discussions about calcium, carbonate, boron, the Alps, sponge, life, the universe and everything...likewise for everything, I 'have to' thank Jan Fietzke shortening and deepening column preparations and scientific congresses and reminding me on the essentials when being deeply immersed into work. A special thank to both, Jan and Florian for the programming!

Not directly involved but having accompanied the study from afar, are Klaus Peter Jochum, Brigitte Stoll, Kirstin Herwig, Michael Seufert and Susanne Schwenzer from the MPI in Mainz convincing me to continue science, encouraging me over the entire term and taking care for little ailments. From a longer distance Michaela Bock shared my worries and pleasures during the last three years.

Lastly, my family in particular my parents prepared the ground I step at. This work is not at least due to their efforts, commitment, reliance and love.

Tab. A1, Description and localization of the hydrothermal fluids and background seawater samples taken from different vent sites during the cruises HYDROMAR I and II, and MARSÜD.

sample ID	fluid amount* [%]	depth [m bsl]	comments	site
Logatchev field				
HYDROMAR I				
29 ROV-2 B2	4	2976	extreme black smoke	IRINA I
29 ROV-3 B7	4	2976	extreme black smoke	IRINA I
53 ROV-4 B2	21	2957	very close to smoker outflow; lots of black particles	IRINA I
53 ROV-5 B3	6	2959	close to smoker outflow; lots of black particles	IRINA I
53 ROV-7 B4	6	2959	close to smoker outflow; lots of black particles	ANNA-LOUISE
64 ROV-6 B2	7	2948	discrete smoker with strong black smoke at the crater rim; little fauna	ANNA-LOUISE
64 ROV-8 B3	7	2948	discrete smoker with strong black smoke at the crater rim; little fauna	IRINIA II
66 ROV-10 B3	11	2959	black smoke of a single smoker at the border of the field	IRINIA II
73 ROV-3 B2	11	3033	small smoker	IRINIA II
73 ROV-6 B3	13	3033	small smoker (same position as 73-2)	IRINIA II
73 ROV-8 B3		3033	small smoker (same position as 73-2)	IRINIA II
CTD/rosette samples				
17 CTD-6	0	3500	reference station	14°40' N 44°59'W (south of LHF)
17 CTD-16	0	2500	reference station	14°40' N 44°59'W (south of LHF)
HYDROMAR II				
224 ROV B15	72	3038	black smoke	IRINIA II
232 ROV-7 B9	0	3037	source of shimmering water	between IRINA II and QUEST
257 ROV-8 B10	88	2978	smoke	SITE B
266 ROV-10 B10	74	3003	smoke	SITE B
277 ROV-5 B2	11	3046	grey smoke from small black smoker, mineral complex (anhydrite?!) at the top of the chimney	IRINIA II
281 ROV-5 B2	51	3053	small chimney of 6 black smokers in central depression	QUEST
CTD/rosette samples				
217 CTD	0	2666	Background station	13°30' N 45°00' W (south of LHF)
231 CTD-8	0	3038	Plume mapping and sampling	14°45' N 44°59' W (NW of LHF)
Ascension area				
MARSÜD				
114 ROV N2	0	2993	diffuse flow	TURTLE PITS
123 ROV-B11	15	2990	small smoker	TURTLE PITS
141 ROV-11	63	2985	extreme black smoke	TURTLE PITS
125 ROV B11	14	2986	discrete smoker	WIDEAWAKE
125 ROV-13	10	2986	discrete smoker	WIDEAWAKE
146 ROV-B1	3	2973	extreme black smoke	RED LION
146 ROV-B9/10	65	2973	extreme black smoke, close to smoke outflow	RED LION
146 ROV-B11	20	2973	extreme black smoke	RED LION
146 ROV-B12	17	2973	extreme black smoke	RED LION
200 ROV-11/13	5	1496	diffuse outflow	LILLIPUT

* Fluid amounts deduced by extrapolation Mg concentration to zero (after Schmidt et al., in press)

Tab. A2, Description and localization of the rocks and hydrothermal mineral precipitates from the Logatchev hydrothermal field (LHF) and and the surrounding area (ODP LEG 209) and the vent fields at the Mid-Atlantic Ridge 5°S (MAR 5°S) investigated in this study.

sample ID	depth [m bsf]	comments	site
LHF			
anhydrites			
35 GTV-7/4	0	anhydrite	IRINIA II
64 ROV-10C	0	chips of sphalerite-anhydrite	ANNA-LOUISE
Serpentinite leachates			
49 GTV-1A-3 (L)	0	leached peridotite with calcite-filled fractures	WORKING AREA II
67 GTV-2A (L)	0	leachate of serpentinized peridotites with aragonitic veins	WORKING AREA I
67 GTV-2B (L)	0		
67 GTV-2C (L)	0		
ODP Leg 209			
calcites			
1271A 1R2 28-31	2.8	calcite dolomitic; hosted by altered dunite;	
1271A 5R1 30-33	38.5	calcite; containing dunite clasts;	
aragonites			
1271B 1R1 8-15	0.15	aragonite; totally altered peridotite (dunite/gabbro); chrysotile	
1271B 14R1 58-62	70.4	aragonite; host: gabbro/dunite; chrysotile	
1271B 15R1 53-57	75.3	aragonite; host: gabbro/dunite	
1274A 12R2 9-13	61	aragonite; host: harzburgite	
1274A 13R1 61-66	65.2	aragonite; host: harzburgite; chrysotile	
1274A 15R1 61-65	74.6	aragonite; host: harzburgite	
MAR 5°S			
anhydrites			
114 ROV-5B	0	Chimney anhydrite surrounded by chalcopyrite	TURTLE PITS
123 ROV-4A	0	From anInactive recrystallized sulfide chimney	TURTLE PITS
123 ROV-4C1	0		TURTLE PITS
130 ROV-1C	0	chimney fragment	TURTLE PITS
139 GTV-4A3	0	sulfide-anhydrite assemblage	TURTLE PITS
139 GTV-4C3	0	sulfide-anhydrite assemblage	TURTLE PITS
basalts			
109 GTV-1	0	glass fragments from sheet flow	TURTLE PITS
109 GTV-2	0	glass fragments from sheet flow	TURTLE PITS

Tab. A3, Comparison of the $\delta^{44/40}Ca_{(SW)}$ values in selected samples subject to different digestion procedures ($Diss_{HF}$ and $Diss_{HBr}$).

sample ID		$\delta^{44/40}Ca_{(SW)}$	2sem	*n*
DTS-1	$Diss_{HF}$	-0.34	0.12	*8*
	$Diss_{HBr}^{*}$	-0.42	0.1	*7*
PCC-1	$Diss_{HF}$	-0.67	0.09	*7*
	$Diss_{HBr}^{*}$	-0.71	0.10	*6*
BM90/21	$Diss_{HF}$	-0.89	0.08	*11*
	$Diss_{HBr}^{*}$	-0.77	0.12	*8*
BM90/21-G	$Diss_{HF}$	-0.80	0.08	*12*
	$Diss_{HBr}^{*}$	-0.79	0.12	*4*
BHVO-2	$Diss_{HF}$	-1.03	0.08	*14*
	$Diss_{HBr}^{*}$	-0.96	0.13	*6*
IAPSO^{+}	$Diss_{HF}$	-0.05	0.07	*4*

*blank corrected
$^{+}$normalized to average long-term IAPSO

Tab. A4, Two glass splits were compared for their Ca isotope compositions in order to test the homogeneity of the MPI-DING reference glasses. Aliquots of BHVO-2 and BIR-1 were processed within the individual chemical preparation procedures as quality-controls.

split		**#1**				**#2**					
sample ID	**$\delta^{44/40}Ca_{(SW)}$**	**2sem**	***n***	**variance**	**$\delta^{44/40}Ca_{(SW)}$**	**2sem**	***n***	**variance**	**mean**	**2 RSE [%]**	**p-value**
ATHO-G	-0.92	0.12	*7*	0.03	-0.93	0.06	6	0.01	-0.93	7.44	0.81
St. Hs6/80-G	-1.13	0.14	*9*	0.04	-1	0.07	7	0.01	-1.07	8.28	0.13
T1-G	-0.97	0.09	*6*	0.01	-1.01	0.07	8	0.01	-0.99	5.60	0.56
KL2-G	-1.13	0.09	*9*	0.02	-1.1	0.06	6	0.01	-1.12	5.26	0.66
ML3B-G	-1.15	0.06	*11*	0.01	-1.03	0.12	6	0.02	-1.09	5.87	0.06
GOR 128-G	-1.11	0.04	*6*	0.00	-1.04	0.15	7	0.04	-1.08	7.15	0.43
GOR 132-G	-1.31	0.08	*6*	0.01	-1.19	0.07	5	0.01	-1.25	5.02	0.05
BM 90/21-G	-0.8	0.09	*7*	0.01	-0.81	0.15	6	0.03	-0.81	9.56	0.87
BHVO-2	-1.03	0.09	*8*	0.02	-1.02	0.15	6	0.01	-1.03	7.76	0.66
BIR-1	-1.06	0.05	*8*	0.01	-1.11	0.16	6	0.04	-1.09	6.84	0.51